

MAGYAR ÁLLAMI
EÖTVÖS LORÁND
GEOFIZIKAI INTÉZET

EÖTVÖS LORÁND
GEOPHYSICAL INSTITUTE
OF HUNGARY

GEOFIZIKAI
KÖZLEMÉNYEK

GEOPHYSICAL TRANSACTIONS

CONTENTS

A new isostatic model of the Earth	K. F. Tyapkin	3
Interpretation of complex resistivity and dielectric data Part II	W. H. Pelton, W. R. Sill, B. D. Smith	11
Scalar audiomagnetotelluric measurements in Hungary	A. Ádám, P. Kaikkonen, S. E. Hjelt, J. Tiikkainen	47
Two- step deconvolution of gamma-ray logs	J. Šamšula, J. Zemčíková	63
Spectral measurement of natural gamma-rays under model and borehole conditions	R. Dorkó	73
Computer log evaluation in Tertiary coal basins	S. Mareš, J. Křestan	83
A statistical interpretation techniques for incomplete set of logs in sand-shale complex	B. Kiss, L. Kormos	93
Comparison of accuracy of control systems for various focused-current logging instruments	I. Kubina	107

ВЕНГЕРСКИЙ
ГЕОФИЗИЧЕСКИЙ
ИНСТИТУТ
ИМ Л. ЭТВЕША

ГЕОФИЗИЧЕСКИЙ
БЮЛЛЕТЕНЬ

VOL. 30. NO. 1. APRIL 1984. (ISSN 0016—7177)



BUDAPEST

Tartalomjegyzék

Egy új izosztatikus Föld-modell	K. F. Tyapkin	10
Komplex ellenállás- és dielektromos adatok értelmezése II. rész	W. H. Pelton, W. R. Sill, B. D. Smith	45
Skaláris audiomagnetotellurikus mérések Magyarországon	Ádám Antal, P. Kaikkonen, S. E. Hjelt, J. Tiikkainen	61
A gamma-sugár szelvények két lépéses dekonvolúciója	J. Šamšula, J. Zemčíková	72
A természetes gamma sugárzás spektrális mérése modell- és fúróluk viszonyok között	Dorkó Róbert	82
Számítógépes szelvénykiértékelés harmadkori szénmedencékben	S. Mareš, J. Křestan	92
Statisztikus értelmezési eljárások alkalmazása agyagos homokkő tárolókban, hiányos szelvényválaszték esetén	Kiss Bertalan, Kormos László	106
A különféle típusú fókuszált áramterű szelvényező berendezésekben használt szabályozó rendszerek összehasonlítása a pontosság szempontjából	Kubina István	117

Содержание

Новая модель геоизостазии	К. Ф. Тяпкин	10
Интерпретация данных о комплексных спектрах сопротивления и диэлектрических спектрах Часть 2	В. Г. Пелтон, В. Р. Сил, Б. Д. Смит	45
Скалярные аудиоманнитотеллурические измерения в Венгрии	А. Адам, П. Кайконэн, С. Э. Хельт, Й. Тикайнэн	62
Двухступенная деконволюция гамма-каротажных измерений	Й. Шамшула, Й. Земчикова	72
Измерение естественного гамма-излучения в модельных и скважинных условиях	Р. Дорко	82
Машинная обработка каротажа при разведке бурого угля	С. Мареш, Й. Кржестян	92
Статистический метод интерпретации для разрезов, слагающихся глинистыми песчаниками	Б. Киш Л. Кормош	106
Сопоставление по точности регулирующих систем различных типов для бокового каротажа	И. Кубина	117

A NEW ISOSTATIC MODEL OF THE EARTH

Konstantin F. TYAPKIN*

The proposed new model, called geostatic model, based on the assumption that the weights of the Earth's sectors being cut off by similar spatial angles, should be equal. The differences between geoid and corresponding spheroid may serve as a criterion of the Earth's equilibrium. Based on this assumption the equilibrium can be quantitatively investigated using gravity anomalies.

d: isostasy, geoid, spheroid, gravity anomalies

I. Introduction

The theory of the equilibrium state of the Earth, isostasy, originated from geophysical investigations in the middle of the 19th century. It was established that the form of the Earth approximates the equilibrium figure a rotating liquid. The spheroid, or theoretical geoid, slightly differs from the sphere and is characterized by flattening $\alpha = 1/298$ depending on the angular velocity and the law of mass distribution in the interior part of the Earth [LEIBENSON 1955].

The theory of isostasy and the history of its development being widely known, we confine ourselves to the essential notions necessary for further explanations.

a) Even at the beginning of its development, practical considerations required that the isostasy theory consider the Earth's crust equilibrium instead of that of the Earth as a planet. Such an approach has been observed up till now though, "the Earth's crust" has been substituted by "lithosphere". By isostatic state we understand a state such that the Earth's crust is placed over the substrate as if it had "swum" over the latter obeying Archimedes law [LUSTICK 1957]. The natural consequence of such a supposition is the equality of pressure upon some surface in the substrate called the compensation surface.

b) The gravitational method was and remains fundamental but not unique in isostatic investigations of the Earth's crust. In the development of the isostasy concept various models were proposed [Airy, Pratt, Bowie, Vening-Meinesz, etc]. The distinguishing feature of all these models is that the surface relief served as the only indicator both of mass distribution in the Earth's crust and of the state of its equilibrium in particular. Consequently, all conclusions concerning the isostasy of the continents based on those schemes would correspond only to the influence of equilibrium of the masses above the geoid level.

* Dnepropetrovsk Mining Institute, Department of Geophysics, POB 14, Dnepropetrovsk USSR
Manuscript received: 2 August, 1983

GOLYIZDRA [1972] developed the concept of isostasy of plane areas in which the above-mentioned schemes of the Earth's crust equilibrium were also taken as a basis but, along with topographic masses, the heterogeneities in the upper part of the Earth's crust revealed using geological and geophysical methods were taken as the indicators of the equilibrium state of the lithosphere. The author showed that under the conditions of plane relief of the Ukrainian shield if surface heterogeneities are available and the amplitude variations of the gravitational field are within a hundred milligals, the Earth's crust state in general approaches isostasy.

c) Since all current isostatic models are based on the interrelation between the relief changes, the heterogeneities in the upper parts of the Earth's crust and the distribution of the compensational masses in the lithosphere, the question was often raised concerning the dependence between isostasy and tectonics [see, e.g. VENING-MEINESZ 1940; ARTEMYEV and ARTYUSHKOV, 1967].

Though the interrelation between mass redistribution in the lithosphere and tectonics seems to be the closest the concrete role of isostatic forces in the formation of tectonic structures has not yet been established. It is quite remarkable that recent crustal movements registered in different regions are oriented both in the direction of equilibrium as determined by the above-mentioned models as well as in the opposite direction. The distinct dependence may be observed only in the direct relation between the imbalance manifestations and the recent tectonic activities in different regions.

d) The isostasy concept assumes that the rotational regime of the Earth (angular velocity and position of axis of rotation) is constant as is the corresponding figure of equilibrium.

2. Geoisostasy

Isostatic compensation models used for equilibrium studies of the Earth's crust in the initial period of the isostasy concept were accepted because at that time most geologists thought that the Earth's crust "was floating" over magma. Modern concepts of the Earth's structure show that such models are incomplete because they deal only with the upper part of the planet and neglect the remainder. An attempt to substitute the role of magmatic substrate by a hypothetical asthenosphere layer does not improve the situation.

Here it appears more constructive to introduce a new model of the equilibrium state of the Earth as a planet; we will name this "geoisostasy". Such a model should correspond to a state of the Earth which the latter would take if all the substrate were liquid without being mixed. This would allow Earth to be characterized by a system of equipotential surfaces which are similar to spheroids in whose formation the whole of the Earth would have taken part including the hydrosphere the atmosphere and even the associated physical fields. Obviously the special role of spheroid coinciding with the geoid must be emphasized. As mentioned above the latter is characterized by flattening

$\alpha = 1/298$. Flattening of internal spheroids decreases gradually towards the centre of the Earth.

It is pointed out that even though it is not absolutely essential to introduce in geostasy, in its general sense being equivalent to Pascal's law, equal weights of the Earth's sectors cut off by the similar spatial angles (*Fig. 1a*) may be taken as one of the equilibrium conditions. It can be expressed as

$$\Delta\Omega \int_0^{\infty} \sigma(r)g(r)r^2 dr = \text{const}, \quad (1)$$

where $\sigma(r)$ is the density distribution function $g(r)$ the acceleration due to gravity at points of the sector at a distance r from the centre of the Earth.

Expression (1) may be given as

$$\Delta\Omega \left\{ \int_0^{R_i} \sigma(r)g(r)r^2 dr + \int_{R_i}^{R_e} \sigma(r)g(r)r^2 dr + \int_{R_e}^{\infty} \sigma(r)g(r)r^2 dr \right\} = \text{const}, \quad (2)$$

where R_i is the external radius of the Earth's quasi-liquid core; R_e the mean radius of the geoid in the sector observed.

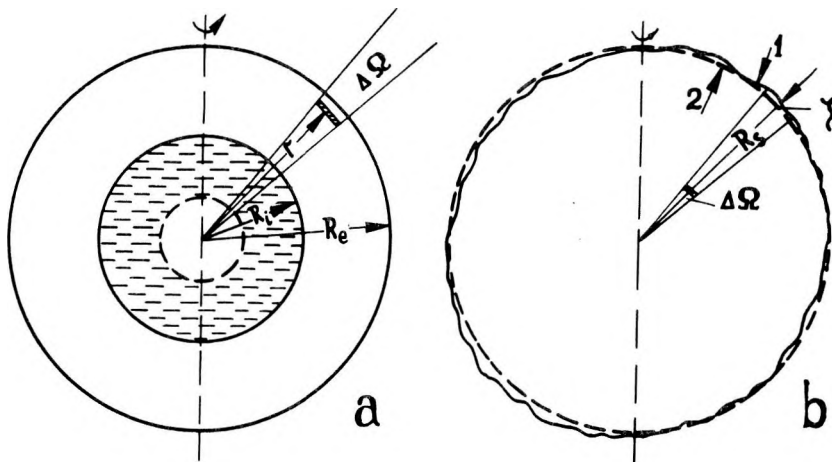


Fig. 1. Determination of geostasy model

1. ábra. A geozosztázia modelljének meghatározása

Рис. 1. Определение модели геозостазии

Using geostasy, this condition may be simplified by neglecting the first and third members on the left-hand side of equation (2)

$$\Delta\Omega \int_{R_i}^{R_e} \sigma(r)g(r)r^2 dr = \text{const} \quad (3)$$

The first member of equation (2) may be ignored if we assume a quasi-liquid core: "In the case of fluid Earth the equipotential surfaces are at the same time the surfaces of equal pressures" [MIKHAILOV 1938]. The third member of equation (2) can be neglected because of its negligible value compared with the second member. It is of essential value only when studying the atmospheric phenomena.

Condition (3) is necessary but not sufficient to support geostostasy.

The second geostostasy condition makes a provision for the range of densities in the interior parts of the Earth within which the potential values would correspond to those of the level surfaces calculated in assuming that the shells of the rotating Earth are liquid. Therefore, the divergences of the actual level surfaces from the theoretical ones would serve as a criterion for the Earth's equilibrium at each of those points. For practical purposes it would be more convenient to estimate the Earth's equilibrium for the points of its outer shell (geoid). As a criterion for the Earth's equilibrium we take the differences in heights (ζ) between the geoid and the corresponding spheroid

$$\zeta = R_g - R_s, \quad (4)$$

where R_g represents the radius of the geoid; R_s the radius of the spheroid in the Earth's sector to be studied. In the case of equilibrium:

$$\zeta = 0. \quad (5)$$

This definition is both acceptable and convenient for measuring the degree of geoid decline from its equilibrium state and can be determined directly from gravity data according to the well-known Stokes' formula [GRUSHINSKY 1963]

$$\zeta(R_0, \varphi_0, \lambda_0) = \frac{1}{2\pi\gamma R} \iint_{(s)} \Delta g(R, \varphi, \lambda) F(\Psi) ds, \quad (6)$$

where R, φ, λ are the spherical coordinates of a variable point over the surface of the Earth taken as a sphere of radius R ; $R_0, \varphi_0, \lambda_0$ the spherical coordinates of the point under investigation; $\Delta g(R, \varphi, \lambda)$ gravity anomalies; γ the mean value of normal gravity over the surface of the Earth; ds an element of the Earth's surface;

$$F(\Psi) = \operatorname{cosec} \frac{\Psi}{2} - 6 \sin \frac{\Psi}{2} + 1 - 3 \cos \Psi \ln \left(\sin \frac{\Psi}{2} + \sin^2 \frac{\Psi}{2} \right) - 5 \cos \Psi$$

Stokes' function and the angle are determined from the equation

$$\cos \Psi = \sin \varphi \sin \varphi_0 + \cos \varphi \cos \varphi_0 \cos (\lambda - \lambda_0) \quad (8)$$

Thus, to attain geostasy it is necessary to put into effect two conditions determined by expressions (3) and (5). It is pointed out that even though it is not absolutely essential to introduce the term "geostasy" since isostasy also describes the model of the Earth's equilibrium proposed by us in practice isostasy has previously been taken to be the model of hydrostatic balance of the Earth's crust (lithosphere) according to Archimedes and to Pascal's law.

3. Geostasy and tectonics

From the above-introduced model of geostasy it follows that all sorts of redistributions of masses are closely associated with changes in the equilibrium state of the Earth. To establish this interdependence we must turn to the rotation hypothesis of the tectonic structure formation in the Earth's crust which gave rise to the following scheme [TYAPKIN 1977]:

a) an interaction of the Earth and its surroundings changes in the rotational regime and in particular leads to variations in the spatial position of the Earth relative to its axis of rotation;

b) the equilibrium state changes to imbalance, and stresses appear to restore equilibrium corresponding to the new rotational regime of the Earth;

c) being influenced by the stresses, redistribution of masses occurs which leads to minimizing those stresses. In turn, mass redistribution results in tectonic formations accompanied by certain geological processes in the upper layers of the Earth usually called the tectonosphere.

Thus the essential tectonic forces are those which tend to bring our planet to an equilibrium state, i.e. the geostatic forces.

Figure 2 shows scheme of a geoid with homogeneous upper layer formed by the reorientation of the Earth relative to its axis of rotation which towers over the concentric spheroid. The character of stresses associated with this process and the process of their relaxation were discussed earlier [TYAPKIN 1977, TYAPKIN 1981]. In the given case, we would just like to compare the deviations between geoid and corresponding spheroid, having obtained from the rotation hypothesis of the structure formation and those calculated by Zhongolovich [1952] from gravity data (*Fig. 3*)

Analysis of *Figs. 2* and *3* leads to a number of important conclusions, viz.

a) the scheme of geoid undulation caused by the Earth's reorientation relative to the axis of its rotation regionally almost completely agrees with that calculated from gravity data.

b) the good agreement between the two pictures may be considered as one of the key factors in determining the laws of tectonic deformations of the Earth's ellipsoid [TYAPKIN 1981];

c) lack of correlation between geoid undulation and distribution of continents and oceans (*Fig. 3*) demonstrates that the topographic masses cannot be adopted as the decisive factor in reaching geostasy.

Let us now turn to the processes aiming to bring the Earth into equilibrium.

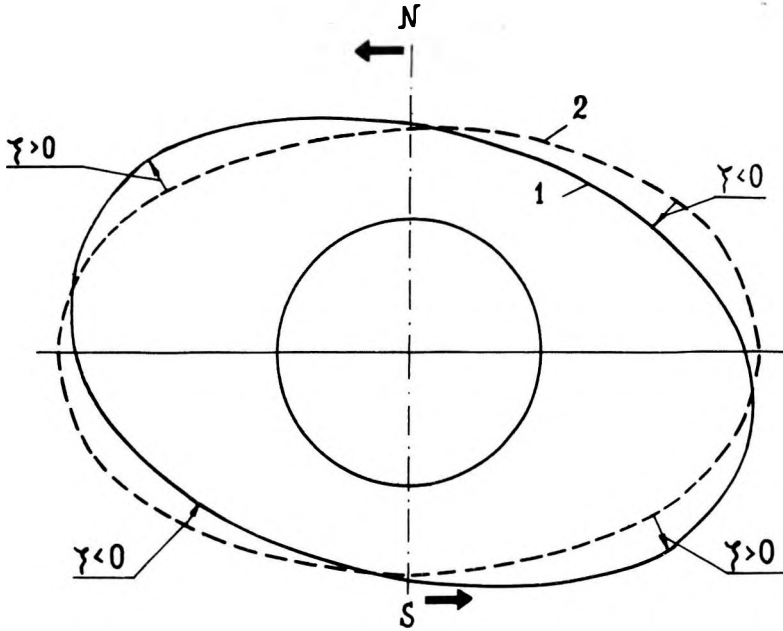


Fig. 2. Scheme of geoid's deviations from the spheroid according to the rotation hypothesis of structure formation
1 — geoid; 2 — spheroid

2. ábra. A geoidnak a szferoidtól való eltérései a rotációs szerkezetképződési hipotézis szerint
1 — geoid; 2 — szferoid

Рис. 2. Схема отклонений геоида от сфероида по гипотезе вихревого образования структур
1 — геоид; 2 — сфероид

On the ground of the variational principle of minimum action, Klushin [1963] showed that within sufficiently large sectors the local changes of the Earth's radius should be accompanied by vertical density redistributions.

Density redistribution inside the Earth's sector cut off by spatial spherical angles $\Delta\Omega$ is regulated by the law of conservation of momentum i.e. by its kinetic energy of rotation. It is a fourth degree function of the distance between the masses and the centre of the planet. Thus, it is of essential importance for geospheres at a distance from the centre of more than 0.8 of the Earth's radius. Almost half the kinetic energy and the momentum determined by masses concentrated at depths from 0 to 700–900 km, i.e. at the interval corresponding to the tectonosphere. All these considerations make it clear that the geological development of the upper layers of the Earth must have been directed towards making the regions with $\zeta < 0$ "heavier" and the regions with $\zeta > 0$ "lighter".

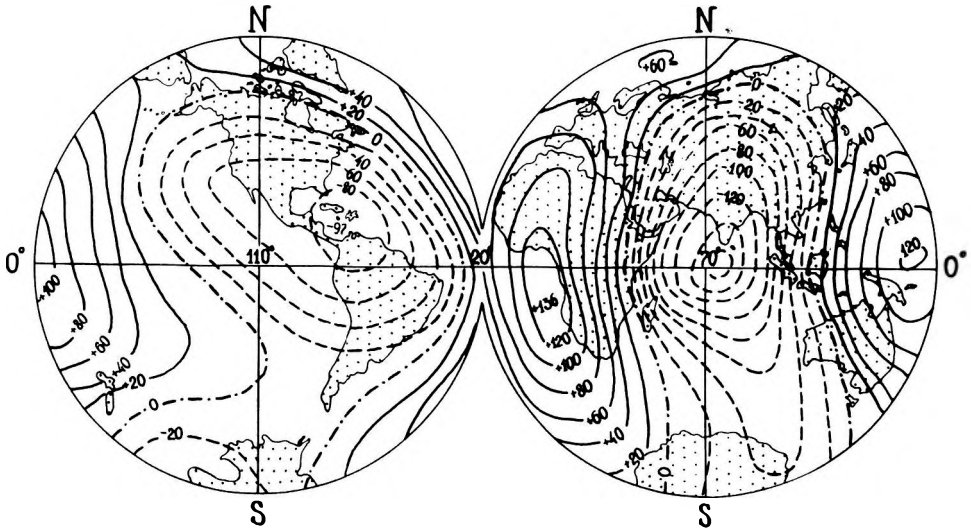


Fig. 3. Scheme of geoid undulation calculated from gravity data [ZHONGOLOVICH 1952]

3. ábra. A gravitációs adatokból számított geoid undulációk [ZHONGOLOVICH, 1952]

Рис. 3. Схема ондуляций геоида, рассчитанных по гравиметрическим данным [Жонголович, 1952]

What are the most probable physical and geological processes taking part in setting up geostasy? The loading of geoid fragments may be achieved by the following processes: the uplift of the Earth's crust blocks; glaciation; filling up the lowered parts of geoids with water; "saturation" of the upper parts of the Earth's crust by more dense basaltoids and ultrabasites (formation of dykes); formation of plateau basalts; upward displacement of the Moho discontinuity as a result of basalt-eclogit type phase transition.

The unloading of geoid fragments takes place by means of: subsidence of the Earth's crust; denudation of the Earth's crust or melting of the ice accumulated in previous epoch of glaciation; filling of the upper parts of the Earth's crust with lighter magmatic formations of acidic composition; downward displacement of the Moho discontinuity as a result of basalt-eclogit type phase transition.

Without proceeding with this enumeration, it remains to note that all the masses capable of displacement including the subsurface waters and atmosphere, take part in the restoration of the disturbed equilibrium. And though their contribution to the balancing processes is small, they are of importance in investigating nature and the laws governing those phenomena.

REFERENCES

- ARTEMYEV M. E., ARTYUSHKOV YE. V., 1967: Isostasy and tectonics. *Geotectonics*, 5, Moscow, pp. 41–57 (in Russian).
- GOLYIZDRA G. YA., 1972: On the isostatic equilibrium of the Ukrainian shield's earth crust (in Russian). *Reports of the Academy of Sciences of the USSR. Fizika zemli*, 10, pp. 14–55. Moscow.
- GRUSHINSKY N. P., 1963: The theory of the earth's shape (in Russian). Moscow, Publishing House for Physical and Mathematical Literature, p. 446.
- KLUSHIN I. G., 1963: Interaction of tectonic movements and earth's magmatism based on the variation principle of minimum action (in Russian). *Notes of Leningrad Mining Institute*, publication 2, Leningrad, v. 46, pp. 33–50.
- LEIBENSON L. S., 1955: *Collection of Works*, v. I., Moscow–Leningrad, publication of the Academy of Sciences of the USSR, pp. 169–396 (in Russian).
- LUSTICK E. N., 1957: Isostasy and isostatic hypothesis (in Russian). Moscow, publication of the Academy of Sciences of the USSR, p. 90.
- MIKHAILOV A. A., 1938: The course of gravimetry and the earth's shape (in Russian). Moscow, p. 432.
- TYAPKIN K. F., 1977: A new rotation hypothesis on the development of the tectonic system of the Earth's crust. *Geophysical Transactions*, 24, pp. 39–53.
- TYAPKIN K. F., 1981: Formation of geosynclines in the light of the new rotation hypothesis. *Geologica Balca.*, 11, 3, 3–12.
- VENING-MEINESZ V. A., 1940: Gravity observations at sea (in Russian). Moscow, p. 324.
- ZHONGOLOVICH L. D., 1952: The earth's outer gravity field and its fundamental related constants (in Russian). *Transactions of the Institute of Theoretical Astronomy of the Academy of Sciences of the USSR*, publication 3, Moscow, p. 126.

EGY ÚJ IZOSZTATIKUS FÖLD-MODELL

K. F. TYAPKIN

A javasolt új modell – a geozosztatikuss modell – azon a feltételezésen alapul, hogy az egyenlő térszöget elfoglaló Föld-szektorok egyenlő súlyúak. A Föld egyensúlyát jellemző kritériumnak a geoid és a megfelelő szferoid közötti eltérést tekinthetjük. Ezen feltevés alapján az egyensúly kvantitatív vizsgálata a gravitációs anomáliák segítségével végezhető.

НОВАЯ МОДЕЛЬ ГЕОИЗОСТАЗИИ

К. Ф. ТЯПКИН

Ставится вопрос о неправомерности использования традиционных моделей изостазии земной коры (литосферы) в связи с тем, что в них искусственно обособляется эта часть Земли от всей остальной планеты.

Предлагается новая модель геостазии, в основе которой лежит выполнение условия: равный вес секторов Земли, вырезанных одинаковыми центральными телесными углами. Критерием уравновешенности Земли в каждой точке могут служить отклонения геоида от соответствующего ему сфероида. Одним из достоинств такого подхода является возможность количественной оценки равновесного состояния отдельных участков Земли по гравитационному полю.

INTERPRETATION OF COMPLEX RESISTIVITY AND DIELECTRIC DATA PART II

W. H. PELTON¹, W. R. SILL², B. D. SMITH³

We have attempted to distinguish clearly between complex resistivity phenomena and complex dielectric behavior, based on the concept of conduction current and displacement current. As a result it is possible to use ridge regression inversion to solve simultaneously for parameters describing the contribution of each phenomenon to observed spectra. In a similar manner it is possible to carry out limited identification of other important processes such as membrane polarization, double layer capacitance, and inductive electromagnetic coupling.

Perhaps the most important single use of inversion in rock properties analysis, however, is to reduce spectral curves to a few numbers, so that changes in spectra with important physical variables such as temperature, mineral composition, concentration and grain size, may be characterized and described accurately.

An outgrowth of our examination of simple relaxation models in all three domains (frequency, time and distribution function), is the capability to transform broadband measurements made in one domain to any other domain or to another type of measurement made in the same domain: for example, amplitude to phase. This is accomplished by using ridge regression inversion to fit a sum of simple relaxation models to the observed data. The determined parameters, and the known analytical form of the models in all other domains can then be used to construct any desired representation of the observed data.

d-complex resistivity, dielectric behavior, ridge regression, membrane polarization, double layer capacitance

7. Ridge regression inversion

We have spent the first part of this paper considering various proposed models for relaxation. What we will now discuss, is an inversion method which can be used to fit automatically the various proposed relaxation models to observed data. In addition to fitting the data, the inversion program provides 1) goodness-of-fit information (which can be used to help select the most appropriate model), 2) quantitative estimates of model parameters (so that the essential features of the relaxation may be plotted against other physical variables such as temperature, composition, grain size and concentration) and 3) information on the importance of each data point regarding the resolution of the total model or of individual parameters (necessary for efficient data collection and experiment design).

¹ Phoenix Geophysics Limited, Willowdale, Ontario, Canada

² Department of Geology and Geophysics, University of Utah, Salt Lake City, Utah, USA

³ U.S. Geological Survey, Denver, Colorado, USA

The algorithm

The algorithm which we have used in order to obtain estimates of model parameters, p , from observed complex resistivity or dielectric data, y , is

$$\Delta p = (\mathbf{A}^T \mathbf{A} + \lambda \mathbf{I})^{-1} \mathbf{A}^T \Delta y \quad (88)$$

where \mathbf{A} is the matrix containing derivatives of every data point with respect to every parameter,

$$A_{ij} = \left. \frac{\partial y_i}{\partial p_j} \right|_{p_j}, \quad (89)$$

\mathbf{A}^T is the transpose of \mathbf{A} , \mathbf{I} is the identity matrix, and λ is a small positive constant which gives stability to the inversion.

When λ is exactly equal to zero, (88) is the Newton-Raphson algorithm which is very fast, but which may diverge if $\mathbf{A}^T \mathbf{A}$ is nearly singular. Thus in order to facilitate convergence in spite of a poor initial guess or poorly-determined parameters, we slightly modify $\mathbf{A}^T \mathbf{A}$ before inversion [LEVENBERG 1944, FOSTER 1961, MARQUARDT 1963]. Since $\mathbf{A}^T \mathbf{A}$ is symmetric and non-negative definite, the addition of λ to its diagonal elements ensures that none of the eigenvalues of the modified matrix will be zero, and therefore the matrix will not be singular. In the limit, as λ becomes very large, the algorithm approaches the gradient method, which always converges but which is very slow. In order to maintain stable yet fast convergence, λ must usually be changed at each new iteration during the inversion. Computer algorithms which accomplish this are known as ridge regression methods.

The general inversion program used in this research on rock properties evolved from earlier work by SMITH [1975] and was later modified to incorporate ridge regression and simultaneous inversion of multiple data sets [PELTON et al. 1974, PELTON et al. 1976]. Since formulation is in terms of discrete parameters, the inversion program is ideally suited to problems which are naturally posed in terms of discrete parameters (such as simple relaxation models); however reasonable success has also been achieved in using the program to determine continuous functionals such as resistivity versus depth [RIJO et al. 1977, PETRICK et al. 1977]. The main factor influencing effective use of the inversion technique is appropriate parameterization of the problem.

Parameterization

Perhaps the most fundamental consideration regarding parameterization is: will the parameters determined by the inversion produce the desired information from the data? For example, if we wish to find the chargeability of a rock

sample from amplitude and phase measurements of the complex resistivity, then we should formulate amplitude and phase in terms of chargeability, and not in terms of other related parameters, such as resistances in an equivalent circuit.

Another important consideration is to exclude solutions which are physically meaningless. Since negative resistivity has no meaning, it is expedient to use $\log R$ instead of R as the parameter specifying the resistivity at zero frequency. As a result, negative resistivities cannot in any way be included in an estimate of the parameter confidence interval for R .

The third important consideration concerns linearization of the problem. All of the relaxation models which we have discussed, except for the simple resistance, have observables such as amplitude and phase which are non-linear functions of the model parameters. However, our ridge regression algorithm utilizes only the first derivative of the data with respect to the parameters. Thus it makes the implicit assumption that the relation between each observable and every model parameter is approximately linear. How good this assumption is will affect the speed of the convergence and the accuracy of estimates for the uncertainty in the determination of each parameter. We will attempt to illustrate later with an example, how different parameterization can result in extremely poor and extremely good linear approximations for the true behavior of the observable.

Data error and weighting

For the inversion algorithm given by (88) we have tacitly assumed that no weighting of the data was required since all the data were equally influenced by noise. For the simultaneous inversion of multiple data sets or inversion of data containing a few bad points, this assumption is no longer valid and we must first multiply the unweighted derivative matrix, \mathbf{B} , and unweighted data difference vector, Δg , by a weight matrix, \mathbf{W} , in order to obtain satisfactory results;

$$\mathbf{A} = \mathbf{W}\mathbf{B} \quad (90)$$

and

$$\Delta y = \mathbf{W}\Delta g \quad (91)$$

If the error in each measurement is independent of the error in the other measurements, as is usually assumed, then \mathbf{W} reduces to a diagonal matrix with entries which are inversely proportional to the standard deviation of each data point:

$$W_{ii} = \frac{1}{\sigma_i} \quad (92)$$

We could possibly estimate σ_i by making a large number of repeat measurements at each point, however this would be rather time-consuming. It is much

simpler to assign relative weights to the data and then later obtain an estimate for the data error from the reduced chi-square statistic,

$$\chi_v^2 = \frac{\Delta y^T \Delta y}{n - m}, \quad (93)$$

where n is the number of data points and m is the number of parameters. As discussed by BEVINGTON [1969], χ_v^2 will be the best estimate for the data variance at those data points associated with weights of 1.0 if the relative weights were indeed correct, the theoretical model was appropriate, and the errors were normally distributed.

Obviously the easiest relative weights to assign are weights which all have the same value for each data set. It is thus expedient to choose as observables those quantities which have roughly constant measurement error at all frequencies. This is one main consideration behind our choice of log amplitude as a common observable. For measurement of both complex resistivity and complex permittivity, the error in amplitude is very often a relatively constant percentage of the amplitude value. Thus if we chose amplitude and not log amplitude as the observable we would be required to specify weights which are inversely proportional to the magnitude of each measurement. Choice of log amplitude as the observable is possible, because amplitude can never be negative, and is desirable in that it eliminates this weight requirement.

Although easy specification of weights is certainly one consideration in the total problem formulation involving choice of both parameters and observables, we must also remain aware that the selection of observables will affect the linearization of the problem just as much as the selection of parameters. In our later example of linearization we change both parameters and observables in order to illustrate good and bad linear approximations.

Our emphasis so far in problem formulation has been on the choice of parameters (either relaxation parameters or equivalent circuit parameters) and on the proper choice of observables: either real and imaginary, amplitude and phase or amplitude and loss tangent, or perhaps logarithmic instead of linear, or possibly reciprocal as opposed to normal (conductivity instead of resistivity). All these different formulations are possible after we have decided on a specific relaxation model. The question remains: how do we choose this model in the first place? The most straightforward approach would be to base our model on the physical processes taking place; however, we may be attempting to determine the dominant process influencing our data out of several possible mechanisms. In such cases it is sometimes useful to employ the reduced chi-square as a goodness-of-fit criterion. We note that since the reduced chi-square is obtained by dividing the square error $\Delta y^T \Delta y$ by $n - m$, the smallest reduced chi-square will be obtained by the model which provides the best fit with the fewest parameters. This is commensurate with the philosophy that if we do not know exactly the physical process, the best model is the simplest model which still fits the data.

Information density

If we wish to find out which data points are contributing the most information toward the determination of our model, one method would be to examine the \mathbf{A} matrix. Large positive or negative values will indicate which data points are important in determining each of the various parameters. For an estimate of which data points are important in the resolution of the total model, however, it is often convenient to examine the information density matrix given by

$$\mathbf{S} = \mathbf{A}\mathbf{H} \quad (94)$$

where

$$\mathbf{H} = (\mathbf{A}^T\mathbf{A})^{-1}\mathbf{A}^T \quad (95)$$

is the generalized inverse. We find that \mathbf{S} is a symmetric, diagonally dominant matrix with dimensions $n \cdot n$. Thus an approximate idea of which data points are the most important may be obtained from examination of the diagonal elements of \mathbf{S} . This also provides a useful check on our original choice of weights for the problem. For example, if we expect that two different data sets should be providing roughly equal information, but find that the diagonal elements of \mathbf{S} are an order of magnitude smaller for one data set than for the other, our choice of weights may be seriously in error.

Parameter statistics

Once we have reached convergence and obtained a set of parameters which provide the best least-squares fit to our data, the next most important requirement is to obtain some idea of the uncertainty in the parameters. If our problem is very poorly posed we may find that $\mathbf{A}^T\mathbf{A}$ still remains singular even at convergence. In such cases it is necessary to maintain a non-zero value of λ merely to eliminate the zero eigenvalues and thus permit inversion of the matrix. A very approximate idea of which parameters have high uncertainty may then be obtained by examining the diagonal elements of the resolution matrix,

$$\mathbf{R} = \mathbf{H}\mathbf{A} \quad (96)$$

where \mathbf{H} is now given by

$$\mathbf{H} = (\mathbf{A}^T\mathbf{A} + \lambda\mathbf{I})^{-1}\mathbf{A}^T \quad (97)$$

Those diagonal elements of \mathbf{R} which are significantly less than 1.0 indicate parameters which are very poorly resolved [ANGORAN 1975].

Usually, however, it is more desirable to deal with models which are not overly complex and to acquire sufficient data to determine adequately the model parameters. In such cases $\mathbf{A}^T\mathbf{A}$ will not be singular at convergence and the resulting resolution matrix, with λ set equal to zero, will be very nearly equal

to the identity matrix (within numerical roundoff). For these well-posed, over-determined problems a more accurate estimate of the uncertainty in each parameter may be obtained by examining the parameter covariance matrix, given by

$$\text{cov}(p) = x_v^2 (\mathbf{A}^T \mathbf{A})^{-1} \quad (98)$$

The best estimate of variance for each parameter may be simply obtained from the diagonal elements of $\text{cov}(p)$. We may also obtain, by appropriate normalization of $\text{cov}(p)$, the parameter correlation coefficients,

$$\text{cor } p_{ij} = \frac{\text{cov } p_{ij}}{(\text{cov } p_{ii} \cdot \text{cov } p_{jj})^{1/2}} \quad (99)$$

Correlation coefficients near 1.0 indicate that only the difference of two parameters is well-resolved, whereas correlation coefficients near -1.0 indicate that only their sum is well-resolved. If the inversion is carried out with respect to log parameters (as we have done in the remainder of this paper), correlation coefficients of $+1.0$ and -1.0 indicate that only the quotient or product of two parameters is well-determined.

8. Applications

There are a large number of areas where inversion can be very usefully applied in the analysis of complex resistivity and dielectric data. It will not be possible to cover all of these areas in this paper, or even to discuss in rigorous detail all the relevant statistical information for the few examples that we have chosen. Our approach, instead, will be to focus on small segments of the interpretation of a fairly broad range of data. In this way we may perhaps indicate the variety of rock property problems that can be attacked with inversion and the usefulness of the technique.

Model selection

Our first application of inversion to analyzing the electrical properties of rocks will concern selection of the simplest relaxation model fitting given complex resistivity or dielectric data.

Bingham Granite Stock. Shown in *Figure 12a* normalized amplitude data from laboratory measurements of the complex resistivity of a mineralized sample of the Bingham stock. The data were kindly provided by NELSON [1975]. We have attempted to fit five models of the Cole—Cole family to the data. The model which provides the lowest value of the reduced chi-square, shown in *Figure 12b*,

is No. 5, which corresponds to the Madden—Cantwell relaxation model (Table 1 in Part one). It is evident that increasing the complexity of the model to the Cole—Cole relaxation (No. 8) and to the generalized Cole—Cole relaxation (No. 10), does not appreciably improve the data fit. The only result is to increase the number of model parameters, thus decreasing the degrees of freedom, $n-m$, and consequently increasing the reduced chi-square. From this simple analysis we might conclude that out of the five models considered, the Madden—Cantwell model is the most appropriate model for the data.

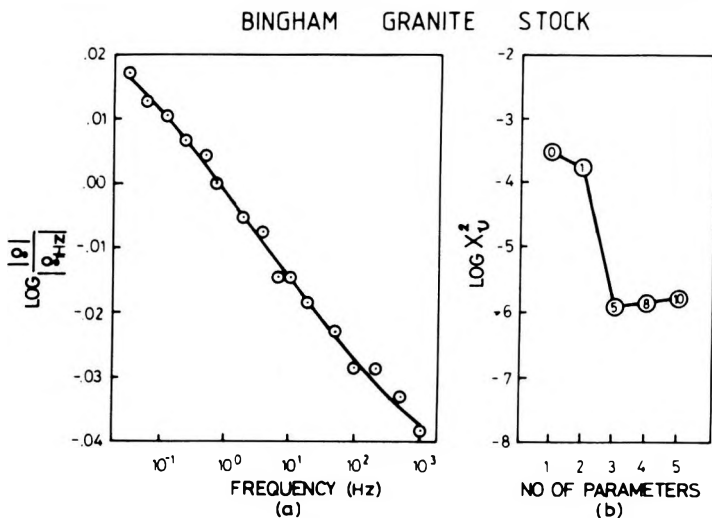


Fig. 12. (a) Inversion of $|g(\omega)|$ obtained from laboratory measurements of a sample of the Bingham granite stock. The circles represent the observed data; the solid line represents the best-fitting relaxation model (No. 5)

(b) Goodness-of-fit values for the five relaxation models which were used to fit the data in (a)

12. ábra. (a) A Bingham gránittömszöböl vett mintán végzett laboratóriumi mérések $|g(\omega)|$ -jának inverziója. A körök jelentik a mért adatokat, a folytonos vonal jelenti a legjobban illeszkedő relaxációs modellt (5. számú)

(b) Öt, az (a) ábra adataihoz illesztett relaxációs modell illesztés-jóságai értéke

Рис. 12. а) Инверсия $|g(\omega)|$, полученного по лабораторным измерениям образца гранитового массива Бингэм. Кружками обозначены измеренные данные, сплошная линия изображает релаксационную модель, обеспечивающую наилучшую аппроксимацию (№ 5).

б) Значение доброты аппроксимации пяти релаксационных моделей, использованных для аппроксимации к данным рис. а.

A further comparison of the data and the best-fitting Madden—Cantwell model, shown as the solid curve in Figure 12a, tends to confirm our conclusion. There is no obvious bias; any difference between the model and the data appears to be random measurement error. This brings us to the subject of a recent controversy [NELSON and VAN VOORHIS 1977; ZONGE and WYNN 1977]. We do not plan to take sides in this controversy; however, we do wish to illustrate how

inversion might be used to evaluate the accuracy of rock electrical measurements. The value for the reduced chi-square obtained for model No. 5 in Figure 12b was $1.42 \cdot 10^{-6}$. Since the theoretical model adequately fits the data without apparent bias, we might assume that this value provides a reasonable estimate for the true variance of the data. Our resulting conclusion is that the amplitude measurements, shown plotted on a double logarithmic scale in Figure 12a (vertical exaggeration 10 : 1), were made with an average accuracy of 0.27% over the four and one-half decades of frequency. In contrast, the total frequency effect over this range was 14%.

Lunar Rock 73,275-8 105 °C We continue with the subject of model selection by examining the phase angle data from measurement of the dielectric constant of a lunar rock shown in Figure 13a. We again attempted to fit several members of the Cole—Cole family of models to the data. In this case, the outcome, shown in Figure 13b, was rather different. The model which provided the lowest value of the reduced chi-square was the most complex of the series. The results suggest that the phase data is significantly non-symmetric and consequently is not well-fitted by the simple Cole—Cole model or by special cases of this model.

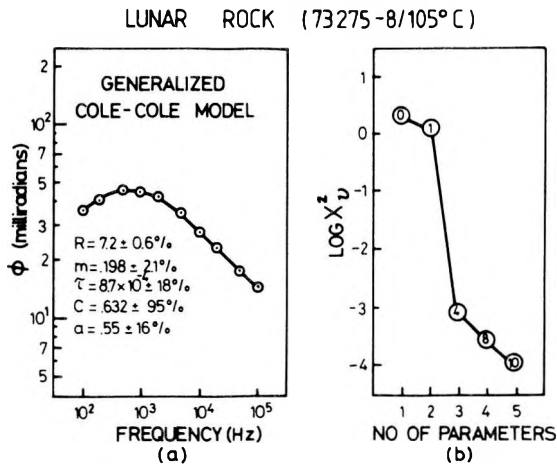


Fig. 13. (a) Inversion of phase data obtained from measurement of the dielectric constant of lunar rock 73 275-8 at 105 °C. The circles represent the observed data; the solid line represents the best-fitting relaxation model (no. 10)

(b) Goodness-of-fit values for the five relaxation models which were used to fit the data in (a)

13. ábra. (a) A 73 275-8 holdközeten, 105 °C-on végzett dielektromos állandó mérések fázis adatainak inverziója. A körök jelentik a mért értékeket, a folytonos vonal jelenti a legjobban illeszkedő relaxációs modellt (10. számú)

(b) Öt, az (a) ábra adataihoz illesztett relaxációs modell illesztés-jóssági értéke

Рис. 13. а) Инверсия фазовых данных по измерениям диэлектрической постоянной, проведенным при 105 °C ха лунной породе 73275-8. Кружки означают измеренные значения, а сплошная линия — релаксационную модель, обеспечивающую наилучшую аппроксимацию (№ 10).

б) Значение доброты аппроксимации пяти релаксационных моделей, использованных для аппроксимации к данным рис. а.

Iron Mountain 5 Our next example illustrating choice of an appropriate relaxation model concerns in-situ complex resistivity data from an open pit magnetite mine near Iron Springs, Utah. Both amplitude and phase data were obtained and were inverted simultaneously to produce the resulting best-fitting Cole—Cole model shown in *Figure 14*. Also shown in the figure are the estimated parameter standard deviations. Since our problem formulation involved log parameters as well as log data, the estimated parameter standard deviations are precisely displayed as percentages.

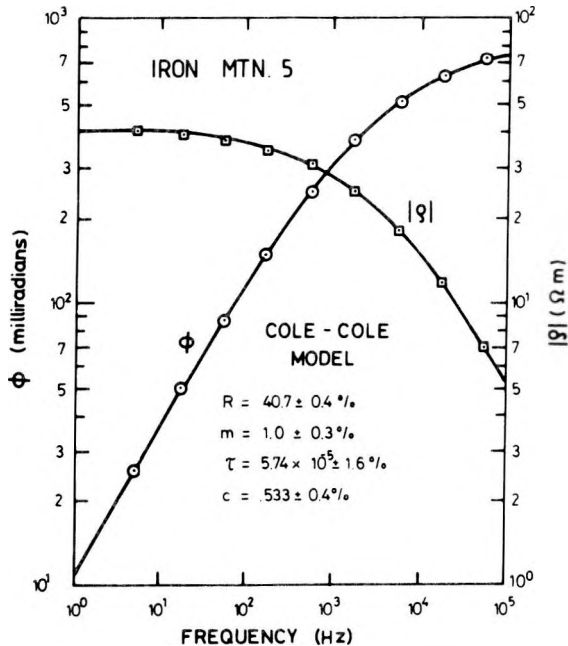


Fig. 14. Inversion of in-situ complex resistivity data obtained over massive powdery magnetite mineralization near Iron Springs, Utah. The observed data are represented by circles and squares; the solid lines indicate the best-fitting Cole—Cole complex resistivity model

14. ábra. Iron Springs (Utah) közelében lévő masszív, porszerű magnetit ércesedésen kapott in situ komplex ellenállás adatok inverziója. A mért adatokat körök és négyzetek jelzik, a folytonos vonalak a legjobban illeszkedő Cole—Cole komplex ellenállás modellt jelentik

Рис. 14. Инверсия данных комплексного сопротивления, полученных в условиях естественного залегания на массивном, порошкообразном оруденении вблизи Айрон Спрингс, Ютэх. Измеренные данные показаны кружками и четырехугольниками, а сплошные линии означают комплексную модель типа Кол-Кол сопротивления, обеспечивающую наилучшую аппроксимацию.

We mentioned previously that appropriate problem formulation requires consideration of several factors, not the least of which is the requirement that the resulting problem be adequately linear. We will now attempt to illustrate with the Iron Mountain 5 model and data, how two different problem formulations can lead to two vastly different linear approximations.

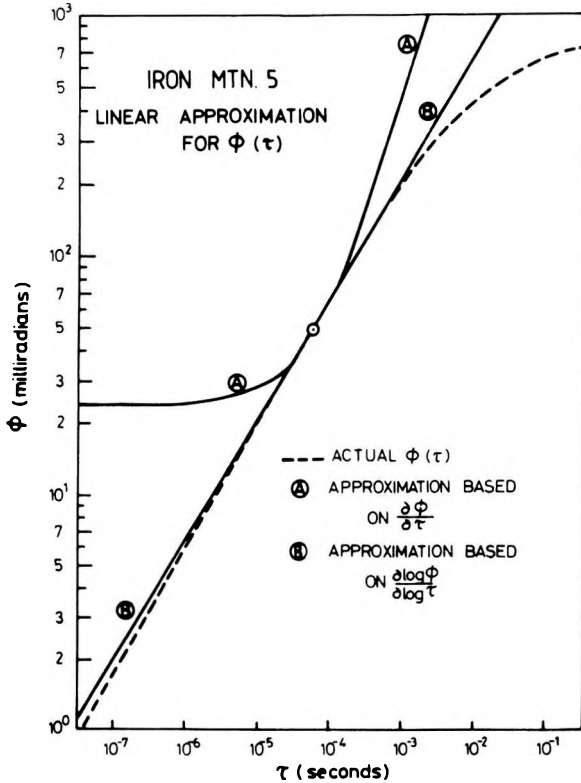


Fig. 15. Two different approximations for phase as a function of time constant

15. ábra. A fázis — időállandó függvény két különböző közelítése

Рис. 15. Две разные аппроксимации функции фаза-постоянная времени

Shown in Figure 15 are three curves passing through the phase angle measurement made at 17.8 Hz. The curve labelled "A" corresponds to a problem formulation involving linear phase (not logarithmic) and linear parameters. Thus each of the columns of the derivative matrix will be composed of simple first order derivatives of phase with respect to each of the model parameters: R , m , τ , and c . If we select τ as our parameter of interest, the single element of the derivative matrix, corresponding to the τ parameter and the 17.8 Hz frequency measurement, attempts to predict the behavior of phase as a function of τ by the formula,

$$\Phi(\tau) = \Phi_0 + \frac{\partial \Phi}{\partial \tau}(\tau - \tau_0), \quad (100)$$

where Φ_0 is 48.2 milliradians, τ_0 is $5.74 \cdot 10^{-5}$ seconds, and the derivative is 425.9 milliradians per second. As shown in Figure 15 this formula is a very poor approximation to the actual curve for $\Phi(\tau)$ except in the region immediately surrounding $\tau = \tau_0$.

A much better approximation of the true $\Phi(\tau)$ behavior can be made if we

formulate the problem in terms of $\log \Phi$ and $\log \tau$. Since the appropriate element of the derivative matrix is 0.51, the approximation for $\Phi(\tau)$ on a double logarithmic scale becomes simply a straight line through (Φ_0, τ_0) with slope 0.51. This approximation (the "B" curve in Figure 15) is very good over a five decade range of τ , and thus suggests that this formulation will result in rapid convergence from a poor initial guess, and accurate prediction of the parameter confidence interval.

Tyrone 1 Our last example of simple model selection and fitting involves in-situ complex resistivity data from the Tyrone porphyry copper deposit near Silver City, New Mexico. Two main dispersions are very evident in the phase angle data shown in Figure 16. In order to fit the data we chose a transfer function formed by the multiplication of two Cole—Cole models.

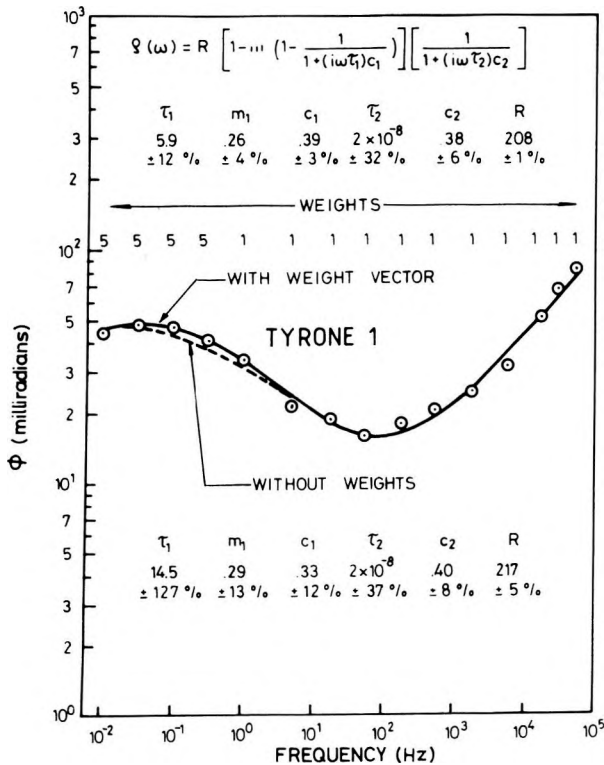


Fig. 16. Inversion of in situ complex resistivity data obtained over the Tyrone porphyry copper deposit

16. ábra. A Tyrone porfirós rézérc előfordulásán kapott in situ komplex ellenállás adatok inverziója

Рис. 16. Инверсия комплексных данных сопротивления, полученных в условиях естественного залегания на месторождении порфириродной медной руды Тайрон.

During the inversion process we encountered difficulty at the lower frequencies. Although the phase angle measurements in this region describe a smooth curve, and thus appear relatively accurate, there is only a slight suggestion of what the low frequency phase behavior might be. This slight character in the curve is actually below the noise level of the phase angle measurements made at higher frequencies. As a result, when an attempt was made to fit the $\log \Phi$ data without using weights, the inversion routine treated the slight bend in the curve at low frequencies as noise, and produced a poor data fit with resulting high parameter standard deviations.

In order to produce a more acceptable fit to the data, we effectively introduced our own bias into the inversion through our selection of relative weights. Use of larger weights at the lower frequencies forced a more precise fit to the data in this region and substantially reduced the estimated uncertainty in the parameters describing the low frequency phase angle peak. The actual credibility of these new small parameter standard deviations is, however, directly dependent on our assumption that the low frequency measurements have a substantially lower noise level than those at higher frequencies. The estimated uncertainty in the parameters, τ_2 and c_2 , describing the high frequency dispersion were left relatively unchanged by the new weights.

Identification of physical processes

Often the ultimate goal of our attempts to fit relaxation models to complex resistivity and dielectric data is really to try to determine, and then characterize, the poorly-understood physical processes taking place.

Pyrite electrode—electrolyte interface In our first example we will try to examine the basic mechanism responsible for the complex resistivity behavior of mineralized rocks. Shown in *Figure 17* is an equivalent circuit which is quite often used to model the resistive, capacitive, and diffusive behavior of the semiconductor—electrolyte interface [WARD and FRASER 1967]. Also shown in *Figure 17* are values of the circuit components obtained from inversion of amplitude and phase measurements made on pyrite electrodes over seven decades of frequency [KLEIN and PELTON 1976]. In *Figure 18* we show the observed amplitude and phase data, and the theoretical curves obtained from inversion. The agreement is excellent. This suggests that the simple circuit in *Figure 17* adequately describes the impedance of the pyrite-electrolyte interface, and that we thus may evaluate the relative importance of the different conduction processes by more closely examining the values of the circuit components. One conclusion is that, for pyrite electrode data shown in *Figure 18*, the reaction resistance is an extremely minor component of the total electrode impedance. It is essentially undetectable relative to the other components of the equivalent circuit. Another conclusion is that the double layer capacitance is also quite small (a few microfarads per square centimeter) and therefore does not provide appreciable conduction across the interface at frequencies much below 1 kHz.

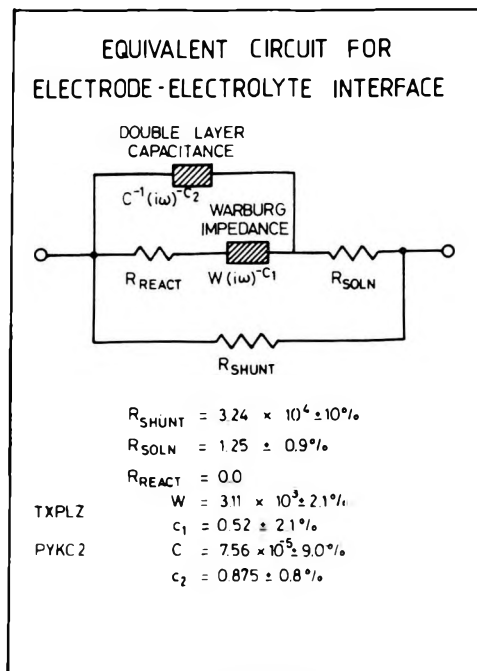


Fig. 17. Equivalent circuit for an electrode—electrolyte interface plus parameters obtained from the inversion of the spectra shown in Figure 18.

17. ábra. Egy elektróda — elektrolit határfelület ekvivalens áramköre és a 18. ábrán mutatott spektrumok inverziójából kapott paraméterek

Рис. 17. Эквивалентная электрическая схема раздела электрод-электролит и параметры, полученные по инверсии показанных на рис. 18 спектров

By allowing the exponents of the Warburg element and the double layer capacitance to vary we were able to model effectively non-ideal components; however, we found that the exponent c_1 was very close to that of the ideal Warburg ($c = 0.5$) and that the exponent c_2 was quite close to that of ideal capacitive behavior ($c = 1.0$).

The higher frequency dependence of the capacitive behavior of the interface is strikingly displayed in Figure 18 by the steep high frequency asymptotic slope of the phase curve.

Scott—West Artificial Rocks We devoted considerable discussion in the first part of this paper toward attempting to define and separate complex resistivity and complex dielectric phenomena. We will now illustrate with an example how inversion might be used to achieve this separation. The data shown in Figure

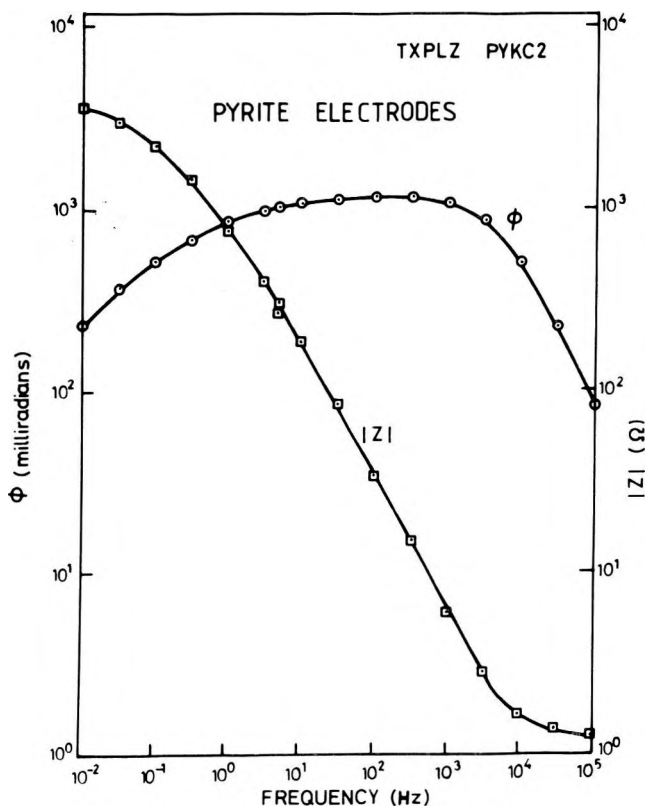


Fig. 18. Amplitude and phase spectra obtained from measurement of the impedance of two pyrite electrodes

18. ábra. Két pirit elektróda impedanciájának méréséből kapott amplitúdó és fázis spektrum

Рис. 18. Спектр амплитуд и фаз, полученный по измерению импеданса двух пиритовых электродов.

19 and Figure 20 were obtained from complex resistivity measurements of artificial rock samples prepared by SCOTT and WEST [1965] from cement, quartz and pyrite. Due to the high pressures applied during preparation, the samples have very low porosity and consequently, very high resistivity. Thus for at least the highest frequencies, we might expect a substantial decrease in the measured complex resistivity, due to dielectric conduction phenomena.

Sample 124B contains no pyrite mineralization and exhibits relatively simple spectra. By casual comparison of the theoretical phase angle curves in Figure 5 with the results shown in Figure 19, it appears that a single Cole—Cole resistivity dispersion might adequately fit the data. This was attempted; however it was found that the theoretical high frequency phase angle curve was very definitely lower than the observed data. Another possible model, which gave a

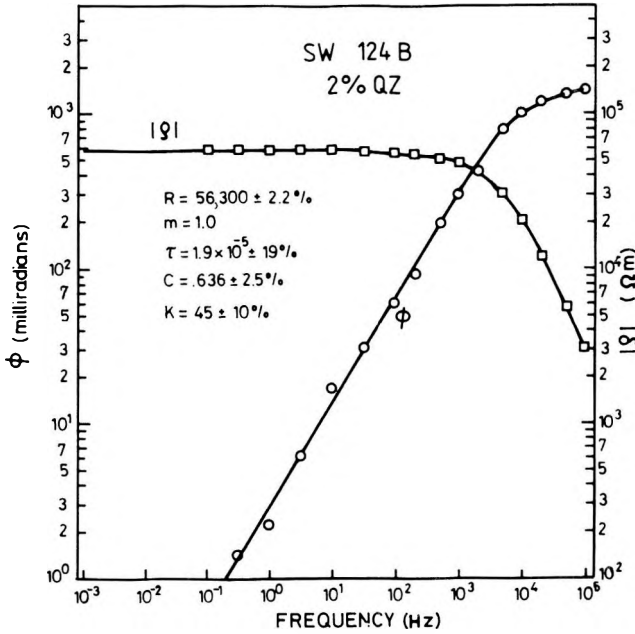


Fig. 19. Inversion of complex resistivity spectra obtained from measurement of Scott-West sample 124B (no pyrite)

19. ábra. A 124B Scott—West mintán (pirit nélküli) végzett mérésekből kapott komplex ellenállás spektrumok inverziója

Рис. 19. Инверсия комплексных спектров сопротивления, полученных по измерениям на двух образцах 124В Скотт—Уэст (без пирита)

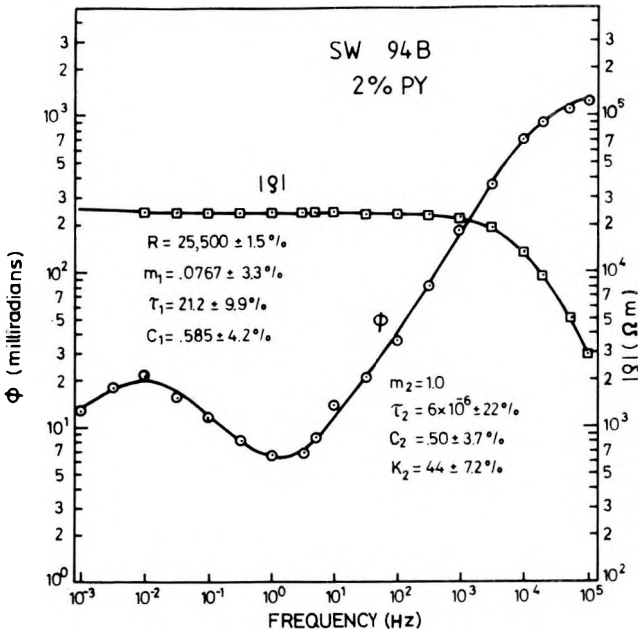


Fig. 20. Inversion of complex resistivity spectra obtained from measurement of Scott-West sample 94B (containing 2% pyrite)

20. ábra. A 94B Scott—West mintán (2% pirit tartalom) végzett mérésekből kapott komplex ellenállás spektrumok inverziója

Рис. 20. Инверсия комплексных спектров сопротивления, полученных по измерениям на образце 94В Скотт—Уэст (с содержанием пирита 2%).

better fit to the data, included a constant resistivity with a single Cole—Cole dielectric dispersion. However, this model requires an unreasonably high value of the dielectric constant at the lower frequencies (in the range of several thousand). The third model which we tried gave the best fit to the data and is shown in Figure 19. We have assumed a single Cole—Cole resistivity dispersion and an entirely real dielectric constant (which was subsequently determined to be 45).

Our conclusion from this exercise is that the major physical process taking place is a complex resistivity relaxation, although dielectric conduction does become important at the highest frequencies. Since there was no metallic mineralization in the sample, we cannot attribute the Cole—Cole resistivity dispersion to metallic electrode polarization.

Shown in Figure 20 are the results from measurements of the complex resistivity of sample 94B which contained 2% pyrite. In addition to the presumed dielectric and membrane polarization behavior at high frequency, we also have a prominent low frequency dispersion apparently caused by the pyrite. The time constant of this relaxation is much longer than the time constants obtained for pyrite mineralization in other artificial rocks [GRISSEMAN 1971, SILL and DEWITT 1976]. This is most likely due to the abnormally high D.C. resistivity of the Scott-West samples (notice the equations for the time constant in Figure 2; τ is strongly dependent on the D.C. resistivity for each of the three equivalent circuits).

As a final note on these artificial rocks we have plotted in Figure 21 the diagonal terms of the information density matrix corresponding to the data from sample 94B. Our formulation of the problem was in terms of log phase,

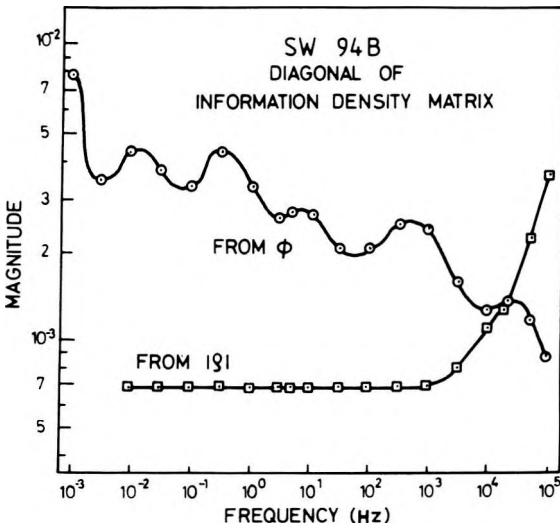


Fig. 21. Diagonal of information density matrix obtained from inversion of Scott—West sample 94B

21. ábra. A 94B Scott—West minta inverziójából kapott információ sűrűségi mátrix átlója

Рис. 21. Диагональ матрицы плотности по информации, полученной из инверсии образца 94Б Скотт—Уэст.

log amplitude and log parameters. However, since we did not specify different relative weights between the phase and amplitude data sets, by default we made

the assumption that the percentage error in the phase measurements was roughly equal to the percentage error in the amplitude measurements. Since this assumption is really quite debatable, it was useful to check the information density matrix and confirm that the values for the two data sets were at least not different by several orders of magnitude. We note that the information density is quite low for those amplitude data which are flat and featureless, but that the values strongly increase at the higher frequencies where the amplitude exhibits strong curvature and the phase becomes flat and featureless. The two data sets thus tend to complement each other in providing useful information over the total frequency range.

Roosevelt KGRA We have noted what appears to be very pronounced effects due to membrane polarization in the Scott-West rocks. Lest the reader obtain the impression that these effects occur only under unusual circumstances in artificial rocks, we present in *Figures 22 and 23* results obtained from complex resistivity measurements of drill cores from the Roosevelt Hot Springs geothermal area [TRIPP 1976].

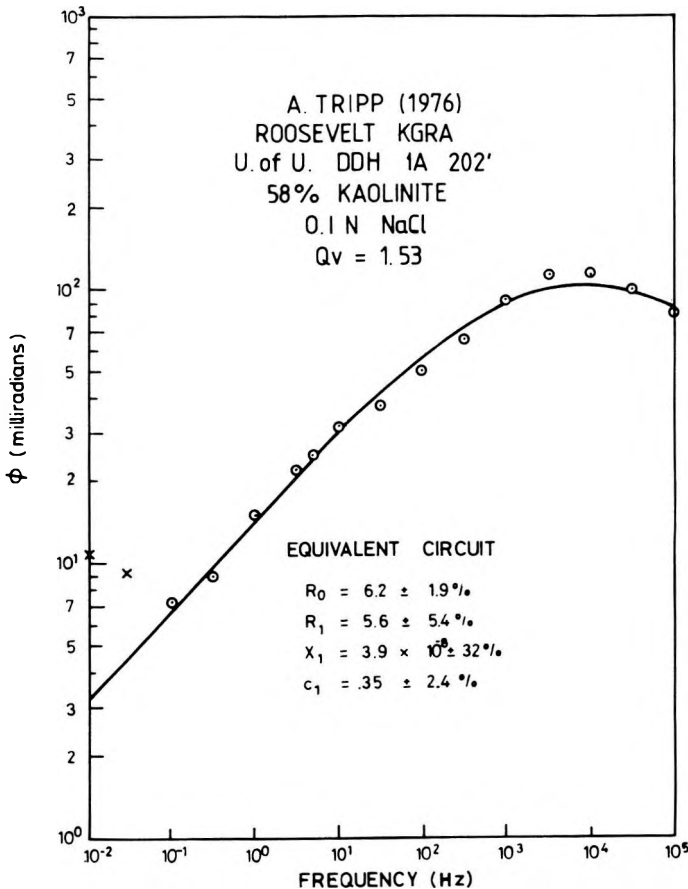


Fig. 22. Inversion of complex resistivity data obtained from measurement of a clay-altered drill core sample from Roosevelt Hot Springs KGRA

22. ábra. A Roosevelt Hot Springs KGRA-ból kapott agyagos bontású magmintán végzett mérések komplex ellenállás adatainak inverziója

Рис. 22. Инверсия данных комплексного сопротивления, полученных по измерениям на глинистой разновидности кернового образца от Рузвельт Хот Спрингс КГРГА

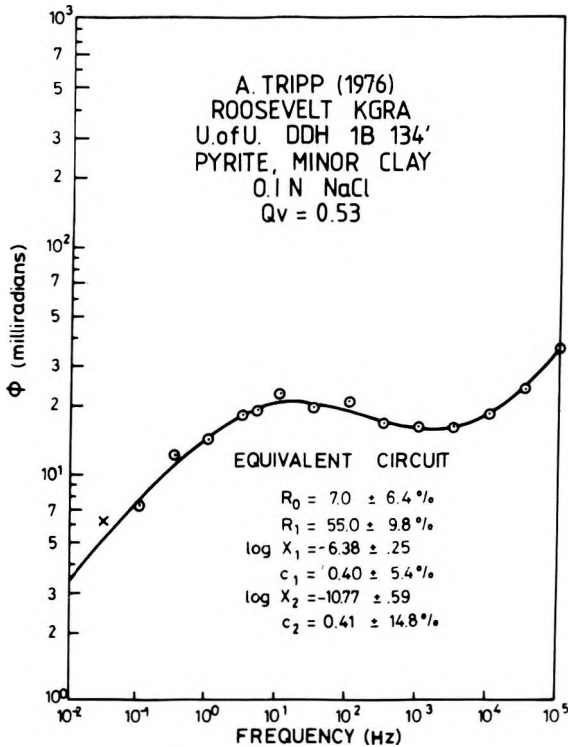


Fig. 23. Inversion of complex resistivity data obtained from measurement of a drill core sample having very minor clay alteration but noticeable iron staining, suggesting pyrite mineralization

23. ábra. Olyan magmintán végzett komplex ellenállás mérések inverziója, amelyben csak nagyon kicsi volt az agyagos bontás, de szemmel látható volt a vasas elszíneződés, ami pirites ércesedésre utal

Рис. 23. Инверсия измерений комплексного сопротивления на керновом образце с весьма низким глинистым разложением, но с очевидным железным загрязнением, что указывает на пиритовое оруденение.

The phase angle results shown in Figure 22 correlate with a very highly altered section of the drill log where the rock was 58% kaolinite. The cation exchange capacity per unit pore volume (Q_v) is large and the sample exhibits a prominent complex resistivity dispersion at the higher frequencies, in spite of the fact that no metallic-conducting minerals were observed present. In order to fit the data we have assumed that conduction through the clays acts in parallel with the normal ionic conduction through pore passages in the rock. The result is an equivalent circuit representation which is the same as that shown earlier in Figure 2a. Although the circuit is known to produce Cole—Cole relaxational behavior we have inverted for the components of the equivalent circuit rather than the Cole—Cole model parameters.

These circuit components may be more readily compared with those fitting the data for the second drill core sample shown in Figure 23, where we have considered a more complex equivalent circuit than that giving rise to a single Cole—Cole relaxation. This second sample exhibited little clay alteration but showed prominent iron staining, suggesting the presence of pyrite. In order to fit the two indicated dispersions in the phase angle spectra we have utilized the equivalent circuit shown in Figure 24, which has two frequency-dependent paths. In total, there are three parallel current paths, by which we have attempted to simulate three conduction mechanisms: conduction through the normal unblocked rock pores, through clay blocked pores and through pyrite blocked pores. Since the phase angle data shows no indication of rolling over at high frequency, we are unable to determine any value for R_2 ; the other parameters, however, are all reasonably well determined. The relatively low values of the two frequency dependences (c_1 and c_2 in Figure 23) suggests diffusion phenomena rather than capacitive or inductive behavior.

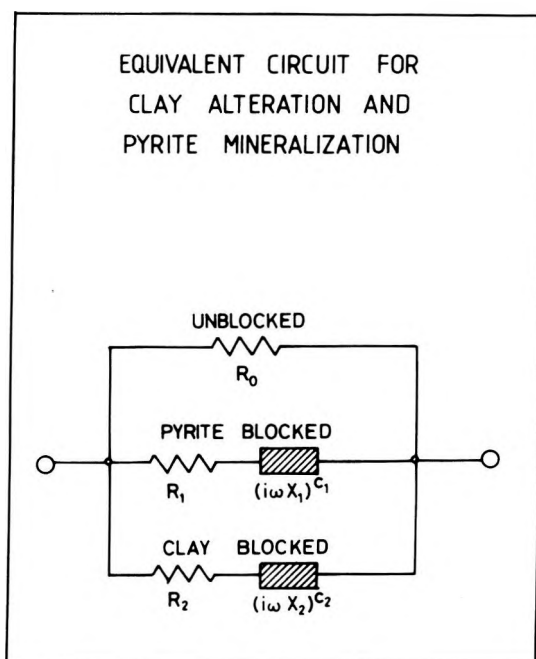


Fig. 24. Equivalent circuit for rocks containing both pyrite mineralization and clay alteration

24. ábra. Pirites ércesedést és agyagos elváltozást is mutató közetek ekvivalens áramköre

Рис. 24. Эквивалентная электрическая схема пород, показывающих как пиритовое оруденение, так и глинистое изменение.

Inductive coupling recognition The last topic under this general discussion of recognition of physical processes, we will only briefly mention since it has been discussed elsewhere [PELTON et al. 1978]. But basically, inductive coupling response is perhaps the easiest process to identify in complex resistivity observations. We have noted that metallic electrode polarization and membrane polarization both result from diffusion phenomena, thus the only hope of distinguishing between the two rests on perhaps identifying statistically significant differences in the time constant and chargeability (field experience and our limited laboratory measurements suggest that membrane polarization has a relatively short time constant). There are similar difficulties in distinguishing between dielectric effects and ionic conduction processes in resistive laboratory samples. Dielectric conduction in the Scott-West rocks was manifested by only a slight increase in phase at the very highest frequencies.

The effects produced by inductive electromagnetic coupling on complex resistivity data are by comparison relatively easy to detect. All solutions for inductive coupling so far [MILLET 1967, HOHMANN 1973], indicate that the frequency dependence for coupling response is very close to 1.0. This is consistent with the observation that many EM problems can be cast in terms of an induction number which involves frequency to the first power. In contrast, the frequency dependence of the complex resistivity response arising from natural earth materials is very low, typically about 0.25. Thus inductive coupling effects should be readily recognizable by a prominent increase (or decrease, depending on whether the coupling is positive or negative) in the slope of the phase angle response on a double logarithmic plot.

Quantitative evaluation of spectra

Our analysis thus far has been mainly concerned with identification of models and physical processes. However, perhaps the most immediate, useful application of our inversion routine will be in the quantitative evaluation of spectra.

Lunar Rock 73275-8 27 °C In Figure 25 we show complex dielectric data obtained from measurement of the same lunar rock for which data was presented earlier in Figure 13. This latter data set was acquired with the rock temperature held constant at 27 °C instead of 105° C. Again we have fitted a generalized Cole—Cole model to the data so that the new parameter values may be usefully compared with the previous parameter values obtained at 105 °C. If we had several sets of data at intermediate temperatures it would be possible to identify and trace relatively subtle variations in the relaxation parameters with temperature. This may be useful in regard to two objectives: first, to provide desired engineering information on the dielectric constant as a continuous function of temperature, and second, to use the known variation with temperature to identify more accurately the physical processes responsible for the dielectric behavior.

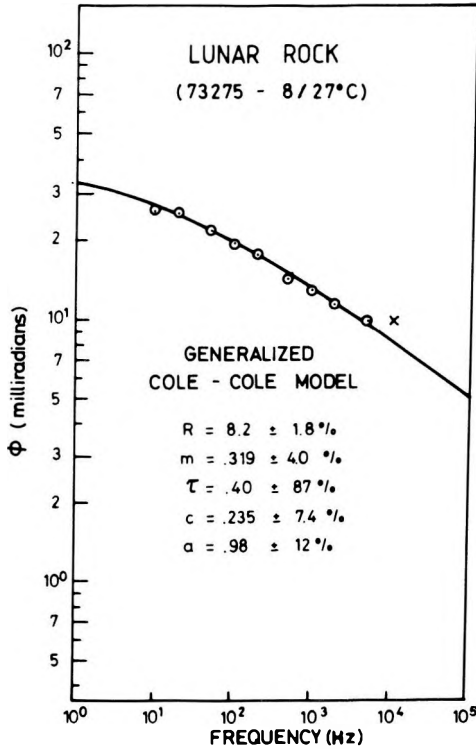


Fig. 25. Inversion of phase angle data from measurements of the complex dielectric constant of lunar rock 73 275-8 at 27 °C

25. ábra. A 73 275-8 holdközeten, 27 °C-on végzett dielektromos állandó mérések fázisszög adatainak inverziója

Рис. 25. Инверсия данных о фазовом угле по измерениям диэлектрической при 27 °C на лунной породе 73275-8.

Grisseman data Another area where engineering information is badly needed is the complex resistivity measurement of mineralized rocks. Although accurate IP measurements have been made for more than twenty years, we still have very little precise, reliable data on the variation in IP response due to mineral concentration and grain size.

Shown in *Figure 26* is an example of some of the data which has been collected. The plot shown is of real conductivity normalized by the real conductivity at 10⁴ Hz. The data were acquired by GRISSEMAN [1971] during a study of artificial rocks composed of cement, quartz and pyrite in varying concentrations and grain sizes. In order to interpret the results, we assumed a Cole—Cole model for the complex resistivity, then took the logarithm of $\text{Re}[1/\rho(\omega)]$ as our observable. The fit to the data, shown in *Figure 26*, is remarkably good. The

average data error is only 0.36%, yet the conductivity varies by 300% over the four decades of frequency. Since the data error is very low, the parameters for the Cole—Cole resistivity relaxation are very precisely determined, as indicated by the small standard deviations shown in the figure.

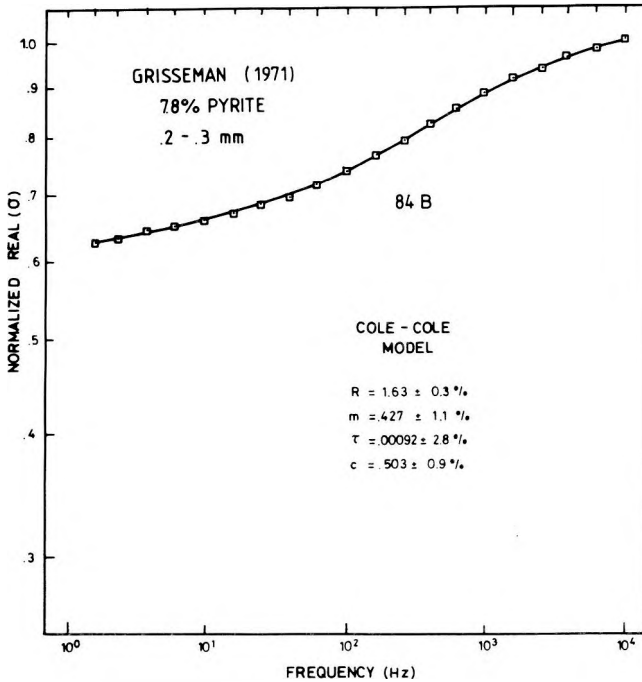


Fig. 26. Inversion of real conductivity data obtained by GRISSEMAN [1971] from measurement of artificial rock sample 84B

26. ábra. A 84B mesterséges kőzetmintán GRISSEMAN [1971] által végzett mérések valós vezetőképesség adatainak inverziója

Рис. 26. Инверсия данных об истинном проводимости по измерениям Грисмана (1971 г.) на образце искусственной породы 84Б

We were able to fit simple Cole—Cole models to all of the artificial rock real conductivity data obtained by Grisseman. It was then possible to plot the variation in Cole—Cole parameters with pyrite grain size and concentration. Shown in Figure 27 is one such plot. The slope of 2.0 on the double logarithmic plot indicates that the time constant is proportional to the square of the pyrite grain size.

Once the Cole—Cole model parameters are obtained from inversion of a data set, it is a simple matter to construct a theoretical curve for any desired observable. For example, if we achieve a good fit to real resistivity data, we may immediately calculate the imaginary resistivity curve by substituting the determined parameters into the analytical expression for the Cole—Cole transfer function and taking the imaginary part. This is one reason why we only briefly

mentioned, in the first part of this paper, the Hilbert transform relation between the real and imaginary parts of a causal transfer function. In theory, the relation is simple, but in practice it is quite difficult to perform a Hilbert transform numerically on noisy observed data and obtain meaningful results [WILSON 1977].

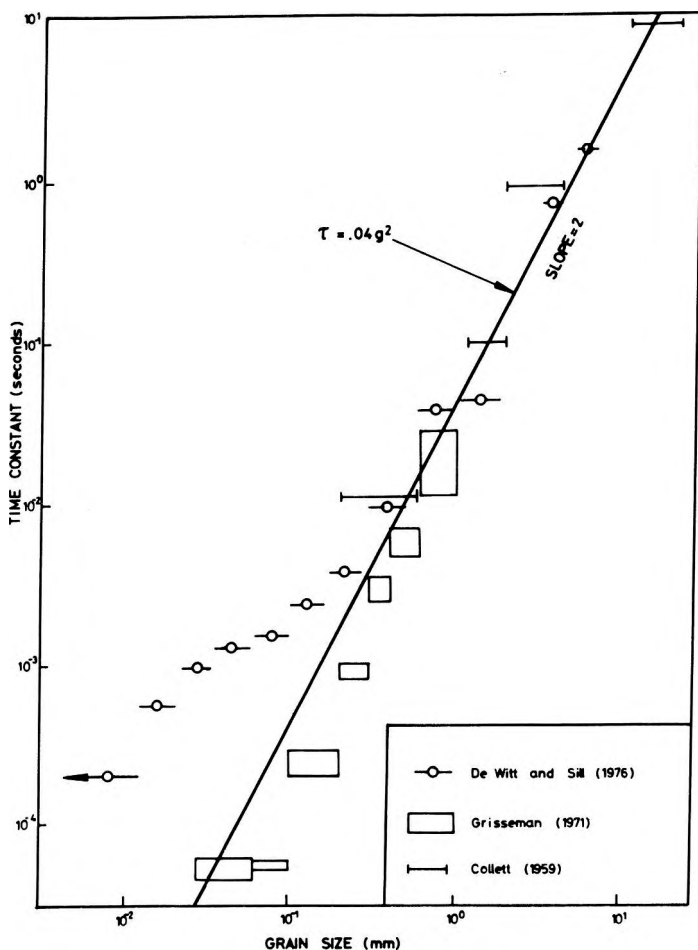


Fig. 27. Time constant versus pyrite grain size obtained from inversion of data gathered by COLLETT [1959], GRISSEMAN [1971], and DEWITT and SILL [1976]

27. ábra. Az időállandó – pirit szemcseméret függvény a COLLETT [1959], GRISSEMAN [1971], valamint DEWITT és SILL [1976] által kapott adatok inverziójából

Рис. 27. Функция постоянная времени — размер зерн пирита по инверсии данных, полученных Колетом (1959 г.) Грисманом (1971 г.), а также ДзВитом и Силлом (1976 г.)

We will now use the Cole—Cole parameters obtained from the inversion in Figure 26, and the Hilbert transform relations inherent in our causal relaxation model, to check Grisseman's results. Shown in Figure 28 is a plot of the tangent of the phase angle, determined from our Cole—Cole parameters, along with actual observations of the tangent of the phase angle reported by GRISSEMAN [1971]. The two curves are in reasonable, but no perfect agreement. The authors are here indebted to WONG [1977] for bringing to our attention the correct logarithmic scale for Grisseman's original data. Our first analysis gave very poor agreement, indicating that the observations were not causal, and that therefore time invariance or linearity were not maintained, or that there was some problem with the measuring apparatus or data reduction.

Examples of measurements which obey the causality requirements almost perfectly are shown in Figure 18 and 19. The solid curves for amplitude and phase were calculated from the same model parameters.

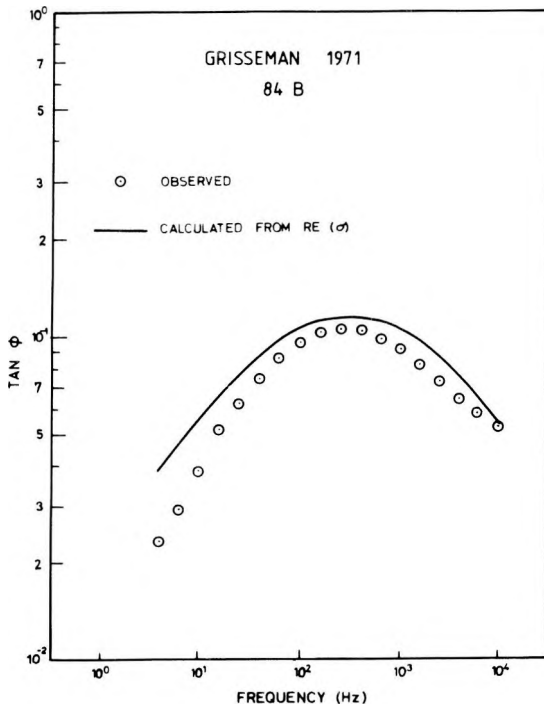


Fig. 28. $\tan \Phi$ observed by GRISSEMAN [1971] compared with $\tan \Phi$ calculated from Cole—Cole model parameters obtained in Figure 26.

28. ábra. A Grisseman által mért (1971) $\tan \Phi$ értékek összehasonlítása a 26. ábrán kapott Cole—Cole modell paramétereiből kapott $\tan \Phi$ értékekkel

Рис. 28. Сопоставление значений $\tan \Phi$, измеренных Грисманом (1971 г.) с значениями $\tan \Phi$, полученными по параметрам модели Кол-Кол на рис. 26.

Time domain data All of our examples of interpretation of complex resistivity and dielectric data have so far concerned measurements made only in the frequency domain. We mentioned in the first part of this paper that frequency domain measurements tend to be easier to make, and to interpret, than time domain measurements, particularly when information is desired over several decades of time or frequency.

However, to illustrate how similar complex resistivity and dielectric interpretation might be carried out in the time domain we will discuss some decay curves published by MADDEN and CANTWELL [1967]. Shown in *Figure 29* are decay data from artificial rocks originally obtained by COLLETT [1959] but replotted by MADDEN and CANTWELL [1967]. The dashed curve in the figure was calculated by MADDEN and CANTWELL [1967] from their approximate derivation of the IP decay, corrected for the 1 second switching time used by COLLETT [1959]. Since the calculated curve fits only the data for smaller grain sizes, Madden and Cantwell suggest that Collett's data for the larger grains was adversely affected by high current densities and the unusual pore geometry created in artificial rocks. We would like to offer here a considerably different interpretation for change in decay shape with increasing grain size, and at the same time to illustrate the various steps required in the interpretation of time domain data.

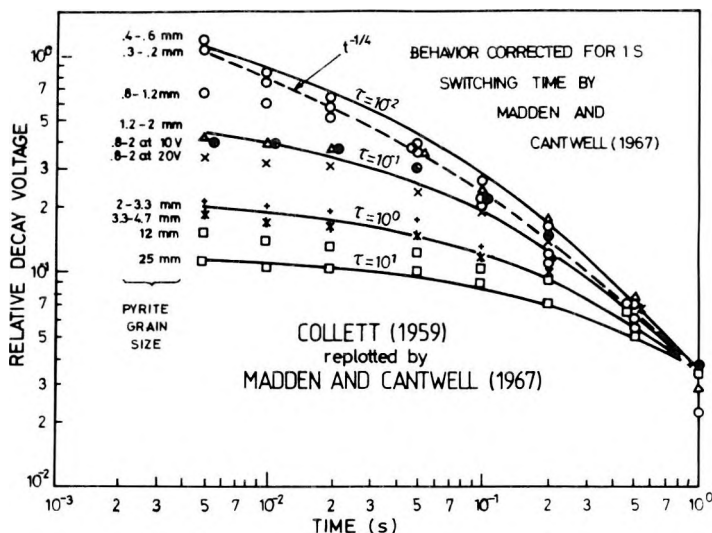


Fig. 29. Decay data obtained by COLLETT [1959] from measurement of artificial rocks which were replotted by MADDEN and CANTWELL [1967], compared with theoretical curves

29. ábra. COLLETT [1959] mesterséges kőzetmintákon végzett méréseinek lecsengési adatai — amelyeket MADDEN és CANTWELL [1967] rajzolt át — elméleti görbékkel összehasonlítva

Рис. 29. Данные затухания по измерениям Колета (1959 г.) на образцах искусственных пород — которые были перечерчены Мадденом и Кэнтвелом (1967 г.) —, в сопоставлении с теоретическими кривыми.

In our analysis of Grisseman's frequency domain data (Figure 26) we obtained a very good fit to his real conductivity measurements using a Cole—Cole complex resistivity model with frequency dependence very nearly equal to 0.5. This value ranged between 0.45 and 0.55 for almost all of his data on artificial rocks.

Good fits to Cole—Cole models with values of c near 0.5 were also observed for our measurements of the Scott-West artificial rocks (Figure 20) and for other recent measurements of artificial rocks at our laboratory [SILL and DEWITT 1976]. It is thus our tentative conclusion that where a very restricted range of grain sizes is involved, as in most artificial rocks, the relaxation behavior closely follows that of a Cole—Cole model with the frequency dependence approximately equal to 0.5 (our "Warburg" model in Table 1). For natural mineralized rocks where the range of grain sizes is typically broader, the dispersion is broader, and the value of the frequency dependence is typically near 0.25, although it ranges from 0.5 to as low as 0.125 [PELTON et al. 1978].

Thus in order to interpret the time domain decay curves shown in Figure 29, where the grain size in each sample was rigidly controlled, we decided to adopt the Warburg relaxation model. In the first part of this paper we derived the exact negative step function response for this model and then corrected for two common transmitter switching waveforms. The results, shown in Figures 8a, and 8b, were two sets of curves, whose decay shape depends on only one variable, the ratio of the relaxation time constant to the transmitter pulse length. We have displayed four of these theoretical decay curves as solid lines in Figure 29. Since the transmitter pulse length was 1 second, they correspond to different relaxation time constants ranging from 0.01 seconds to 10 seconds. It is now apparent from Figure 29, that the strange, systematic change in decay shape, noted by MADDEN and CANTWELL [1967], can be very simply explained by an increase in time constant as a function of grain size, without resorting to nonlinear behavior or unusual pore geometry.

As an exercise, to compare the trends observed in Collett's data, Grisseman's data and data from DEWITT and SILL [1976], we plotted all three sets of results in Figure 27. The similarity of trends is remarkable, considering that absolutely no effort was made to create the same porosity in the different sets of samples, or to use similar electrolyte concentrations.

MADDEN and CANTWELL [1967] also published nine other decay curves for natural mineralized rocks. We have plotted only two of these data sets in Figure 30 since the other seven decay curves fall between these two. The measurements were made using sequential switching with a transmitter pulse length of 7 seconds. The solid lines shown in the figure are two of our theoretically calculated curves based on a Warburg model and corrected for sequential switching. It is apparent that the two different curve shapes might possibly be explained by a factor of 10 difference in the time constant.

We would like to be more thorough here, and to use our ridge regression inversion routine to solve in the time domain for all the Cole—Cole model parameters, including the frequency dependence, c ; rather than assuming a

value of c and then superimposing type curves to estimate the time constant. This can certainly be easily accomplished, and would be desirable, if more and better quality data in the time domain become available.

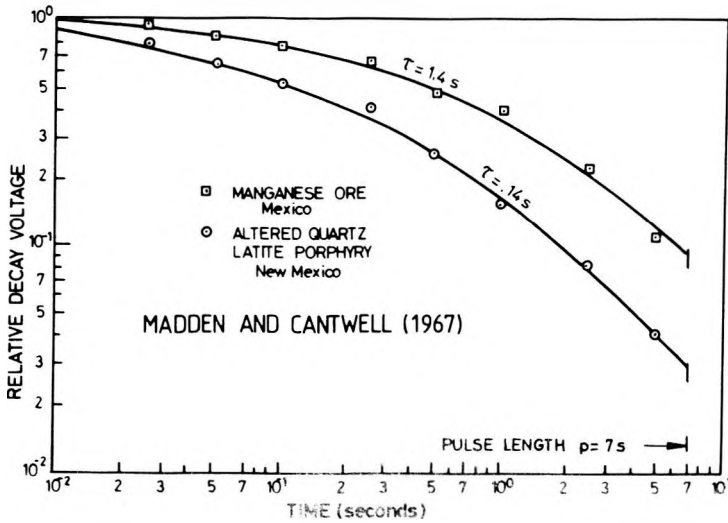


Fig. 30. Decay data obtained by MADDEN and CANTWELL [1967] from measurement of natural rocks, compared with theoretical curves

30. ábra. MADDEN és CANTWELL [1967] természetes kőzeteken végzett méréseiből kapott lecsengési adatok, elméleti görbékkel összehasonlítva

Рис. 30. Данные затухания по измерениям Маддена и Кэнтвелла (1967 г.) на естественных породах, в сопоставлении с теоретическими кривыми.

Transformation between domains

The final subject we will consider, involves numerical transformation from one set of measurements to another; notably from the frequency domain to the time domain. First, however, we will discuss transformation between the two types of common measurements made in the frequency domain.

Phase versus frequency effect If we were to assume a constant phase model for complex resistivity (such as the Drake model when $\omega\tau \gg 1$), it would be very easy to establish a universal relationship between frequency effect and phase. The frequency effect measurement,

$$FE_{l-h} = \frac{|\varrho(l)| - |\varrho(h)|}{|\varrho(h)|} \quad (101)$$

can be considered as merely an attempt to specify the slope of $|\varrho(\omega)|$ on a double logarithmic plot, by taking the first backward difference. The true slope, for the Drake model with parameters R , τ and a , when $\omega\tau \gg 1$ is simply

$$\begin{aligned} \text{FE}_T &= a \text{ decades/decade} \\ &\cong 100 a e^\circ/\text{decade} \end{aligned} \quad (102)$$

for $a \ll 1$ and $e = 2.71828$. . . The phase, Φ , is also readily given in terms of a by

$$\begin{aligned} \Phi &= a \frac{\pi}{2} \text{ radians,} \\ &= 500a\pi \text{ milliradians} \end{aligned} \quad (103)$$

[VAN VOORHIS et al, 1973]. Thus we have the very simple relationship

$$\Phi \cong \alpha \cdot \text{PFE}_T \quad (104)$$

where

$$\begin{aligned} \alpha &= 5 \frac{\pi}{e} \text{ milliradians} \\ &= 5.8 \text{ milliradians} \\ &= 0.33 \text{ degrees} \end{aligned} \quad (105)$$

and PFE_T represents percent frequency effect per decade.

We tested this theoretical relation by plotting $\Phi_{0.1 \text{ Hz}}$ against $\text{PFE}_{0.1-1.0 \text{ Hz}}$ for in-situ data obtained by PELTON et al. [1977]. Each black dot in *Figure 31* is essentially free of measurement error since we first inverted the spectra, and then used the theoretical relaxation model to calculate $\Phi_{0.1 \text{ Hz}}$ and $\text{PFE}_{0.1-1.0 \text{ Hz}}$. Thus the scatter in the diagram arises solely from the fact that the in-situ spectra were not constant phase, and thus all calculated α were slightly different from 0.33 degrees.

To obtain an average value for α we conducted a simple linear regression in double logarithmic space, and then converted the estimated percentage standard deviation for α to a linear standard deviation. Shown in *Figure 31*, along with our least-squares fit (solid line; $\alpha = 0.35 \pm 0.02$ degrees) are dashed lines corresponding to other relations obtained by ZONGE [1972] and SCOTT [1971]. Scott graphically derived several different values for α ranging from 0.30 degrees to 0.35 degrees to 0.43 degrees, whereas Zonge used a different theoretical approach than ours to obtain a value of $\alpha = 0.31$ degrees.

The main purpose of this exercise was to illustrate that a reasonably accurate linear relation between PFE and phase can be derived extremely easily using the Drake model. Substantial differences from this theoretical relation indicate that the phase is not constant. A few rapid calculations using PFE and phase obtained from a Cole—Cole model reveal that large values of α correspond with large time constants or decreasing phase with frequency, whereas small values of α correspond with small time constants or increasing phase. The scatter diagram of *Figure 31* roughly indicates how much variation might be expected in noise-free measurements of α over natural mineralization.

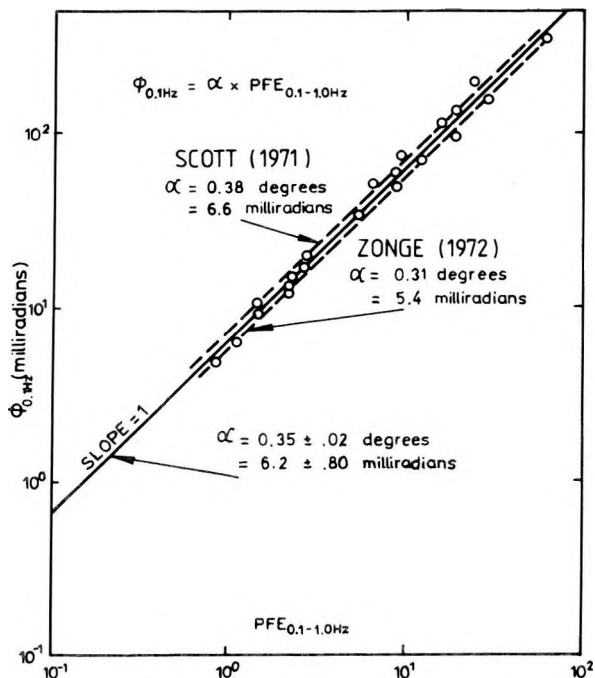


Fig. 31. Phase angle versus PFE obtained from essentially noise-free in situ data

31. ábra. Fázisszög — PFE függvény lényegében zajmentes in situ adatok alapján

Рис. 31. Функция фазовый угол — PFE по данным, полученных в условиях естественного залегания практически без шума.

Frequency domain—time domain conversion By now the reader is probably all too well aware of our fascination with the Cole—Cole model. The reason for this preoccupation is that the model is extremely general, to the extent that can fit virtually any relaxation transfer function with either one or a combination of several of these models. (Remember that the Debye model, which corresponds to a delta function representation in the distribution domain, is just a special case of the Cole—Cole model.) Yet in spite of this generality, the model has a very simple mathematical form which is easily programmable in both the frequency domain and the time domain.

We have already examined two sets of time domain data, and attempted to fit a special case of the Cole—Cole model ($c = 0.5$) to the data. If we were able to obtain, with confidence, all of the Cole—Cole model parameters through analysis of the time domain data (obtaining m , for example, through measurement of m_{obs} , knowledge of the transmitter waveform, and use of Figure 9) we could then simply calculate any observable in the frequency domain, such as amplitude or phase, through the relation for $h(\omega)$ given by (21).

Similarly, we can use the parameters determined by inversion in the frequency domain, to calculate the time domain response. This exercise has been carried out with the parameters obtained from inversion of the Iron Mountain 5 in-situ data shown in Figure 14. The expressions (47) and (50) were programmed on an HP-67 pocket calculator and used to obtain the calculated step function decay curve shown in Figure 32.

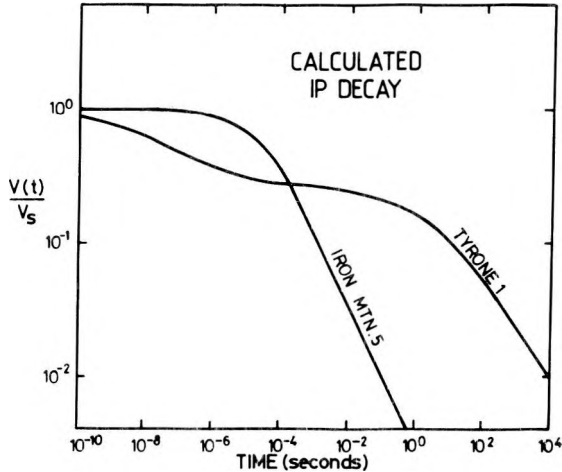


Fig. 32. Calculated IP decay curves for Iron Mountain 5 and Tyrone 1 in situ spectral data

32. ábra. Az Iron Mountain 5 és Tyrone 1 in situ spektrális adatokból számított GP lecsengési görbék

Рис. 32. Кривые затухания ВП, рассчитанные по спектральным данным Айрон Моунтин 5 и Тайрон 1, полученным в условиях естественного залегания.

To illustrate transformation of more difficult spectra, we re-examined the Tyrone 1 in-situ data shown in Figure 16. The frequency domain model which was originally fitted to the data was not very satisfactory since it was a multiplication of two Cole—Cole models which, in turn, corresponds to convolution of two Cole—Cole models in the time domain. Since convolution of two functions over seven decades was beyond the capability of our pocket calculator (or the University of Utah Univac 1108, for that matter) we decided to re-invert the spectral data to the following model:

$$g(\omega) = R \left[\frac{m}{1 + (i\omega\tau_1)^{c_1}} + \frac{1-m}{1 + (i\omega\tau_2)^{c_2}} \right]. \quad (106)$$

The parameters, R , m , τ_1 , and c_1 previously produced a good fit to the low frequency phase angle peak, so they were held constant. The new model parameters, τ_2 and c_2 were determined to be

$$\tau_2 = 1.70 \cdot 10^{-8} \pm 14.8\%, \quad (107)$$

and

$$c_2 = 0.360 \pm 2.4\%, \quad (108)$$

and the resulting new “addition model” curve was found to be virtually identical to the old “multiplication model” curve shown as a solid line in Figure 16. However, since addition in the frequency domain corresponds to addition in the time domain (because the Fourier transform is linear) it was consequently a simple matter to add together two Cole—Cole decay curves to produce the “double decay” curve for (106) shown again in Figure 32.

We have plotted the decay for Tyrone 1 over fourteen decades of time, in order to illustrate its asymptotic behavior. However, this behavior is not really well known since we only have seven decades of frequency information ($10^{-1} < \omega < 10^6$). Thus the decay could be a little faster or slower for $10^1 < t < 10^{-6}$.

Also, both the decays assume an infinitely long charging time. If the transmitter pulse length is not very long compared to τ_1 , the decay curves must be corrected for the effects of switching by adding the appropriate series of positive and negative step function responses.

The point we are trying to make in this section, is that transformation between the frequency domain and the time domain can be carried out relatively easily using inversion and sums of Cole—Cole models (or of any other relaxation models, such as the Cole—Davidson model, which have easily programmable response in both domains).

Partly because the time domain decay is so long and drawn out (Tyrone 1 takes roughly 10 decades to decay one decade), and partly because 10^7 point Fast Fourier Transforms are not readily available, it is not possible to transform broad-band data between the time and frequency domains directly, by using the FFT. A 1024 point FFT, for example, corresponds to less than three decades of information. An alternative, innovative method of transformation is described by WILSON [1977]. He first transforms to a logarithmic frequency scale then finds that the Hilbert transform and decay spectra relations become algebraic rather than integral equations. His method is advantageous in that transformation is not dependent on any particular relaxation model; however, extrapolating functions are required at high and low frequencies, and the transformation is adversely affected by noise in the observed spectra. In contrast, our method is model dependent, but has the advantage that no extrapolating functions are required at high and low frequency, since the asymptotic behavior of $h(\omega)$ is automatically specified. In addition, the transformation is relatively immune to noise in the observed spectra. Although some noise does persist through to the time domain (in the form of parameter uncertainties) much of the measurement error is very effectively filtered out at the start, through the least squares fit to the data provided by the inversion.

9. Discussion and summary

This concludes our attempt at treating a reasonably broad subject: the analysis of complex resistivity and dielectric data. By our original choice of this topic we were almost predestined to commit a cardinal sin: the production of a research paper which is longer than the average reader's time and patience. However, the alternative was to produce several smaller, self-contained papers on special topics such as the forward problem, quantitative evaluation of spectra and transformation between the different domains. This would result in an unfortunate lack of integration and unnecessary redundancy.

In the single paper which we have written instead, we have attempted to summarize briefly the essential requirements of relaxation models for complex resistivity and dielectric behavior. This led to a consideration of the behavior in the frequency domain and in the time domain of many of the simple relaxation models which have been proposed. The true time domain behavior of virtually all of these relaxation models (all except the Debye model) we have had to derive for the first time. An asymptotic solution for the Cole—Cole decay was obtained by MADDEN and CANTWELL [1967] for very long times and an asymptotic solution for the Drake model decay was obtained by VAN VOORHIS et al. [1973] for very short times. However, these asymptotic solutions can not be accurately applied for intermediate times, where precise observations can be made most easily, and where most of the information on the relaxation parameters is located.

Under ideal circumstances, with the transfer function analysis approach outlined in this paper, we should be able to collect rock electrical data in either the frequency domain or the time domain and then invert to identify and characterize, all of the important conduction processes occurring in the rock. In practice, of course, this sort of ideal interpretation is almost never achievable. We are always faced with the following difficulties: 1) measurements of finite accuracy over a limited frequency band or time range, containing transient effects produced by time or frequency waveforms of finite length, 2) the basic non-uniqueness produced by the infinite number of possible equivalent circuits for the rock conduction, 3) the inherent ambiguity between metallic electrode polarization and membrane polarization and even between complex resistivity and complex permittivity (all our IP behavior, for example, could be considered due to an abnormally large, complex dielectric constant), and 4) the spectral smearing due to ranges of grain size, variable pore width and interpore connections, etc.

In spite of these difficulties we believe that we can use the data analysis and inversion techniques outlined herein to 1) discern the most reasonable model out of several models proposed for a particular data set, and thereby perform limited identification of physical processes, 2) conduct quantitative evaluation of spectra so that variations in response with density, temperature, mineral composition, grain size, sulfide concentration, clay content, porosity, solution resistivity or other physical variables may be adequately characterized, and 3)

achieve accurate, and relatively easy transformation between the frequency domain and the time domain, or between the different types of measurements made in either domain.

Perhaps the most important feature of our paper, we believe, is that the theory and technique outlined herein, are relatively simple to implement. All of the forward problems which we have discussed may be programmed easily on a pocket calculator. All of the inversions of spectral data were carried out on the University of Utah Univac 1108 computer. The time required for each inversion was less than 1 second (for virtually any marginally reasonable initial guess) and the memory requirements were less than 40K. No attempt was made to optimize time or memory requirements since the cost for each inversion was always less than 10 cents.

Acknowledgements

The authors wish to acknowledge the encouragement, financial support, and equipment provided by Dr. P. H. Nelson and Dr. G. W. Hohmann of Kennecott Exploration, Incorporated, and by Mr. J. Roth of Amax Exploration, Ltd. Additional financial support was provided by National Science Foundation Grant GA-31571. Constructive discussions were held with Dr. Ralph Shuey on relaxation response and with Mr. Wesley Wilson on transformation from the frequency domain to the time domain. The spectral data from drill cores obtained at Roosevelt Hot Springs were provided by Mr. Alan Tripp. The interpretation of the spectral data from the pyrite electrodes was carried out in conjunction with Mr. James D. Klein, and the measurement of the Scott-West rocks was assisted by Mr. Grant DeWitt. Mr. J. Wong was very helpful in pointing out an error in our processing of Grisseman's data. Finally, Dr. S. H. Ward was responsible for the original direction and ultimate supervision of this research as well as creating the rock properties laboratory and academic environment which allowed the work to proceed.

REFERENCES

- ANGORAN Y. E., 1975: Induced polarization of metallic minerals, a study of its chemical basis. Ph. D. thesis, MIT, 189 p.
- BEVINGTON P. R., 1969: Data reduction and error analysis for the physical sciences. New York, McGraw-Hill Book Co., Inc., p. 336
- COLLETT L. S., 1959: Laboratory investigation of overvoltage, in *Overvoltage research and geophysical applications*. New York, Pergamon Press
- FOSTER M., 1961: An application of the Wiener-Kolmogorov smoothing theory to matrix inversion. *J. Soc. Indust. Appl. Math.*, **9**, pp. 387-392
- GRISSEMAN C., 1971: Examination of the frequency dependent conductivity of ore-containing rock on artificial models. Scientific Report No. 2, Electronics Laboratory, University of Innsbruck, Austria

- HOHMANN G. W., 1973: Electromagnetic coupling between grounded wires at the surface of a two-layer earth. *Geophysics*, **38**, pp. 854–863
- KLEIN J. D., PELTON W. H., 1976: A laboratory investigation of the complex impedance of mineral-electrolyte interfaces. Paper presented at the 46th Annual International SEG Meeting, October 25 in Houston, Texas
- LEVENBERG K., 1944: A method for the solution of certain nonlinear problems in least squares. *Quart. Appl. Math.*, **2**, pp. 164–168
- MADDEN T. R., CANTWELL T., 1967: Induced polarization, a review, in *Mining Geophysics*, Vol. II, Tulsa, SEG, pp. 373–400
- MARQUARDT D. W., 1963: An algorithm for least squares estimation of nonlinear parameters. *J. Soc. Indust. Appl. Math.*, no. **2**, pp. 431–441
- MILLET F. B., 1967: Electromagnetic coupling of colinear dipoles on a uniform half space, in *Mining Geophysics*, Vol. II, Tulsa, SEG, pp. 401–419
- NELSON P. H., 1975: Personal communication
- NELSON P. H., VAN VOORHIS G. D., 1977: Discussion on “Recent advances and applications in complex resistivity measurements”. *Geophysics*, **42**, pp. 120–121
- PELTON W. H., RIJO L., SWIFT C. M. JR., 1976: Inversion of two dimensional induced polarization and resistivity data. Paper presented at the 46th Annual International SEG Meeting, October 26, in Houston, Texas
- PELTON W. H., SMITH B. D., SILL W. R., 1974: Inversion of complex resistivity and dielectric data. Paper presented at the 44th Annual International SEG Meeting, November 13 in Dallas, Texas
- PELTON W. H., WARD S. H., HALLOP P. G., SILL W. R., NELSON P. H., 1978: Mineral discrimination and removal of inductive coupling with multifrequency IP. *Geophysics*, **43**, pp. 588–609
- PETRICK W. R., PELTON W. H., WARD S. H., 1977: Ridge regression applied to crustal resistivity sounding data from South Africa. *Geophysics*, **42**, pp. 995–1005
- RIJO L., PELTON W. H., FEITOSA E. C., WARD S. H., 1977: Interpretation of apparent resistivity data from Apodi Valley, Rio Grande do Norte, Brazil. *Geophysics*, **42**, pp. 811–822
- SCOTT W. J., 1971: Phase angle measurements in the induced polarization method of geophysical prospecting, Montreal, McGill University, Ph. D. thesis, 288 p.
- SCOTT W. J., WEST G. F., 1969: Induced polarization of synthetic, high-resistivity rocks containing disseminated sulfides. *Geophysics*, **34**, pp. 87–100
- SILL W. R., DEWITT, 1976: Parametric studies of IP spectra: Paper presented at the 46th Annual International SEG Meeting, October 26 in Houston, Texas
- SMITH B. D., 1975: Interpretation of electromagnetic field measurements. Ph. D. thesis, University of Utah, 244 p.
- TRIPP A., 1976: Personal communication
- VAN VOORHIS G. D., NELSON P. H., DRAKE T. L., 1973: Complex resistivity spectra of porphyry copper mineralization. *Geophysics*, **38**, pp. 49–60
- WARD S. H., FRASER D. C., 1967: Conduction of electricity in rocks, in *Mining Geophysics*, Vol. II, Tulsa, SEG, pp. 197–223
- WILSON W. R., 1977: Numerical calculations of electrical dispersion relations in rocks. M. S. thesis, University of Utah, 182 p.
- WONG J., 1977: An electrochemical model of the IP phenomenon in disseminated sulfide ores. Paper presented at the 47th Annual International SEG Meeting, September 30 in Calgary, Alberta
- ZONGE K. L., 1972: Electrical properties of rocks as applied to geophysical prospecting. Ph. D. thesis, University of Arizona, 156 p.
- ZONGE K. L., WYNN J. C., 1977: Reply to discussion on “Recent advances and applications in complex resistivity measurements”. *Geophysics*, **42**, pp. 121–123

KOMPLEX ELLENÁLLÁS- ÉS DIELEKTROMOS ADATOK ÉRTELMEZÉSE II. RÉSZ

W. H. PELTON, W. R. SILL, B. D. SMITH

A vezetési áram és az eltolási áram fogalmát felhasználva arra törekedtünk, hogy világosan megkülönböztessük a komplex ellenállás jelenségét és a dielektromos viselkedést. Ennek eredményeként lehetővé vált, hogy a *ridge regression* inverzió felhasználásával egyidejűleg megkapjuk azokat a paramétereket, amelyek az egyes jelenségeknek a megfigyelt spektrumhoz való hozzájárulását leírják. Hasonló módon más folyamatok, mint a membrán polarizáció, kettősréteg kapacitás és induktív elektromágneses csatolás azonosítása is — korlátozott mértékben — elvégezhető.

A közzétulajdonságok vizsgálatában azonban az inverzióknak talán az a legfontosabb felhasználása, hogy a spektrális görbéket néhány számmá alakítja át, így a spektrum olyan fontos fizikai változók függvényében való változásait, mint a hőmérséklet, ásványos összetétel, koncentráció és szemcseméret, pontosan le lehet írni, vagy jellemezni.

Az egyszerű relaxációs modellek mindhárom tartományban (frekvencia, idő és eloszlás függvény) való vizsgálatának az is eredménye, hogy az egyik tartományban végzett szélessávú mérést át lehet számítani egy másik tartományba, vagy ugyanabban a tartományban végzett másfajta mérésre, például az amplitúdót fázissá. Ez úgy történik, hogy a *ridge regression* inverzió felhasználásával egyszerű relaxációs modellek összegét illesztjük a mért adatokhoz. A meghatározott paraméterek és a modell minden más tartományban ismert analitikus képlete aztán felhasználható a megfigyelt adatok bármely kívánt módon való ábrázolására.

ИНТЕРПРЕТАЦИЯ ДАННЫХ О КОМПЛЕКСНЫХ СПЕКТРАХ СОПРОТИВЛЕНИЯ И ДИЭЛЕКТРИЧЕСКИХ СПЕКТРАХ Часть II

В. Г. ПЕЛТОН, В. Р. СИЛ, Б. Д. СМИТ

Были сделаны на основании понятия тока проводимости и тока смещения явно различить явление комплексного сопротивления и диэлектрическое поведение. В результате этого стало возможным при применении инверсии по регрессии ридж одновременно получить параметры, которые описывают вклад отдельных явлений в наблюдаемый спектр. Подобным образом в ограниченной мере можно распознавать также другие процессы, как мембранную поляризацию емкость двойного пласта и индуктивную электромагнитную связь.

При изучении свойств горных пород, однако, важнейшим видом применения инверсии является преобразование спектральных кривых в некоторые цифры, таким образом изменения спектра в зависимости от важных физических переменных, в том числе температуры, минерального состава, концентрации и размера зерн, можно точно описать или характеризовать.

Результатом изучения простых релаксационных моделей во всех трех областях (функций частоты, времени и распределения) является между прочим и то, что проведенное в одном из областей широкополосное измерение можно перечислить в другой область или в другой вид измерения, проведенного в одном и том же области, напр., амплитуду в фазу. Это производится так, что с помощью инверсии по регрессии ридж сумма простых релаксационных моделей согласуется с измеренными данными. Определенные параметры и аналитическая формула модели, известная по всем другим диапазонам, могут быть применены для представления наблюдаемых по любому желаемому способу.

SCALAR AUDIOMAGNETOTELLURIC MEASUREMENTS IN HUNGARY

Antal ÁDÁM*, Pertti KAIKKONEN**, Sven-Erik HJELT**,
Juha TIIKKAINEN**

Audiomagnetotelluric (AMT) soundings were carried out in Hungary by the French-made "ECA Résistivimètre" in the frequency range of 4.1–2300 Hz to test AMT method for different geophysical problems (Nagycekn electromagnetic observatory, sedimentary basin, a geodynamic test profile, ore prospecting, etc.).

The main conclusions are the following:

- the most reliable information was obtained at the frequency range of the *harmonics of the Schuman resonance* (7.3–23 Hz).
- the reliability of the apparent resistivity (ρ_a) values measured on crystalline rocks is higher than that above sediments because in the latter case the much lower amplitude of the electric field essentially worsens the signal-to-noise ratio.
- the noise level caused by power lines of ~ 50 Hz is the highest at 41 and 230 Hz. Near to the sources of the stray (leakage) currents, mainly in villages, the general level of ρ_a values is increased according to frequency sounding in the "near zone" of the source.
- there is an energy gap between 730 and 2300 Hz which is due to the attenuation of the ELF signals conducted in the Earth—ionosphere cavity and it manifests itself in low ρ_a values.

Because of difficulties in distinguishing between signal and noise EM fields in scalar measurements without coherence control, there is a need to investigate tensorial data processing and the nature of natural audiofrequency field. For this purpose the design of a digital recording system has been started.

d: audio-magnetotellurics, test surveys, signal-to-noise ratio, time variation, tensorial data processing

1. Introduction

In Hungary the magnetotelluric (MT) method is used by institutes for applied geophysics in the frequency range of 0.01–20 Hz to investigate the relief of the basement at depths of some thousands of metres (see *Fig. 1* section MT₁ of the magnetotelluric sounding curve measured in the Nagycekn observatory, after ÁDÁM et al., 1981). For the geoelectric sounding of the Earth's crust and the upper mantle electromagnetic time variations of much lower frequencies are needed, such as the harmonics of the quiet daily variation (S_q) see section MT₂ in *Fig. 1*). For the determination of the layer structure of the sedimentary cover of a basin, ELF signals of 3–3000 Hz should be used for magnetotelluric soundings. For the geophysical survey of near-surface ore bodies and in various

* Geodetic and Geophysical Research Institute of the Hungarian Academy of Sciences, POB 5, Sopron, H-9401, Hungary

** Department of Geophysics, University of Oulu, SF-90570 Oulu 57, Finland

Paper presented at the 28th International Geophysical Symposium, 28 September–1 October 1983, Balatonszemes, Hungary

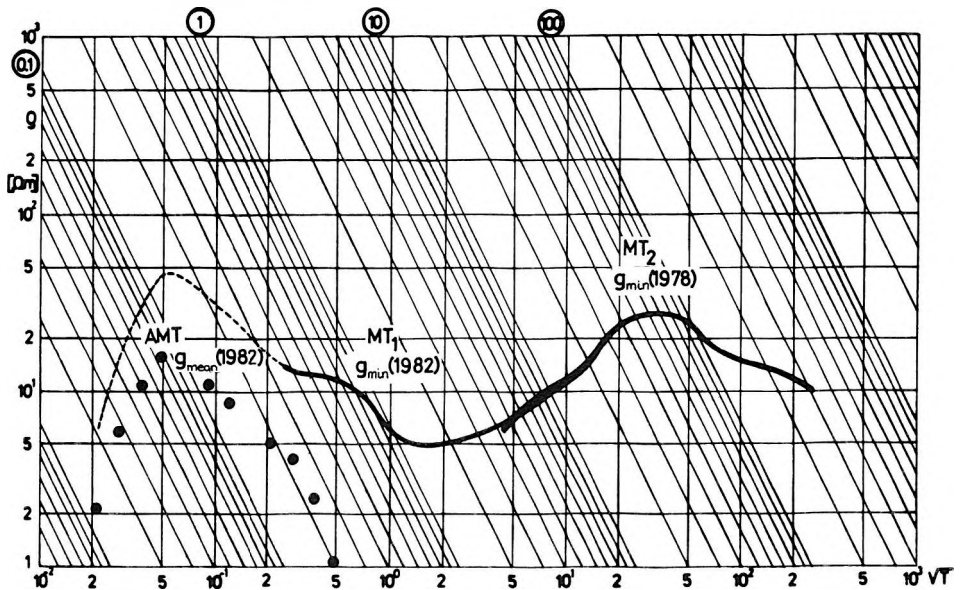


Fig. 1. Magnetotelluric (MT) and audiomagnetotelluric (AMT) sounding curves measured in the Nagycenk observatory. AMT—measured by University of Oulu; MT_1 —measured by ELGI; MT_2 —measured by GGRI

1. ábra. A nagycenki obszervatóriumban mért magnetotellurikus (MT) és audiomagnetotellurikus (AMT) szondázási görbék. AMT — Oului Egyetem munkatársainak mérése; MT_1 — ELGI munkatársainak mérése; MT_2 — GGRI munkatársainak mérése

Рис. 1. Кривые магнитотеллурического (MT) и аудиомангнитотеллурического (AMT) зондирования, полученные в обсерватории Надьценк. AMT — замеры сотругниками Университета в г. Оулу; MT_1 — замеры сотругниками ELGI; MT_2 — замеры сотругниками GGRI

engineering geophysical problems, EM variations in the same frequency range should be analysed. Magnetotelluric sounding using natural ELF signals is called “audiomagnetotelluric” or shortly AMT sounding (see the AMT section in Fig. 1).

The measuring group of Oulu University (Finland) carried out AMT soundings between 16 September and 7 October 1982 in Hungary to test the applicability of AMT measurements at middle latitudes for different geophysical problems:

1. in the Nagycenk observatory above 1500 m thick sediments,
2. along a geodynamic profile between the villages of Ukk and Ötvös, in a shallow basin of the Bakony Mts broken into blocks by seismo-active fractures,
3. in the Little Hungarian Plain being a deep basin filled by some thousand metres of sediments,
4. on ore-bearing formations of the Börzsöny Mts.

The AMT instrument, the French-made ECA 542-0, uses a microprocessor to obtain immediately in the field the apparent (scalar) resistivity value (ρ_0) from the average amplitudes of the electric (E) and magnetic (H) components in

perpendicular directions. There are 12 fixed frequencies between 4.1 and 2300 Hz.

2. Geological description

The task of the geophysical surveys in the first three areas was to determine the structure of the sedimentary basin, including the separation of layers of different resistivities, and the tectonics of the basement. The layer sequence in the Pannonian stage can be well characterized by the alternation of more or less resistive sediments (sand or clay). A similar layer sequence was obtained in the Nagycenk observatory but terrace gravel of higher resistivity is embedded into the near-surface layers.

The horizontal anisotropy of the sedimentary layers near the surface of the deep basins is generally less than the anisotropy of the fractured basement.

The AMT sounding curve measured in the Nagycenk observatory is shown in *Fig. 1* as a continuation of MT curves covering together a period range of 8 orders of magnitude. Irrespective of a systematic scale value difference between the AMT and MT ρ_a values, the AMT curve shifted to the MT₁ curve fits well to it and qualitatively expresses the sedimentary structure described by geoelectric models of the DC soundings. This AMT curve is the geometric mean of 12 measurements. Their mean square errors are shown in *Fig. 2*. Some

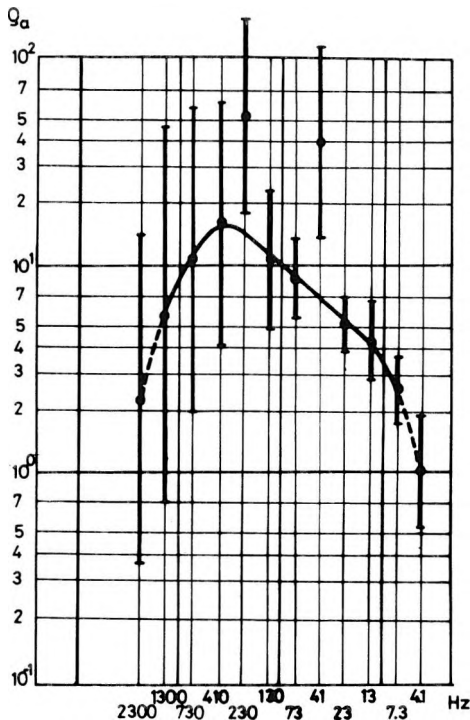


Fig. 2. Mean square errors of the AMT curve in the Nagycenk observatory

2. ábra. A nagycenki obszervatóriumban mért AMT görbe négyzetes középhibái

Рис. 2. Среднеквадратические ошибки кривой AMT в обсерватории Надьценк.

characteristic features of this curve are briefly mentioned here, with more details being given later on.

- Lowest errors of the Q_a values were obtained at the harmonics of the Schuman resonance (7.3, 13, 23 Hz);
- the disturbing fields of power lines of about 50 Hz seriously affect the Q_a values at 41 Hz, and at the fifth harmonic possibly at 230 Hz;
- the attenuation between 410 and 2300 Hz in the Earth-ionosphere cavity decreases the amplitudes of the ELF signals, the uncertainty of the Q_a values significantly increases.

In the Little Hungarian Plain many factors, such as low electric signals over sediments of low resistivity, high level of disturbances due to the power lines in the villages, etc. decreased the reliability of the individual AMT measurements. Therefore, only an average AMT sounding curve was used for the whole area. Such a curve very much resembles the AMT curve of the Nagycenk observatory measured in a quite similar geological situation (*Fig. 3*).

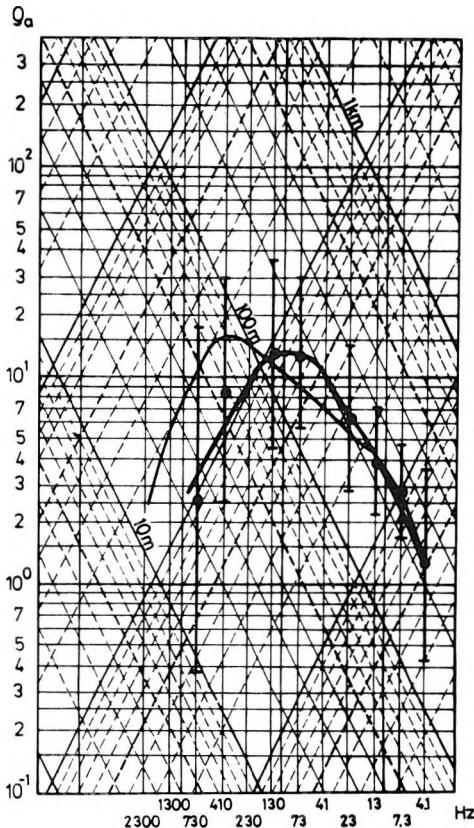


Fig. 3. AMT—measurements at Nagycenk Observatory (thin line) and median of AMT measurements in the Little Hungarian Plain (thick line)

3. ábra. A Kisalföldön mért átlagos AMT görbe (vastag vonal), a Nagycenki Obszervatóriumban mért AMT-görbe (vékony vonal)

Рис. 3. Средняя кривая АМТ, полученная на Малой венгерской низменности (мирной линией), кривая АМТ, полученная в обсерватории Нагьценк (тонкая линия).

Around the villages of Ukk and Ötvös in a shallow basin broken into blocks by deep fractures, the depth of the highly resistive basement varies only some hundreds of meters according to the geological map of Fig. 4. The impedance directions $Z_{xy\max}$ computed on the basis of the MT soundings are connected with the strike of the fractures. In the villages the AMT curves are generally distorted by stray currents. In view of this, at the measuring site 10 an undisturbed area was chosen to illustrate the information content of the AMT curves (Fig. 5). The MTS curve measured at the nearest magnetotelluric point to Ötvös was connected with the AMT curve by a thin line. The anisotropy directions for both of the MT and AMT soundings are assumed to be same. The AMT curve obtained in the direction of 15° E (Q_{\max}) represents the H polarization case. The currents flowing perpendicularly to the strike cannot penetrate below the Eocene limestone embedded into the sediment cover, and so the curve does not indicate sediments below this resistive layer. The E-polarized AMT curve (direction 285°) however, shows the deeper layer sequence.

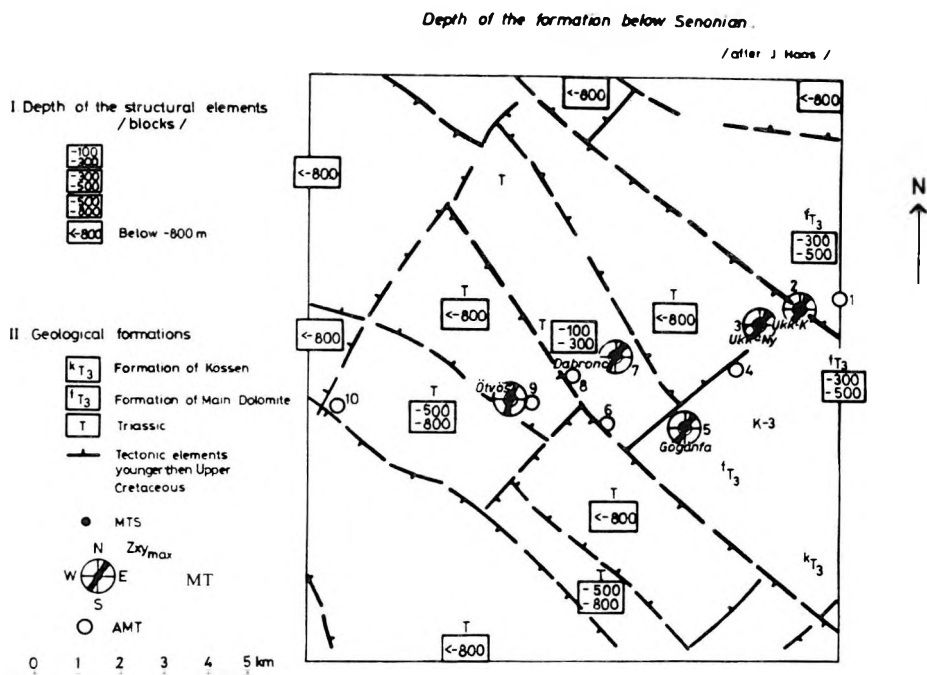


Fig. 4. MT and AMT sites along the Transdanubian geodynamic profile

4. ábra. MT és AMT mérési pontok a dunántúli geodinamikusszelvény mentén

Рис. 4. Места МТ и АМТ зондирования по Задунайскому геодинамическому профилю

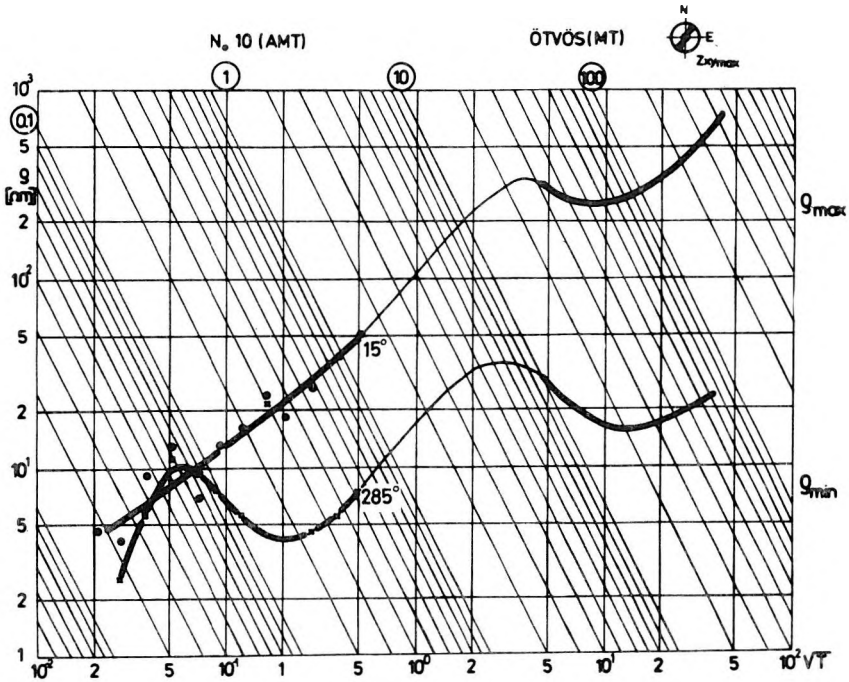


Fig. 5. Connection of MT and the corresponding AMT curve at the measuring site shown in Fig. 4

5. ábra. Az MT és a megfelelő AMT görbe kapcsolata a 4. ábrán bemutatott mérési ponton

Рис. 5. Связь кривой MT с соответствующей кривой AMT на месте зондирования, показанном на рис. 4.

The resistivity changes measured at different frequencies by AMT soundings along this geodynamic profile cannot be connected with the MT isoohm profile and the fractures of the area unless the disturbed data are omitted.

Upon comparing the "filtered" AMT isoohm profiles with the original ones (Fig. 6a and 6b), the increase of the values at 41 and 230 Hz in the villages can clearly be seen. On the "filtered" profiles the minimum q_a values appear above the transversal fractures around the villages Ukk and Dabronc. The same can be seen in the residual profiles, which describe the logarithmic behaviour of q_a at each individual measuring point normalized by the regional average of the q_a (Fig. 7).

In the Börzsöny Mts the Eötvös Loránd Geophysical Institute (ELGI) Budapest, carried out ore prospecting using a combination of different geoelectric and IP methods.

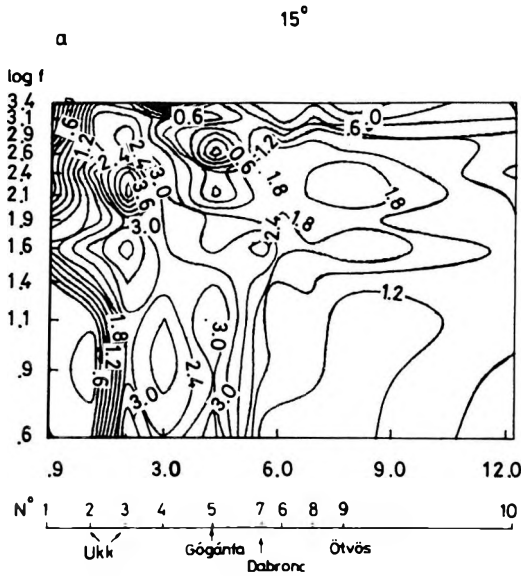


Fig. 6. a. Isohm section along the Transdanubian geodynamic line

6. a. ábra. Izoohm szelvény a dunántúli geodinamikusszelvény mentén

Рис. 6. а. Разрез изоом по Задунайскому геодинамическому профилю

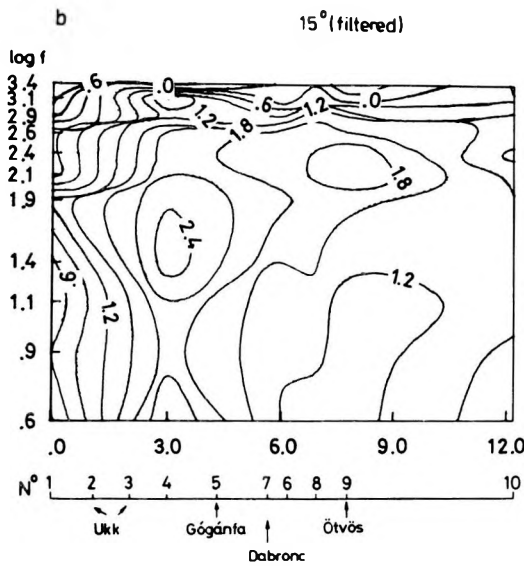


Fig. 6. b. Isohm section along the Transdanubian geodynamic line omitting data of the disturbed points (2, 3, 5, 7) and the r_a values at 41 Hz and 230 Hz

6. b. ábra. Izoohm szelvény a dunántúli geodinamikusszelvény mentén, a zavarral terhelt pontok (2, 3, 5, 7) és a 41 Hz és 230 Hz frekvencián mért r_a értékek kizárásával.

Рис. 6. б. Профиль изоом по Задунайскому геодинамическому профилю с исключением данных, полученных на точках с помехами (2, 3, 5, 7), и значений ρ_a на частотах 41 Гц и 230 Гц

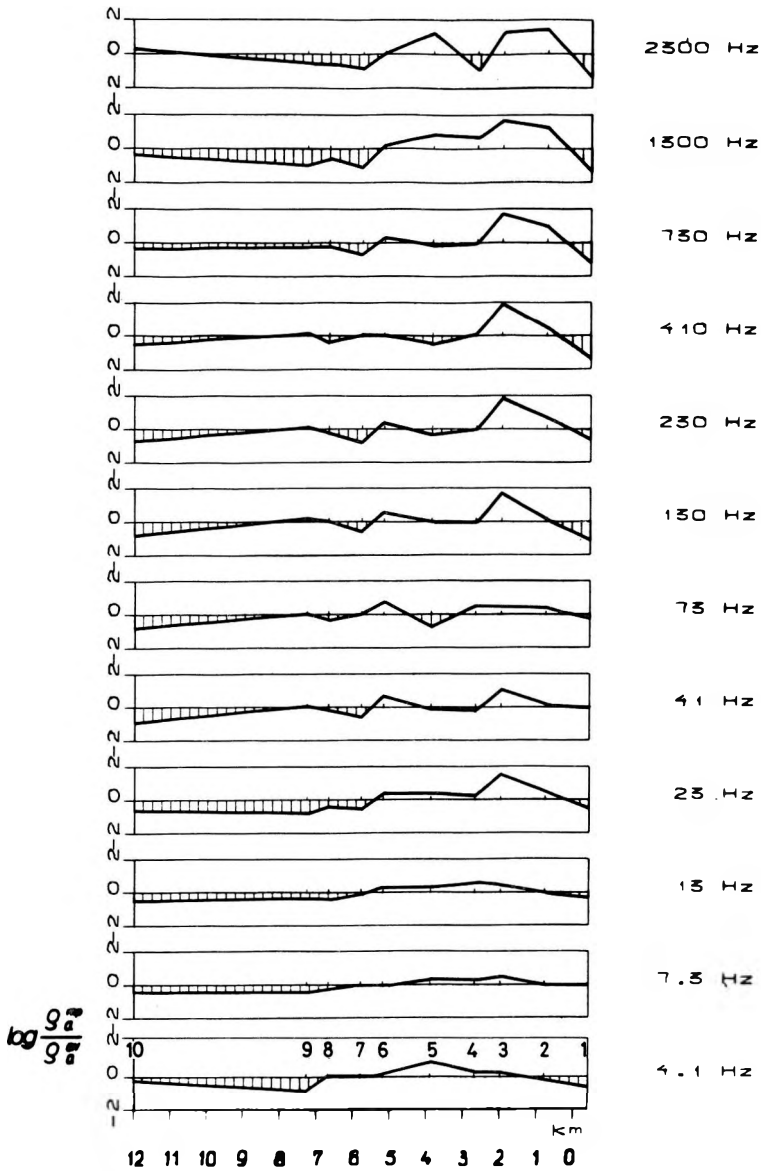


Fig. 7. Residual q_a profiles at each discrete frequency. The direction of the telluric line is 285° (E-polarization)

7. ábra. Maradék q_a szelvények az egyes diszkrét frekvenciákon. A tellurikus vonal iránya 285° (E-polarizáció)

Рис. 7. Профили остаточных значений q_a на каждой дискретной частоте. Направление теллурической линии — 285° (поляризация E)

In Fig. 8 the AMT Q_a -profiles at 4.1 Hz are compared with the resistivity values of a gradient array measured by ELGI above an ore-bearing formation which was verified by a borehole at the point 0.2 km. Irrespective of the different scales, the low resistivity ore formation is well indicated by the AMT profiles in both directions showing its lateral extent, in accordance with earlier experiments of the Oulu group in Finland [PELKONEN ET AL., 1979]. The low-frequency residual profiles in Fig. 9 delineate laterally fairly accurately the ore formation. This formation pinches out at the left side of the profile between 0.1 and 0.15 km, because both polarizations indicate this pinching out at the same point. The different behaviour of the residual profiles of the E- and H-polarization at the lowest frequencies on the right could be explained by the deepening of the top of the formation to the right.

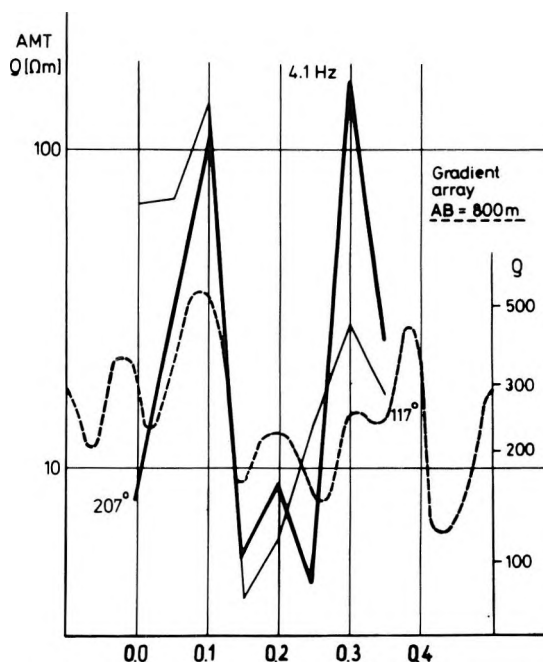


Fig. 8. Geoelectric and AMT profiles measured above an ore-bearing formation in the Börzsöny Mts in the directions of 117° (thin line) and of 207° (thick line)

8. ábra. Geoelektromos és AMT szelvények egy érces formáció felett a Börzsönyben, 117° (vékony vonal) és 207° (vastag vonal) irányban

Рис. 8. Геоэлектрические и АМТ профили, полученные над рудной формацией в горах Бёржёнъ по направлениям 117° (тонкой линией) и 207° (жирной линией)

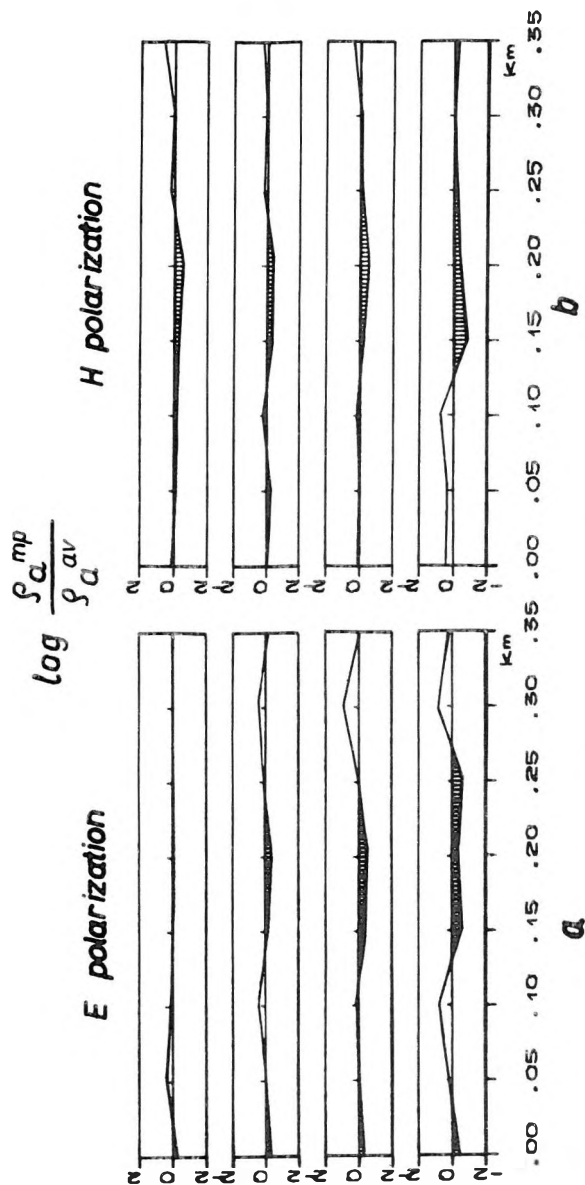


Fig. 9. Residual Q_a profiles above an ore-bearing formation in the Börzsöny Mts. The direction of the telluric line is: a) 207° (E-polarization); b) 117° (H-polarization)

9. ábra. Magadék Q_a szelvény érces formáció felett a Börzsönyben. A tellurikus vonal iránya a) 207° (E-polarizáció); b) 117° (H-polarizáció)

Рис. 9. Профили остаточных значений Q_a над рудной формацией в горах Бёржёнъ. Направления теллурической линии: а) 207° (поляризация Е); б) 117° (поляризация Н).

3. Noise level

As is shown in Fig. 2, the ϱ_a values at 41 and 230 Hz are significantly increased by stray (leakage) currents caused by power lines of about 50 Hz and its harmonics. The same conclusion can be drawn from the original isoohm profiles measured along the geodynamic line between Ukk and Ötvös (Fig. 6a), where the signals are increased by about two orders of magnitude at 41 and 230 Hz in the villages. Since the noise mainly appears in the electric components it increases the ϱ_a values. On the basis of the ϱ_a values measured at 41 Hz, 3 noise groups were supposed. The average sounding curve for these groups indicates that the average level of the most noisy sounding curve (group 3) should be much higher than the background given by the other two average curves (Fig. 10):

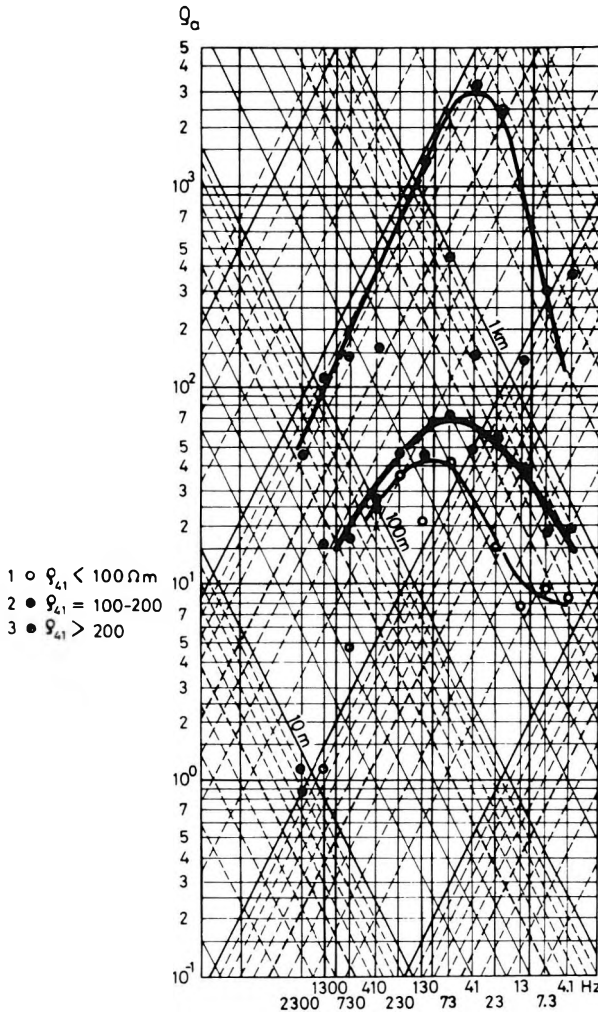


Fig. 10. Median AMT sounding curves of different disturbances

10. ábra. Átlagos AMT szondázási görbék különböző zavarokkal

Рис. 10. Средние кривые AMT зондирования с разными помехами

These results imply that in the neighbourhood of electricity consumers—mainly in villages—AMT measurements should be processed and interpreted with the greatest care. Also, notch filtering at the power line frequency and around its harmonics should be improved in the instruments.

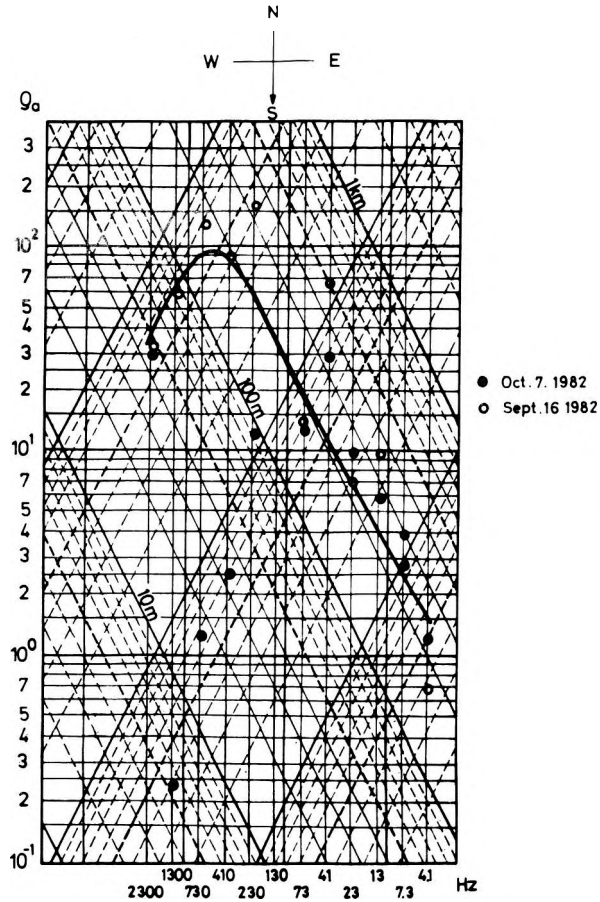


Fig. 11. AMT sounding data measured in the Nagycenk observatory on two different days in N—S direction (the full line indicates the smoothed AMTS-curve obtained on 16 September)

11. ábra. A nagycenki obszervatóriumban két különböző napon É—D irányban mért AMT szondázási adatok (a folytonos vonal a szeptember 16-án mért, simított AMT görbét jelzi)

Рис. 11. Данные AMT зондирования, полученные в обсерватории Надьценк в два разные дни по меридиональному направлению (сплошной линией проведена выравненная кривая AMT, полученная 16-го сентября)

4. Signal level

The attenuation of the electromagnetic field is well known from the literature [e.g. STRANGWAY, 1982]. In connection with Fig. 2 we have already indicated this effect between 410 and 2300 Hz. Due to this attenuation and to the conductive sediments the level of the signal mainly decreases in the electric components. Thus extremely low Q_a values were measured in this frequency band.

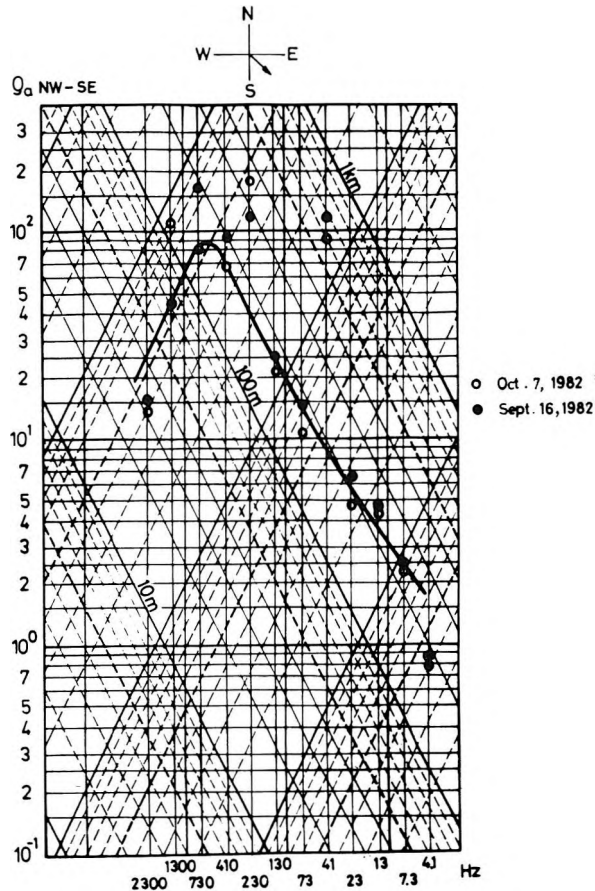


Fig. 12. AMT sounding data and a sounding curve measured in Nagycenk observatory on two different days in NW—SE (i. e. anisotropy) directions

12. ábra. AMT szondázási adatok és átlagos szondázási görbe, melyeket a nagycenki obszervatóriumban mértek két különböző napon, ÉNy—DK (azaz anizotrópia) irányban

Рис. 12. Данные AMT зондирования и средняя кривая зондирования, полученные в обсерватории Надьценк в два разные дни по направлению СЗ—ЮВ (т. е. анизотропии)

The ELF activity generally increases during the local afternoon; this means that the measuring conditions also improve in this frequency band. The signal intensity, therefore the attenuation, varies considerably from time to time. In Finland experience has shown sudden changes in the high frequency part of the AMT band. Very high harmonics contamination has also caused problems [HJELT, 1981]. The time variation in Hungary is demonstrated by two sounding curves measured on two different days: on 7 October much lower q_a values were obtained between 410 and 1300 Hz than on 16 September (*Fig. 11*).

The scatter of the scalar (two-component) AMT resistivity values can be somewhat reduced, i.e. the reliability of the data improved, for 2-D structured if measurements are made in the main structural (MT anisotropy) directions.

According to the basic relations of the magnetotelluric method, the main impedances Z_{xy} and Z_{yx} can be obtained using the following formulae:

$$\frac{E_x}{H_y} = Z_{xx} \frac{H_x}{H_y} + Z_{xy}, \quad \frac{E_y}{H_x} = Z_{yy} \frac{H_y}{H_x} + Z_{yx}$$

where the variation of the magnetic polarization H_x/H_y or H_y/H_x can be neglected in the direction where the secondary impedances Z_{xx} and Z_{yy} approximate zero. With 2-D structures these directions correspond to the anisotropy directions. In the Nagyecenk observatory the daily scatter of the q_a values is much smaller in certain directions than in other ones (see *Fig. 11* and *12*). The directions with lower scatter may be just the anisotropy directions.

5. Conclusions

Since signal and noise conditions generally influence first of all the electric components, the reliability of the measurements can be increased only if the q_a values are calculated from well-correlated electric and magnetic variation components, rather than from their average values. The effect of the time variation of the source field and of the 2-D and 3-D structures can obviously be better taken into consideration if the data processing of the AMT method approximates that of the MT.

The frequent occurrence of sufficiently energetic ELF signals and the use of microprocessor techniques, based on the tensorial relations between the EM field components having a great coherence, enable the use of field data processing for the AMT method. Measurements for a better understanding of the time variation and the coherence of the AMT source fields as well as a study of the data processing technique are aims of a joint Finnish-Hungarian project.

Acknowledgements

We thank A. Erkel, L. Szabadváry and L. Verő of the Eötvös Loránd Geophysical Institute and Z. Nagy and B. Péterfai of the Geophysical Exploration Company for supporting these investigations.

REFERENCES

- ÁDÁM A., VERŐ J., CZ. MILETITS J., HOLLÓ L., WALLNER Á., 1981: The geophysical observatory near Nagycenk. I. Electromagnetic measurements and processing of data. *Acta Geodet. Geophys. et Montanist. Acad. Sci. Hung.* **16** (2-4), pp. 333-351.
- HJELT, S. E., 1981: Scalar AMT in high latitudes — experiences and problems. Paper presented at the IV Scientific Assembly of IAGA, Edinburgh, August 1981.
- PELKONEN R., HJELT S. E., KAIKKONEN P., PERNU T., RUOTSALAINEN A., 1979: On the applicability of the audiomagnetotelluric (AMT) method for ore prospecting in Finland. Dept of Geophysics, Univ. of Oulu. Contribution No. 94, 25 pp.
- STRANGWAY D. W., 1983: Audiofrequency magnetotelluric (AMT) sounding. *Developments in Geophysical Exploration Methods-5*. Published by Applied Science Publishers Ltd, England.
- Tectonic map of the Little Hungarian Plain, constructed By J. Haas (1982)—personal communication to A. ÁDÁM.

SKALÁRIS AUDIOMAGNETOTELLURIKUS MÉRÉSEK MAGYARORSZÁGON

ÁDÁM ANTAL, PERTTI KAIKKONEN, SVEN-ERIK HJELT, JUHA TIIKKAINEN

Audiomagnetotellurikus (AMT) szondázásokat végeztünk Magyarországon a francia gyártmányú „ECA Resistivimètre” típusú műszerrel a 4,1–2300 Hz frekvenciatartományban, hogy megvizsgáljuk az AMT módszer alkalmazhatóságát különböző geofizikai problémák megoldására (a nagycenki elektromágneses obszervatórium környékén, üledékes medencében, földtani alapszelvényen és az érckutatásban stb.).

A fő következtetések az alábbiak:

- A legmegbízhatóbb információt a Schuman rezonancia harmonikusainak tartományában (7,3–23 Hz) kaptuk.
- A kristályos kőzeteken mért látszólagos ellenállás (ρ_a) értékek megbízhatósága nagyobb, mint az üledékeken mértéké, mivel az utóbbi esetben az elektromos tér sokkal kisebb amplitúdója alapvetően rontja a jel/zaj viszonyt.
- A ~50 Hz-es távvezetékek által okozott zajszint a legmagasabb 41 és 230 Hz-en. A kóbor (levezetési) áramok forrásának közelében (főleg falvakban) a ρ_a értékek általános szintje megnövekedett a forráshoz „közeli zóna”-ban végzett frekvenciaszondázás szerint.
- Egy energiahányos szakasz van 730 és 2300 Hz között a Föld-ionoszféra üregben bekövetkező ELF jel csillapodás miatt, itt a ρ_a értékek alacsonyak.

A koherencia ellenőrzése híján a skalár mérésekben nehéz különbséget tenni a jelnek, illetve zajnak tekintendő EM terek között, ezért szükséges a tenzorális adatfeldolgozás és a természetes audiófrekvenciás terek vizsgálata. E célból egy digitális regisztráló fejlesztését kezdtük el.

А. АДАМ, П. КАЙКОНЭН, С. Э. ХЕЛТ, Й. ТИКАЙНЭН

СКАЛЯРНЫЕ АУДИОМАГНИТОТЕЛЛУРИЧЕСКИЕ ИЗМЕРЕНИЯ В ВЕНГРИИ

Аудиомагнитотеллурические зондирования (АМТ) были проведены в Венгрии с аппаратурой французского выпуска «ЕСА Resistivimètre» в диапазоне частот 4,1–2300 Гц с целью изучения возможности применения метода АМТ для решения различных геофизических проблем (около электромагнитной обсерватории с. Надьценк, в осадочном бассейне, по геологическим основным профилям, при поисках и разведке рудных месторождений и т. п.).

По этим работам были сделаны следующие заключения:

- Наиболее надежная информация была получена в диапазоне гармонических резонанса Шумана (4,1–23 Гц).
- Надежность измеренных на кристаллических породах значений кажущегося сопротивления (ρ_a) выше значений, полученных на осадочных породах, так как в последнем случае значительно более низкая амплитуда электрического поля существенно ухудшает отношение сигнал/шум.
- Уровень шумов ~ 50 Гц, вызываемых линиями электропередачи, является наиболее высоким на частотах 41 и 230 Гц. Вблизи источников блуждающих токов (отвода) (главным образом в деревнях) общий уровень значений ρ_a увеличивался по частотному зондированию, проведенному в «близкой зоне» источника.
- Наблюдается участок с дефицитом энергии между 730 и 2300 Гц в связи с затуханием сигнала ELF в полости Земля-ионосфера, здесь получают низкие значения ρ_a .

В отсутствие проверки сходимости по скалярным измерениям трудно различить ЭМ поля, рассматриваемые как сигнал или шум, в связи с этим требуются тензорная обработка данных и исследование естественных полей звуковых частот. Для такой цели начата разработка цифровой регистрирующей аппаратуры.

TWO- STEP DECONVOLUTION OF GAMMA-RAY LOGS

Jiří ŠAMŠULA*, Jarmila ZEMČÍKOVÁ*

The natural radioactivity of rocks in a borehole is measured by gamma well-logging. The measured curve, however, is affected by the measurement itself, the logging equipment and by the interaction, dispersion and mutual shielding of layers. The possibilities of reducing these effects are shown using deconvolution operators supposing knowledge of certain measurement conditions. The corrected values better correspond with the true geological situation.

d: gamma-ray logging, computer evaluation, deconvolution, filter technique

1. Introduction

The application of computer techniques in well-logging measurements has enabled the use of certain transformations in the processing of field data which, even if useful, have not been utilized up to now because of the demands on numerical operations, though these are elementary ones. Many authors have been inspired by this problem and considerations and attempts similar to those proposed here have appeared in the literature [GEORGE ET AL. 1962, 1964, RICE 1962, CONAWAY 1980].

The natural radioactivity of rocks in a borehole is characterized by the intensity of gamma-rays measured by a moving scintillation probe with appropriate integration equipment. However, the measured curve is affected both by the parameters of the measuring equipment, and by the interaction, dispersion and mutual shielding of layers. Consequently, the data from the measurements may only partially correspond to the true geological situation. The borehole profile can be differentiated by the measured curve with partial resolution only. In this paper it is proposed that there may be the possibility to improve the situation by mathematical transformation of the measured curve—by convolution with a suitable operator.

* Geofyzika n.p., Brno, POB 62, 612 46 Brno 12, Czechoslovakia
Paper presented at the 28th International Geophysical Symposium, 28 September–1 October, 1983, Balatonszemes, Hungary

2. Mathematical base

Let us consider the following: for an idealized model course of a physical parameter along a borehole profile the response of the measuring equipment is either known or is to be derived. The relationship between these course is to be defined either with high precision or with a suitable approach by the convolution integral

$$v(h) = \int_{-\infty}^{\infty} g(h - \tau) s(h) d\tau = g(h) * s(h) \quad (1)$$

where $s(h)$ represents the true course of a physical variable depending on a depth h , $v(h)$ the response of the measuring system, and $g(h)$ the impulse response of a linear filter which may represent the measuring system. The convolution integral may be expressed as a weight integration with a shifting weight function $g(h - \tau)$. The analysis of a filtering function has often been carried out in a frequency domain. If the term of frequency has been introduced, then it has to be considered as a variable reciprocal whether to time or length, according to the nature of the solution.

If equation (1) holds, a reciprocal solution is proposed

$$s(h) = v(h) * \frac{1}{g(h)} \quad (2)$$

which implies a theoretical possibility to determine by the convolution operation the true course of a measured physical variable. The possibility, which has long been known, is based on the knowledge of the inversion of the impulse response $1/g(h)$ of a linear filter. In practical applications, however, the above mentioned computation difficulties need to be overcome. The executing of the convolution operation, e.g. for two long numerical series, requires a great number of elementary arithmetical operations.

3. Application to gamma-logging measurements

Let us propose a borehole profile, as outlined in *Fig. 1*, a radioactively barren material with a thin active layer (a). In static measurements along the borehole profile by a sensor we obtain a curve (b). In measurements by a moving sensor the measured curve has been deformed as a function of velocity and direction of the motion—curves (c) and (d)—and partly due to the time constant of the impulse counter. Curve (b) was termed by Conaway (1980) as the Geologic Impulse Response (GIR). This curve represents the physical variable measured along the borehole profile and the input into the measuring

* is the symbol designating the convolution

apparatus, which causes further deformations. If the original geological situation is to be achieved from the measured curve, we proceed in two steps. Firstly, the deforming influence of the measuring channel is to be suppressed, whereby the GIR curve is obtained. Then, by the inversion of the GIR curve the true geological situation is achieved.

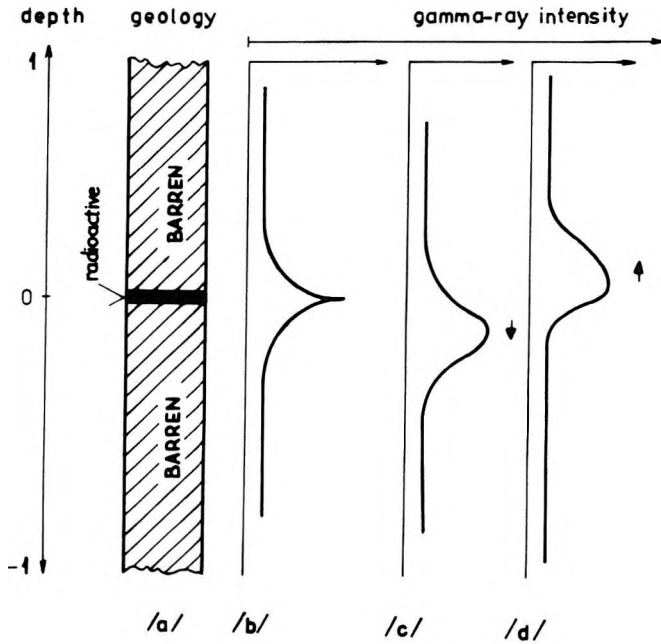


Fig. 1. a) Geologic column showing a thin zone of radioactive material embedded in barren rock

b) Ideal simulated gamma-ray log run past the thin radioactive zone with a digital system having a point detector

c) Simulated log run past the thin radioactive zone with an analog logging system having an exponential ratemeter; log run in downhole direction

d) Same as c) except log run in uphole direction [after CONAWAY 1980]

1. ábra. a) Meddő kőzetbe ágyazott vékony radioaktív zónát szemléltető rétegsor

b) Ideálisan szimulált gamma-sugár szelvény pontszerű detektoros digitális rendszerrel

c) Szimulált szelvény exponenciális rateméterrel működő analóg szelvényező rendszerrel; lefelé való szelvényezés

d) Mint c) de felfelé való szelvényezéssel [CONAWAY 1980 után]

Рис. 1. a) Геологический разрез с тонкой прослойкой радиоактивного вещества, вмещенной в пустой породе

b) Идеально симулированная диаграмма ГК при использовании цифровой системы с точечным детектором

c) Симулированная диаграмма при использовании аналоговой измерительной установки с экспоненциальным счетчиком импульсов; замер был проведен при пуске зонда

d) г. ж. как c) при подъеме зонда
[по КОНЭВЕЙ, 1980 г.]

The reaction of most commercially manufactured counters with integrators can be expressed in a simple exponential function

$$f(h) = 0, \quad h < 0$$

$$f(h) = \frac{1}{vT} \cdot e^{-h/vT}, \quad h \geq 0 \quad (3)$$

where h is the depth, T the time constant of the sensor, and v the velocity of the sensor.

This function can be called the impulse response of the sensing equipment. To eliminate the influence of the sensing equipment one must know the inverse of the $f(h)$ function. This function can be calculated by two methods—either in the frequency or time domain. Using the first method, CONAWAY [1980] calculated a three-element operator of the following type

$$\frac{1}{f(h)} = \left(\frac{vT}{2\Delta h}, \quad 1, \quad -\frac{vT}{2\Delta h} \right) \quad (4)$$

where Δh represents the sampling interval. Essentially, this operator solves the first deconvolution step.

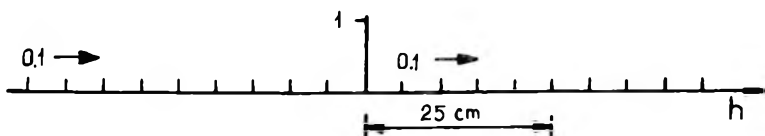
In practical applications of these operators problems may arise. If we take a sampling interval from 5 cm to 50 cm in deep drilling, and consider that the measurement is suppressed by some sort of fluctuations, then the application of the two- or more element operator is undesirable. In practical applications the following procedure and solution have been introduced. Let us calculate with the parameters:

$$v = 0.09 \text{ m/s}, \quad T = 5 \text{ s}, \quad \Delta h = 5 \text{ cm}$$

To calculate the operator elements let us take $\Delta h = 25 \text{ cm}$

$$\frac{vT}{2\Delta h} = 0.9$$

This value enables the operator to be constructed, its marginal elements will be distributed into nine samples:



This procedure is practically a combination of the calculated operator and a smoothing one.

By the above demonstrated transformation we obtain the curve which corresponds to that designated by CONAWAY [1980] as GIR. In theory, the next step—which implies additional inversion—gives a possibility to obtain a model of the original geological situation. The GIR curve in *Fig. 2* has the form

$$(h) = e^{-\alpha(h)} \quad (5)$$

where α is the constant including the influence of the activities of a thin layer, the probe sensitivity, the borehole influence, the dispersing effect of a barren media, etc. While in a preceding procedure for determining the inversion to eliminate the influence of the sensor the parameters v and T remained constant during the measurement, this cannot be stated definitely. In view of this we have carried out the analysis of the relation with respect to the changing of α . Accounting for the unchangeable borehole diameter, the probe diameter approaching the borehole diameter and, further, providing for the non-existence of materials along the borehole profile with the shielding effects for gamma-ray approaching that of lead and similar materials, we can consider the α constant as the invariable along the borehole profile. Nevertheless, the calculation of the concrete value of α still remains difficult. Similarly, the construction of a model in 4π geometry is not simple, nor is its calculation. In the first approach we proceeded as follows: a GIR curve with a double exponential course was proposed and we could estimate the α value directly from the measured curve. If α equals 1, then $\varphi(h)$ is equal to 1 for $h=0$. For $h=1$ the $\varphi(h)$ value decreases to 0.36. If the GK log exhibits an expressive active layer, then the depth interval (distance) in which the anomaly decreases from its 100% to 36% can be considered as characteristic for the α value of the given probe and the given situation in a borehole. Assuming all this, we can derive the inverse for the $\varphi(h)$ function, which represents the deconvolution operator of the second step. We can derive the inverse for the $\varphi(h)$ function by numerous methods. Problems of deriving the inversion model have been analysed and solved by the fundamental approach of ROBINSON [1967], KANASEWICH [1973], KULHÁNEK [1976], and others. In our applications we have advantageously utilized the procedure and algorithms developed by MEREU [1978]. The above quoted author has published a complete description of a computer program to obtain the weights of a time-domain wave-shaping filter program. Although this was developed for seismic applications, its applications may be even wider.

The following table shows the output from the program in which the values

$$\varphi(h)^* = (0.05; 0.13; 0.36; 1; 0.36; 0.13; 0.05)$$

have been introduced in the calculation as the given function (W column). The desired function has been given as the value 1 in column D. The desired operator is calculated in column F. In column H a checking calculation has been entered

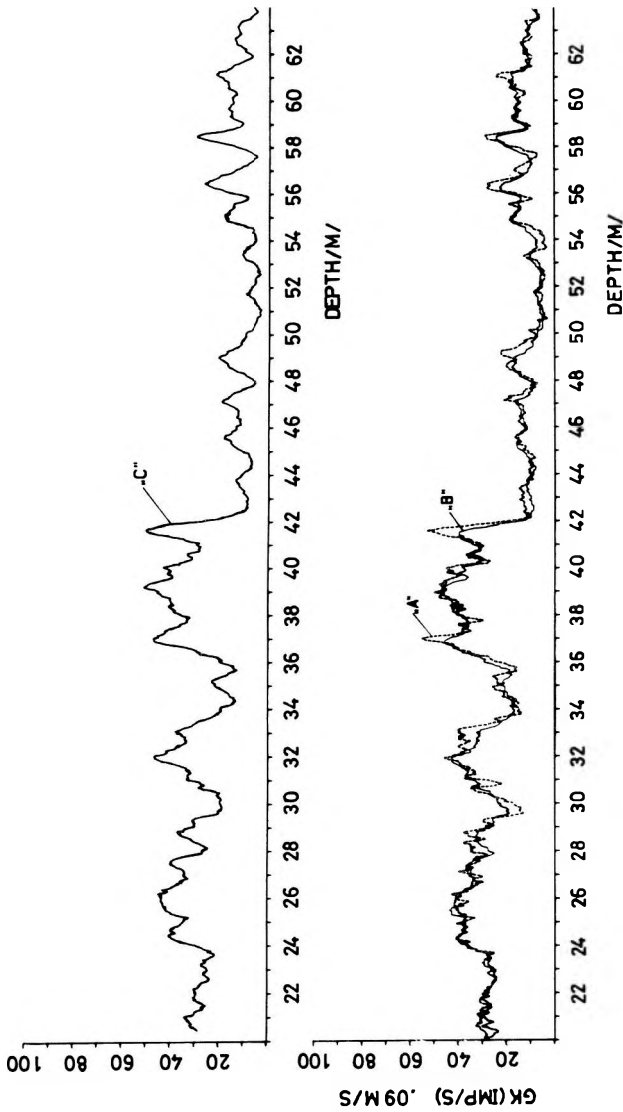


Fig. 2. Gamma-ray log. A — quasi-static measurement; B — measurement with probe velocity 0.09 m/s; C — after filter application

2. ábra. Term. gamma szelvény. A — kvázistatikus mérés. B — 0,09 m/s szondasebességgel való mérés; C — szűrő alkalmazása után

Рис. 2. Диаграмма ГК. А — квазистатическое измерение; В — измерение при скорости подъема 0,09 м/с С — После применения фильтра

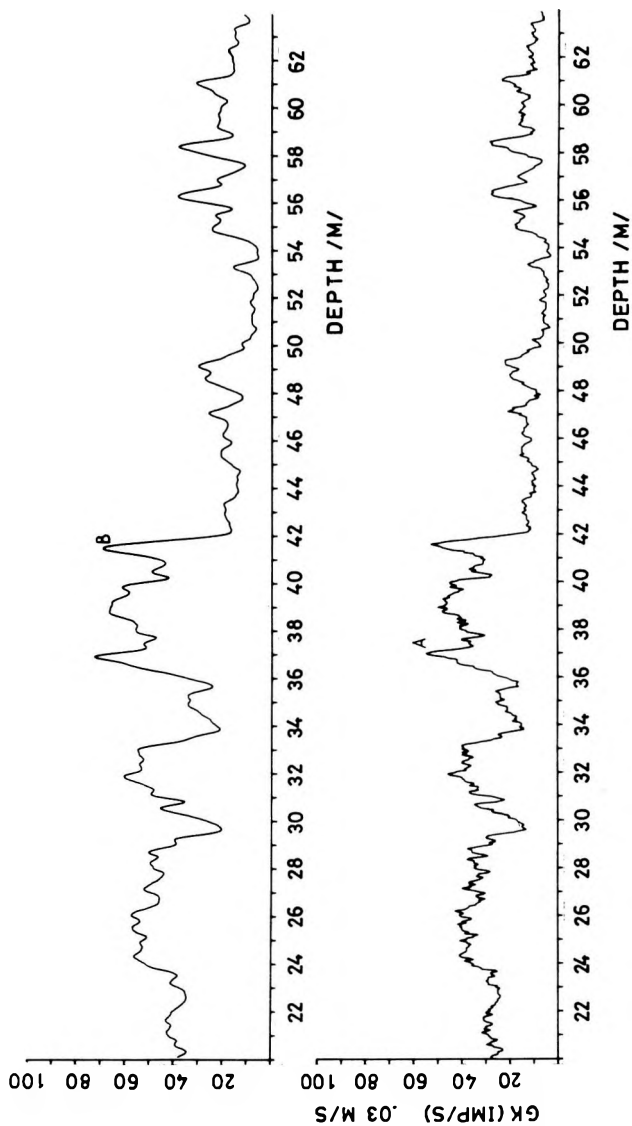


Fig. 3. Experimental application of the second deconvolution. A — primary gamma-ray log;
B — GIR inversion

3. ábra. A második konvolúció kísérleti alkalmazása. A — elsődleges term. gamma szelvény
B — GIR inverzió

Рис. 3. Экспериментальное применение второй деконволюции. А — первичная диаграмма
ГК; В — инверсия GIR

of the calculated operator with the given function. It is evident that we have achieved the value 1 with the error of 0.013, which is certainly sufficient, no matter that some mild oscillations may occur.

Thereby, we have derived the operator for the second deconvolution step and we can proceed to the practical calculation.

Time	Given wavelet		Desired wavelet		Correlation functions		Symmetric filter		Shaping filter		Actual output		Shaping errors	
	W	D	R	S	G	F	H	E						
-5			.013		-.046	-.008	.000	3.E-04						
-4			.053		.104	.030	-.001	-7.E-04						
-3	.050		.194	.050	-.085	-.021	.001	6.E-04						
-2	.130		.426	.130	.193	.001	-.001	-1.E-03						
-1	.360		.827	.360	-1.054	-.400	.007	7.E-03						
0	1.000	1.00	1.304	1.000	1.994	1.277	.987	-1.E-02						
1	.360		.827	.360	-1.054	-.400	.007	7.E-03						
2	.130		.426	.130	.193	.001	-.001	-1.E-03						
3	.050		.194	.050	-.085	-.021	.001	6.E-04						
4			.053		.104	.030	-.001	-7.E-04						
5			.013		-.046	-.008	.000	3.E-04						

4. Example of application

Let us adduce an example of the natural gamma activity measurement in *Fig. 2*. Curve *A* implies the measurement carried out so very slowly that it can be regarded as a static one. The used time constant is 5 s. Curve *B* represents the measurement with the velocity of 0.09 m/s. The decrease of the maxima can distinctly be observed as well as their shifting along the depth axis. Curve *C* represents the result of the operator application, as outlined earlier. It is apparent that the operator restored the values of the maxima and their positions along the depth axis very well.

An experimental application of the second deconvolution step is attempted in *Fig. 3*. The deconvolution operator demonstrated in the table in the preceding section has been applied to curve *A* in *Fig. 2*. For the α constant determination a section of the curve has been utilized at a depth of 41–42 m. where an intense step of the registered gamma-ray intensity occurs. We have estimated the distance of 0.3 m in which the intensity decreases to 0.36%. Then, the α constant is 3.33, which is the input value for the calculation of the double GIR exponential model. This again serves as the input for the MEREU program (see the table in the preceding section). It is clearly seen in *Fig. 3* that after the transformation the resulting curve exhibits an increase in the maxima of approx. 30%, as compared with the original transformed curve. Hence, the credibility of the transformation depends on our ability to estimate correctly the α constant and to accomplish the demand that the α constant be invariable along the borehole profile.

5. Conclusion

In conclusion we may say that the first transformation and its results are directly applicable in practice. The anomaly amplitude is restored and the anomalies are positioned at the proper depth. The second transformation, as stated above, is dependent on the credibility of the α constant determination.

REFERENCES

- CONAWAY J. C., 1980: Exact inverse filters for the deconvolution of gamma-ray logs. *Geoplotation*, **18**, pp. 1–14.
- GEORGE C. F., Jr., SMITH H. W., BOSTICK F. X., Jr., 1962: The Application of inverse convolution techniques to improve signal response of recorded geophysical data. *Proceedings of the I.R.E.*, November.
- GEORGE C. F., Jr., SMITH H. W., BOSTICK F. X., Jr., 1964: Application of inverse filters to induction log analysis. *Geophysics*, **29**, 1, February, pp. 93–104.
- KANASEWICH E. R., 1973: Time sequence analysis in geophysics. The University of Alberta Press.
- KULHÁNEK O., 1976: Introduction to digital filtering in Geophysics. Elsevier Scientific Publishing Company, Amsterdam–Oxford–New York.
- MERU R. F., 1978: A computer program to obtain the weights of a time—domain wave—shaping filter which is optimum. *Geophysics*, **43**, 1, February, pp. 197–215.
- RICE R. B., 1967: Inverse convolution filters. *Geophysics*, **27**, 1, February, pp. 4–18.
- ROBINSON E. A., 1967: Multichannel time series analysis with digital computer programs. Holden-Day, San Francisco, Cambridge, London, Amsterdam.

A GAMMA-SUGÁR SZELVÉNYEK KÉT LÉPÉSES DEKONVOLUCIÓJA

J. ŠAMŠULA, J. ZEMČIKOVÁ

A szerzők természetes radioaktivitás meghatározást végeztek egy fúrásban gamma-szelvényezés útján. A kapott görbét befolyásolják a mérési folyamat és a műszer jellemzői, valamint a rétegek kölcsönhatásai, diszperziós és árnyékolási folyamatai. A cikk bemutat egy dekonvolúciós eljárást, amely lehetővé teszi a zavaró hatások csökkentését, feltéve, hogy bizonyos mérési körülmények ismeretesek. A korrigált értékek jó egyezést mutatnak a földtani viszonyokkal.

ДВУХСТЕПЕННАЯ ДЕКОНВОЛЮЦИЯ ГАММА-КАРОТАЖНЫХ ИЗМЕРЕНИЙ

И. ШАМШУЛА, Я. ЗЕМЧИКОВА

Естественная радиоактивность горных пород в разрезе скважины была измерена при использовании ГК. На измеренную кривую ГК существенное влияние оказывают собственный измерительный процесс и аппаратура, с одной стороны, и взаимное рассеяние и экранирование в пластах с другой. В работе показаны возможности уменьшения этих влияний при помощи операторов деконволюции, допуская, что известны определённые условия измерения. Исправленные величины таким образом лучше соответствуют действительной геологической обстановке.

SPECTRAL MEASUREMENT OF NATURAL GAMMA RAYS UNDER MODEL AND BOREHOLE CONDITIONS

Róbert DORKÓ*

Spectral gamma-ray logs yield useful information for solving complex geological problems. The paper deals with investigations concerning, and calibration of, the gamma-ray measurements under model conditions, in order to lay the foundations of the practical applications. Well logging tools for determining the natural radioactive material content of rocks must be calibrated for energy and quantitatively. The pulse numbers obtained in different energy windows are strongly influenced by the borehole conditions and for correct interpretation of natural gamma-ray spectral measurements these effects should be taken into account.

d: spectral log, gamma-ray methods, models, calibration, borehole conditions

1. Introduction

Investigations using the spectral gamma-ray logging method have been carried out in Hungary for the past ten years. During the same period the first spectral probes were introduced.

When interpreting gamma-ray logs one has to determine the anomaly caused by radioactive elements in the rocks surrounding the borehole.

From the log one can determine the potassium-, uranium-, and thorium content of the rocks thereby obtaining important data on the quantitative and qualitative shale-content of the individual layers, for lithologic studies on the rocks, for stratigraphic correlation, etc.

The method also plays an important role when studying the geological conditions of the genesis of the given mineral constituents. Potassium accumulates as a result of the decomposition of acid magmatic rocks, mainly in shales. Uranium is easily soluble, mobile, it can migrate large distances, and easily be absorbed by organic materials. Thorium associates with highly resistive minerals (zirconium, monazite, rutile); it can also accumulate in bauxites.

Energy—selective well—logging tools consist of three basic parts: borehole equipment, surface analyser, recorder. In the borehole tool we apply an energy-selective NaI (Tl) scintillation crystal detector. Energy stabilization is provided by means of the reference isotope placed in the probe [e.g. ^{65}Zn (1.118 MeV); ^{137}Cs (0.66 MeV)]. The borehole tool is placed in a pressure-tight case (up to 200 atm.), the maximum borehole temperature is 120° C. The probe can be supplemented by an isotope extension for neutron-induced captured gamma-

* Eötvös Loránd Geophysical Institute of Hungary, POB 35, Budapest, H-1440.
Manuscript received: 8 November, 1983

ray measurements. In the most generally used surface analysers four arbitrary spectral windows can be selected. The windows are set either by means of potentiometers determining their lower and upper limits, or by potentiometers adjusting the midpoint and the width of the window. In a technically much simpler version the setting of the window is carried out by a changeable, preset program-plug. This is a very convenient system, although during measurement the operator cannot intervene. In digital well-logging system, a 120 channel analyser is used; the entire energy spectrum appears on the display; recording is in analog form.

2. Measuring technique

The calibration of spectral measuring systems is performed in two steps: calibration of the energy scale and calibration of the energy windows for the corresponding radioactive element content.

Calibration of the energy scale consists in the determination of the gamma-photon energy—signal amplitude (channel number) characteristics of the measuring system. This is achieved by means of mono-radiative calibrating isotopes. The required energy windows are set on the basis of these characteristics. In the case of spectral gamma-ray logging the following windows are used:

Window No.1: (^{40}K isotope 1.46 MeV)	1.34–1.58 MeV
Window No.2: (RaC modification 1.76 MeV)	1.60–2.03 MeV
Window No.3: (Quasi integral)	1.34–3.00 MeV
Window No.4: (ThC'' modification 2.62 MeV)	2.45–3.00 MeV

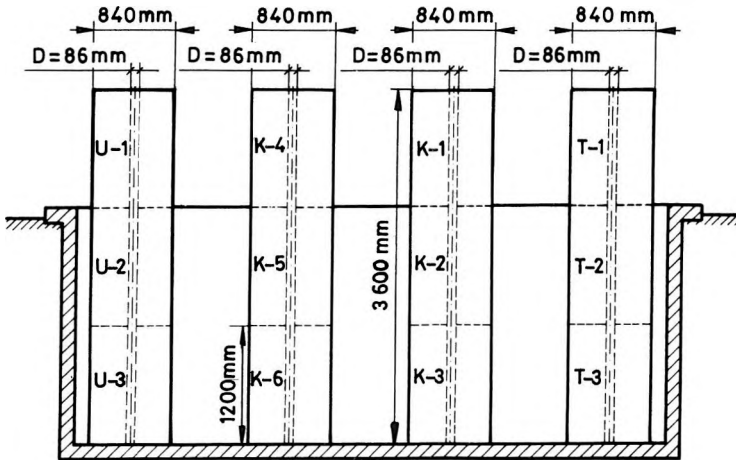


Fig. 1. Schematic outline of the standard series developed by ELGI for spectral gamma-ray logging

1. ábra. A természetes gamma spektrális etalonsor sematikus vázlata

Рис. 1. Схема серии эталонов для спектрального измерения естественного гамма-излучения

3. Calibration

The task of quantitative calibration is to determine a relationship between the content of the radioactive element and the impulse numbers obtained in the energy windows. For this task, ELGI has developed a standard series (Fig. 1). This standard series consists of 6 different potassium layers, and two times 3 layers containing different amounts of uranium and thorium, respectively. The amount of radioactive material in these standard materials spans the range of values usually encountered in well-logging practice, except when directly logging for radioactive ores. The material of the model layers is quartz sand enriched with potassium, uranium or thorium. The homogeneity of the individual layers was earlier checked by analysing 300 samples from different parts

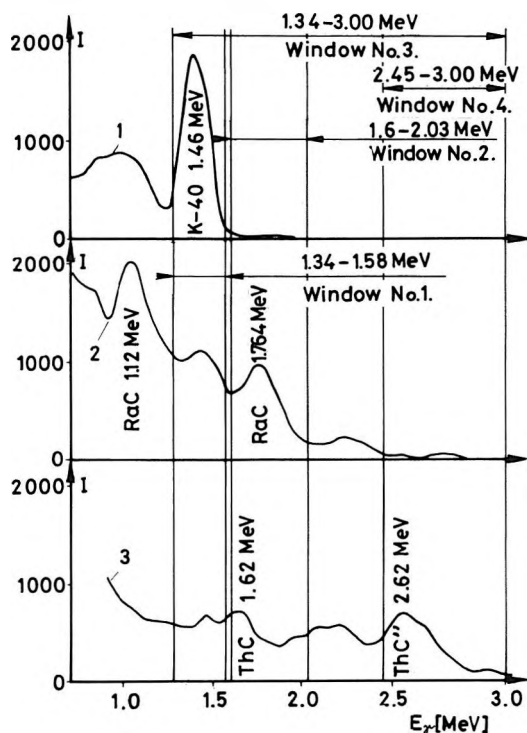


Fig. 2. Gamma-ray energy spectra obtained in the different layers. 1 — layer containing 13.8% potassium; 2 — layer containing 160 ppm uranium; 3 — layer containing 234 ppm thorium

2. ábra. Az egyes etalonrétegekben felvett természetes gamma energia spektrumok. 1. spektrum: 13,8% kálium tartalmú réteg, 2. spektrum: 160 ppm urán tartalmú réteg, 3. spektrum: 234 ppm tórium tartalmú réteg

Рис. 2. Энергетические спектры естественного гамма-излучения, зарегистрированные в отдельных эталонных пластах. Спектр 1: пласт с содержанием калия 13,8%, Спектр 2: пласт с содержанием урана 160 ppm, Спектр 3: пласт с содержанием тория 234 ppm

of the layers. The layers are hermetically sealed from each other to prevent the emanation of radon and thoron gases formed during radioactive decay. The spectral probes developed in ELGI are calibrated using this standards. *Figure 2* shows gamma spectra recorded by a multichannel analyser in layers containing potassium, uranium and thorium, respectively. The energy windows, utilized in the measuring equipment—comprising the KRGE-1-120-60s probe and the KRF-4-12-An surface unit—,are also indicated. *Figure 3* shows the calibration diagram measured by the above-mentioned well-logging equipment in the thorium reference series, for a borehole of 86 mm diameter. The relationship is linear. The same holds for windows Nos. 1 and 2 in the uranium standard series, and for window No.1 in the potassium series. Having obtained the calibration diagrams, the coefficients of the system of equations used for interpretation can be computed for a borehole diameter of 86 mm.

Interpretation is carried out by "spectral stripping". As seen in *Fig. 2*, the impulse number in energy window No.4 depends on the thorium content alone, i.e. the thorium content can directly be determined from the pulse count. The number of impulses measured in energy window No.2 depends on the thorium- and uranium contents. If we subtract the value of the impulse number due to the thorium content from the number of impulses in window No.2, the uranium content can be determined by means of the calibrating diagram obtained in window No.2. Finally, upon subtracting from the number of impulses received in energy window No.1 those counts due to the thorium and uranium contents,

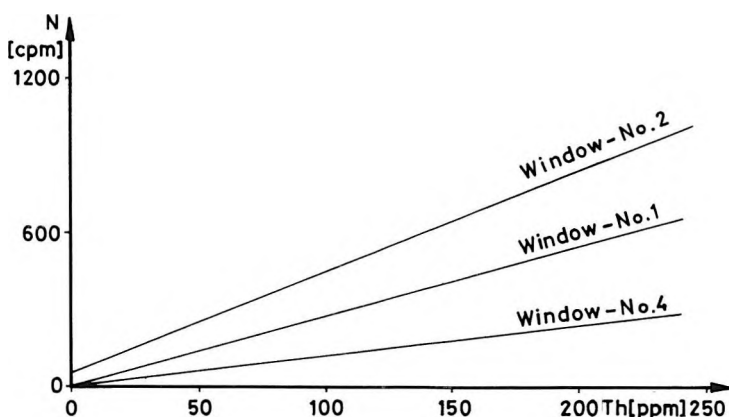


Fig. 3. Calibration diagrams measured in the thorium standard series

3. ábra. A tórium etalonsorban felvett hitelesítő diagrammok

Рис. 3. Калибровка диаграммы, зарегистрированные в серии эталонов тория

respectively, the potassium content can be determined by means of the corresponding calibrating diagram. Accordingly, interpretation is carried out by means of the following formulæ:

$$\begin{aligned} T &= \frac{N_4}{m_{4T}} \\ U &= \frac{N_2}{m_{2U}} - \frac{m_{2T}}{m_{2U}} T \\ K &= \frac{N_1}{m_{1K}} - \frac{m_{1U}}{m_{1K}} U - \frac{m_{1T}}{m_{1K}} T \end{aligned} \quad (1)$$

where T, U, K are the thorium, uranium and potassium contents; m_{iT} , m_{iU} , m_{iK} are the slopes of the calibrating diagrams obtained in the i -th window for the thorium, uranium and potassium series, respectively; N_i is the number of impulses measured in the i -th energy window.

4. Borehole correction and application

When we compared the results obtained from spectral logging with analyses carried out on core samples, it became evident that the borehole conditions (borehole diameter, formation density) and the lack of saturation of the series of standard layers of *Fig. 1* should be taken into account. In the present study the rocks penetrated by the borehole were assumed to be self absorbing cylinders of horizontally infinite extension; inside the cylinder the radioactive radiation sources being uniformly distributed. The axis of the cylinder coincides with that of the borehole. In *Fig. 4* the sufficiently thick layer is also saturated in the vertical direction, at the centre of this layer a detector along the borehole axis would indicate the radioactive intensity:

$$I = I_x - I_1 \quad (2)$$

where I_x is the intensity corresponding to a hypothetical borehole of 0 diameter; I_1 is the radioactive intensity due to the rock mass within the volume determined by the hole and the layer boundaries ($V = R^2\pi Z$). Using the well-known formula, intensity I can be expressed in terms of spherical coordinates as

$$I = I_0 \int_{\varphi=0}^{2\pi} \int_{r=\frac{R}{\cos\vartheta}}^{Z/2 \sin\vartheta} \int_{\vartheta=0}^{\arctg \frac{Z}{2R}} e^{-\mu_0 r} r^2 \cos\vartheta d\vartheta dr d\varphi \quad (3)$$

where I_0 is the intensity of the radioactive radiation source at an arbitrary point of the cylinder; R is the borehole radius; Z the thickness of the layer; ρ the

formation density; μ the mass absorption coefficient, having the following values in the different energy windows:

Window No.1:	0.050 cm ² /g
Window No.2:	0.046 cm ² /g
Window No.3:	0.0447 cm ² /g
Window No.4:	0.039 cm ² /g

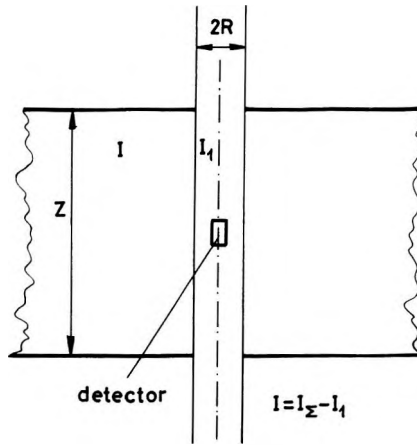


Fig. 4. Gamma radiation in boreholes

4. ábra. A természetes gammasugárzás fúrólukakban

Рис. 4. Естественное гамма-излучение в скважинах

The correction factor for the diameter; computed on the basis of Eq. (3), consists of two parts, as shown by Figs. 5 and 6. Figure 5 shows the correction for the case of a layer which is infinite (saturated) both horizontally and vertically. The vertical axis shows the I_{\max}/I_∞ ratio, where I_∞ is the intensity in a hypothetical infinitely extended layer for 0 borehole diameter; I_{\max} is the intensity to be measured in the middle of the infinitely extended (saturated) layer in the case of borehole radius R . The horizontal axis displays the value $\mu'R$ ($\mu' = \mu\rho$). In Fig. 6 the horizontal axis shows the ratio of layer thickness Z to borehole diameter $D = 2R$, the vertical axis is the value I/I_{\max} , where I_{\max} is the same as in Fig. 5, I is the intensity in the middle of the layer of thickness Z and of finite extension (as far as radioactive intensity is concerned), the parameter of the family of curves is the value $\mu'R$. If the value of $\mu'R$ is known, we read I_{\max}/I_∞ from the vertical axis of Fig. 5; further from the layer thickness and $\mu'R$ we obtain I/I_{\max} from Fig. 6, the product of these values yields the ratio I/I_∞ . This value shows the decrease of the intensity in a layer of thickness Z measured in a borehole of diameter D as compared with I_∞ ; that is, to the intensity measured in the middle of a hypothetical infinitely extended layer penetrated

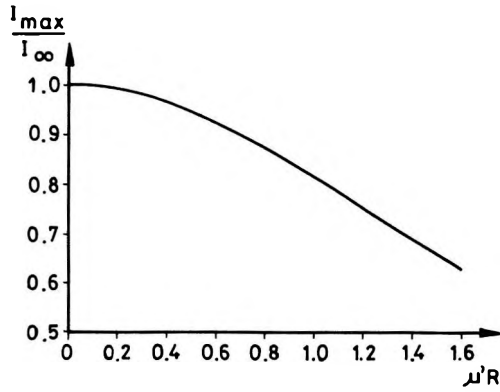


Fig. 5. Correction for a horizontally and vertically infinitely extended layer

5. ábra. A horizontálisan és vertikálisan végtelen kiterjedésű rétegre vonatkozó korrekció

Рис. 5. Поправка для пласта с бесконечным продольным и вертикальным распространением.

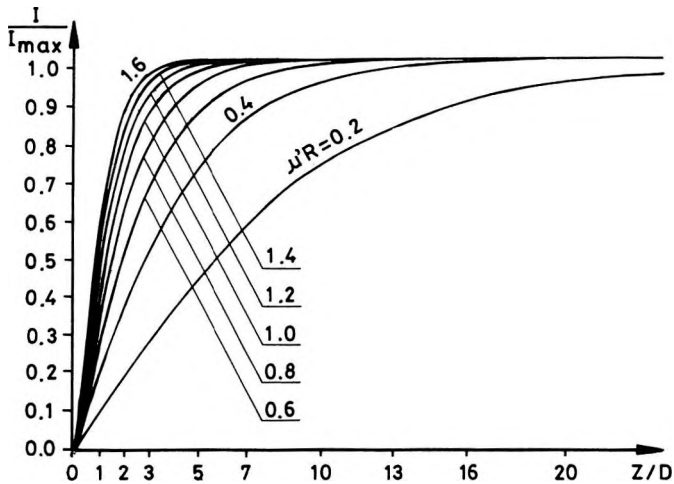


Fig. 6. Diameter correction diagram for spectral gamma-ray log

6. ábra. A természetes gammasugárzás spektrális méréseinek átmérő-korrekciós diagramja

Рис. 6. Поправочная диаграмма спектральных измерений естественного гамма-излучения за изменение диаметра скважины

by a hole of diameter 0. The correction factor for the borehole diameter (C_D) is the reciprocal of this value.

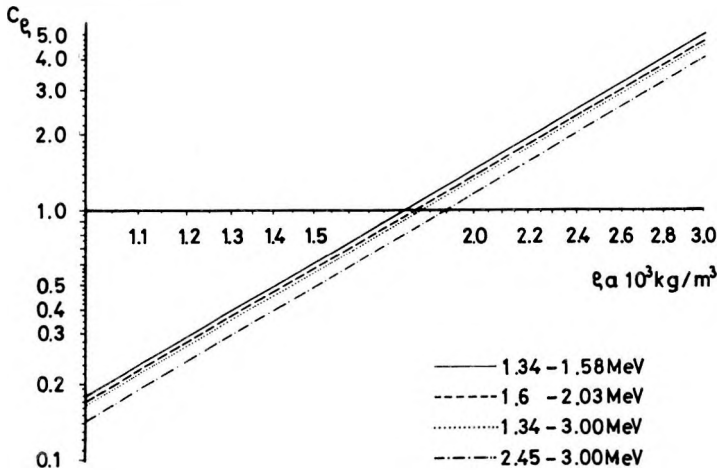


Fig. 7. Density correction diagrams for different energy windows for spectral gamma-ray logging

7. ábra. A természetes gamma spektrális mérések sűrűség-korrekciós diagramja az egyes energia ablakokban

Рис. 7. Поправочная диаграмма спектральных измерений естественного гамма-излучения за плотность по отдельным энергетическим окнам

Figure 7 shows in double logarithmic scale the density correction diagrams for the different energy windows, computed by means of Eq. (3). The horizontal axis is formation density. The density correction factor C_ρ corresponding to the given energy window can be read off. In the computation of the diagrams corrections have been applied to take care of the lack of saturation of the standard layers. This lack of saturation is due to the geometrical dimensions of the standard layers and to their density of $1.6 \cdot 10^3 \text{ kg/m}^3$. For the individual energy windows we have determined composite correction formulae containing the different correction factors, which best approximate the joint effect of the borehole diameter and rock density, and which facilitate computer processing of the well logs. For reference, the corresponding parameters of the standard layers were utilized (geometrical dimensions, density of the layers is $1.6 \cdot 10^3 \text{ kg/m}^3$, borehole diameter is 86 mm). The general approximating formula is

$$C = k\rho^3 \text{ch} (0.3212\mu' D + 0.0216) \quad (4)$$

For the different energy windows we have the following correction formulae:

Window No.1: $C_1 = 0.2520 \rho^3 \text{ch} (0.0257D + 0.0216)$

Window No.2: $C_2 = 0.2509 \rho^3 \text{ch} (0.0240D + 0.0216)$

Window No.3: $C_3 = 0.2506 \rho^3 \text{ ch } (0.0236D + 0.0216)$

Window No.4: $C_4 = 0.2491 \rho^3 \text{ ch } (0.0200D + 0.0216)$

where the borehole diameter D should be given in cm units, ρ is formation density. The number of impulses obtained in the different energy windows should first be multiplied by the correction factors C_i before proceeding to the spectral stripping step of the interpretation.

The well-logging equipment has also been used for spectral gamma-ray logging in some bauxite exploratory drilling. On the basis of the recorded logs, properly corrected as described above, we were able to determine the thorium, uranium and potassium contents of the penetrated formations by means of spectral stripping. The computed radioactive element contents have shown fair agreement with the laboratory analyses carried out on the core samples. Making use of the relationships published by HASSAN et al. [1976], we studied the relationship existing in bauxites between the thorium content and the aluminium or the silicium content respectively. These authors determined the thorium content from natural gamma spectral logs and parameter P was derived from the laboratory analysis of core samples as

$$P = \frac{\text{Al}_2\text{O}_3}{\text{Al}_2\text{O}_3 + \text{SiO}_2}$$

The results are shown in Fig. 8. The relationship between the two quantities can be considered linear in the interval $0.4 \leq P \leq 0.95$, with a correlation coefficient $r = 0.9025$. The line parallel with the vertical axis (Th axis) is the boundary line of the bauxites considered in Hungary as of industrial quality. Consequently, in the exploratory stage of prospecting a knowledge of the thorium content provides useful information for delimiting the likely areas for further prospecting.

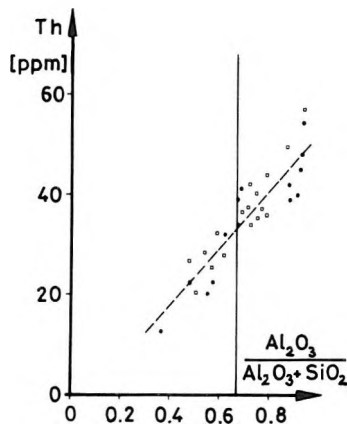


Fig. 8. Results obtained from exploratory drillings for bauxite

8. ábra. Vizsgálati eredmények a bauxitkutató fúrásokban

Рис. 8. Результаты в скважинах, бурящихся на бокситы

BIBLIOGRAPHY

- LEIPUNSKI O. I., NOVOZKILOV B. V. SOKHAROV V. N., 1960: Propagation of gamma radiation in matter (in Russian). Publishing House for Physical and Mathematical Literature, Moscow
- CZUBEK J. A., 1961: Some problems of the theory and quantitative interpretation of the gamma ray logs. Acta geophysica polonica, Vol. VIII, No.1/2
- LOCK G. A., HOYER W. A., 1971: Natural gamma ray spectral logging. The Log Analyst, 12 (5), 3-10, October
- HASSAN M., HOSSIN A., COMBAZ A., 1976: Fundamentals of the differential gamma ray log. Interpretation technique, Paper H., Transactions SPWLA
- FERTL W. H., 1979: Gamma Ray Spectral Data Assists in Complex Formation Evaluation. Transactions SPWLA Sixth European Evaluation Symposium, London

A TERMÉSZETES GAMMA SUGÁRZÁS SPEKTRÁLIS MÉRÉSE MODELL- ÉS FŰRŐLYUK VISZONYOK KÖZÖTT

DORKÓ RÓBERT

A természetes gamma spektrális karotázs hasznos információkat szolgáltat az egyre bonyolultabb földtani feladatok megoldásához. Jelen dolgozat a módszer modell körülmények melletti vizsgálatával a hazai alkalmazást alapozza meg. A kőzetek természetes radioaktív anyagtartalmának meghatározásához szükséges a karotázs mérő berendezések hitelesítése. Az egyes energia ablakokban kapott impulzus számokra igen erős befolyással vannak a fúrési körülmények, ezért ezeket a természetes gamma spektrális mérések kiértékelésénél figyelembe kell venni.

ИЗМЕРЕНИЕ ЕСТЕСТВЕННОГО ГАММА-ИЗЛУЧЕНИЯ В МОДЕЛЬНЫХ И СКВАЖИННЫХ УСЛОВИЯХ

Р. ДОРКО

Спектральное измерение естественного гамма-излучения дает полезную информацию для решения все более сложных геологических задач. В настоящей работе обсуждаются возможности применения этого метода в Венгрии в результате проведения модельных экспериментов и калибровка. Определение содержания естественных радиоактивных веществ в горных породах требует калибровка каротажных измерительных установок по энергии в количественном отношении. Получение в отдельных окнах энергии число импульсов подвергается сильному влиянию скважинных условий. Только при учете таких условий можно провести интерпретацию данных спектрального измерения естественного гамма излучения.

COMPUTER LOG EVALUATION IN TERTIARY COAL BASINS

Stanislav MAREŠ*, Jiří KŘEŠŤAN**

Lignite seams in open-pit mines of the Tertiary coal basins of Northern Bohemia are currently being exploited and geological prospecting and drilling activities are being carried out in new regions in an attempt to discover further resources of solid fuels. All boreholes are logged using a relatively wide range of logging methods (formation resistivity log, gamma-ray log, formation density log, neutron-neutron log, caliper log). Logs digitized directly in the field are subsequently processed on an Eclipse C 300 computer. The results of computer evaluation are presented in the form of formation volume analysis in sandy—clayey overburden and in the form of an ash content log in coal seams.

d: well logging, computer evaluation, brown coal exploration, formation analysis, ash-content log

1. Introduction

The North Bohemian Basin is the largest brown-coal basin in Czechoslovakia. It occupies an area of about 800 km² and is situated at the foot of the Krušné hory Mountains, between the towns of Kadaň in the west and Ústí n. Lab. in the east. The south-eastern margin of the basin is demarcated by the line connecting the localities Korozluky, Postoloprty and Podbořany. The basement is formed of the Krušné hory crystalline complex in the northern part and of Upper Cretaceous sediments in the southern part. The character of the sedimentary filling of the basin is given in *Table 1*. The coal seam is formed from one seam of great thickness or is divided by thin clay layers into 2 or 3 parts. The upper boundary of the coal seam is very sharp, but the transition to the underlying barren rocks is often gradual. The main coal seam is exploited predominantly by open-pit mining. Additional prospecting by means of boreholes is made i) in front of the working face in order to precisely determine the seam structure and the ash content, ii) in as yet unexploited parts of the basin in order to assess new reserves of brown coal.

2. Logging techniques and calibration of logging instruments

All the prospecting boreholes are logged. In the boreholes in front of the mine faces only density logs (GGL) and caliper logs (CL) are measured; in the boreholes of newly prospected areas the above-mentioned logs are complemen-

* Faculty of Sciences, Charles University, Albertov 6, 128 43 Praha, Czechoslovakia

** Stavební geologie, n.p., Gorkého nám. 7, 113 09 Praha 1, Czechoslovakia

Paper presented at the 28th International Geophysical Symposium, 28 September—1 October, 1983 Balatonszemes, Hungary

ted by gamma ray logs (GR), neutron-neutron logs (NNL) and resistivity logs in some simple electrode arrangement (short normal RESN16 with AM electrode spacing 0.4 m and long normal RESN64 with AM = 1.6 m). Borehole logging is carried out using K-500 (Hungarian-made, ELGI) or Prospector 2000 (US-made, Gearhart-Owen Inc.) logging equipment, supplemented by analog-to-digital converters (Czechoslovak-made) [KŘEŠTÁN 1978, MATOUŠEK ET AL. 1978]. Logging data are punched on a tape with a 0.1 m digitization step. Analog logs are recorded on 1 : 100 scale.

All logging tools are calibrated to express all measured data in defined physical units. Density probes (Source ^{137}Cs , activity 10 to 20×10^8 Bq, detector to source distance $L=0.5$ m, the probe with shielded detector pressed against the borehole wall by a steel spring) and neutron probes (source $^{241}\text{Am-Be}$, activity 110 GBq, $L=0.5$ m) are calibrated in large blocks of rock of known

Age	Lithostratigraphic units		Most frequent lithol. types	Thickness (m)
	Series	Formation		
Miocene Aquitain. Burdigal. Helvet. Torton.	producing	Upper clays and sands	mostly clays	up to 250
		coal-seam	brown coal	30–50
		lower clays and sands	sandy-clayey layers	up to 100
	volcanogenic series		sandy—clayey sediments with pyroclastics, tuffs and tuffites	20–50
Oligocene—Middle—Upper	basal complex		sandstones and conglomerates	100

Table I. Geological data on the Neogene North Bohemian Basin [after HAVLENA 1964]

I. táblázat. Az Észak-cseh medence neogén képződményeinek földtani adatai [HAVLENA nyomán, 1964]

Таблица I. Геологические данные Северочешского неогенового бассейна [по ГАВЛЕНА, 1964 г.]

bulk density and porosity; the results of borehole measurements are expressed in g cm^{-3} for bulk density and in % for neutron porosity. The probes for measuring natural radioactivity are calibrated using ^{226}Ra standard of known activity, and the results of borehole measurement are expressed in rate exposure units, pA kg^{-1} . Calipers are calibrated using a set of rings of known diameter; the results of borehole measurements are expressed in mm.

3. Evaluation of logging data and algorithms used

The purpose of logging in coal prospecting is:

- a) to delimit the principal lithological types of sediments and to determine the depth of the basement surface,
- b) to delimit the depth interval of the coal seam and to determine the ash content and heating capacity.

The digitized logs are evaluated by means of the system of SG programs [KŘEŠŤAN, MAREŠ 1977] using an Exlipse C 300 minicomputer [MAREŠ, KŘEŠŤAN 1981]. In the first step (editing program) the measured data usually expressed in mV are converted into the defined physical units using the calibrating constants (see above). Logging data are then statistically analysed (statistical programs). Using frequency graphs, frequency plots and Z-plots (see *Figs. 1–3*) the characteristic physical parameters (density DEN, neutron porosity NPOR, natural radioactivity GR and the apparent resistivity RESN) of clays (indices SH), of clean sands (SD), of the formation matrix (MA) and the limit values for the coal (C) and crystalline rocks (B) are determined. Regression analysis takes one of the most suitable mathematical relationships (linear, exponential, logarithmic, parabolic, hyperbolic) between density DEN and ash content AD and between density DEN and heating capacity QD, calculating the correlation coefficients and the corresponding regression constants. An example of statistically determined rock parameters for the Jiřetin coal district in the North Bohemian Basin is given in *Table 2*.

In the main program the following parameters are calculated:
clay content VSH_{GR} from the gamma ray log

$$\text{VSH}_{\text{GR}} = (\text{GR} - \text{GR}_{\text{SD}}) / (\text{GR}_{\text{SH}} - \text{GR}_{\text{SD}}), \quad (1)$$

clay content VSH_{N} from the neutron—neutron log

$$\text{VSH}_{\text{N}} = \text{NPOR} / \text{NPOR}_{\text{SH}}, \quad (2)$$

resulting clay content VSH

$$\text{VSH} = \text{MIN} (\text{VSH}_{\text{GR}}, \text{VSH}_{\text{N}}), \quad (3)$$

effective porosity EPOR_{D} from the density log

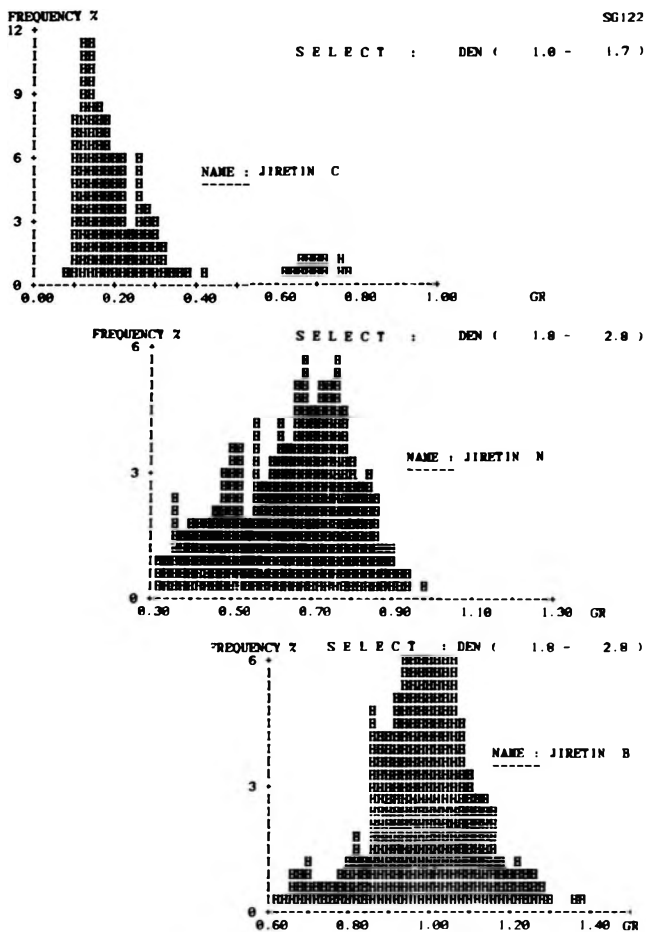


Fig. 1. Frequency graphs of the natural radioactivity GR (pA/kg) for coal (C), Neogene barren sedimentary rocks (N) and crystalline basement — gneiss (B)

1. ábra. A szénrétegek (C), a neogén meddő üledékes kőzetek (N) és a kristályos gneisz fekvő (B) természetes radioaktivitásának gyakorisági görbéi (GR, pA/kg)

Рис. 1. Частотные кривые естественного гамма-излучения GR (pA/kg) (для угля (с), неогеновых непродуктивных осадочных пород (N) и кристаллического фундамента — гнейса (B))

Physical Parameter	Characteristic for				Limit for	
	clay	sand	matrix	coal	coal	cryst. r.
Indices	SH	SD	MA	C	C lim	B lim
DEN (g cm ⁻³)	1.85	2.24	2.50	1.28	1.75	2.26
NPOR (%)	43	15	0	53.5	48	24
GR (pA kg ⁻¹)	0.80	0.40	0.20	0.12	0.54	0.90
K ₁ = 116.48		Q ₁ = -132.33		K ₂ = -0.35		Q ₂ = 30.98

Table II. Characteristic and limit values of physical parameters of sedimentary rocks, coal and crystalline complex (calculation parameters) and regression coefficients for relations (7) and (8)

II. táblázat. Az üledékes kőzetek, a kőszénrétegek és a kristályos öszlet jellemző értékei és határértékei (számítási paraméterek), valamint a (7) és (8) összefüggések regressziós együtthatói

Таблица II. Характерные и предельные значения физических параметров для осадочных пород, угля и кристаллической толши (расчетные параметры) и коэффициенты регрессии для отношений (7) и (8)

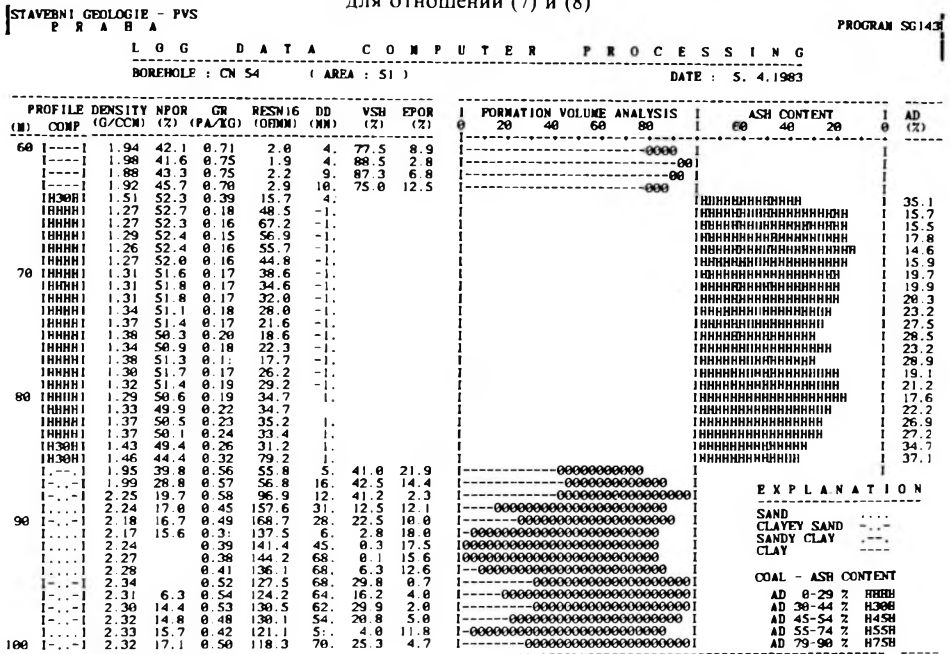


Fig. 4. Listing and schematic graphic representation of logging results from a prospecting borehole in the North Bohemian Basin

4. ábra. Az Észak-cseh medencében végzett kutató fúrás szelvényezési eredményeinek táblázatos és vázlatos grafikus ábrázolása

Рис. 4. Перечень и схематическое графическое изображение результатов измерений в разведочной скважине в Северочешском бассейне

c) logs showing: i) the formation volume analysis in barren sedimentary rocks, ii) the ash content in the coal seam, iii) two original or transformed logging parameters for better delimitation of the coal seam (Fig. 5).

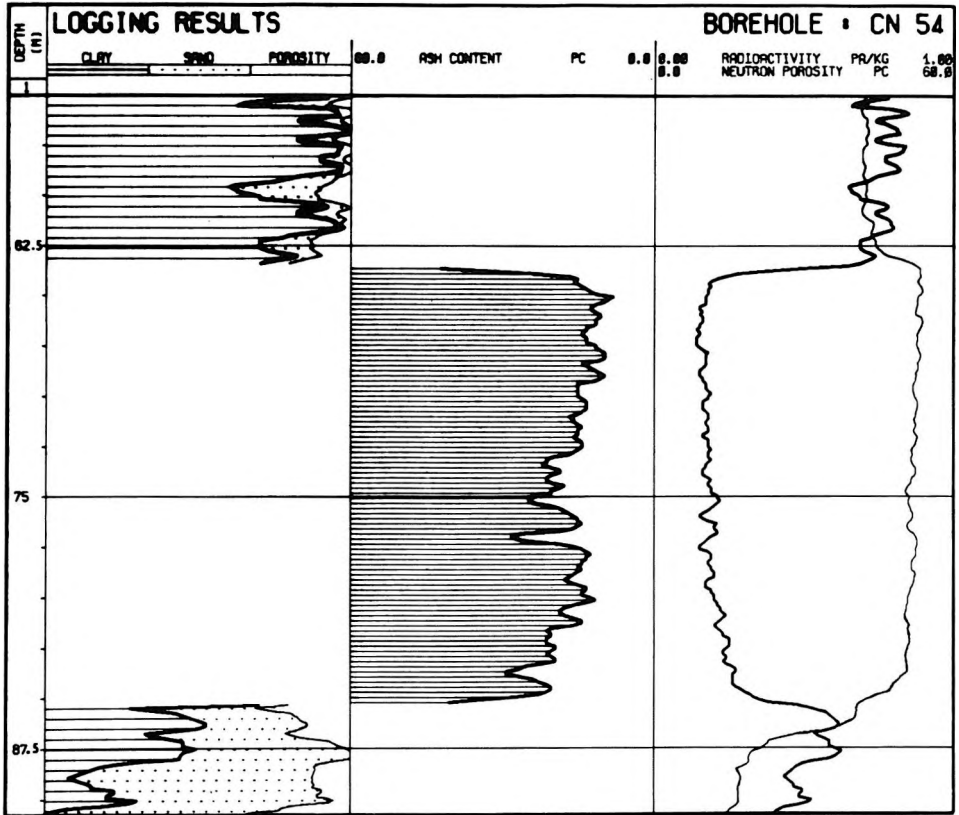


Fig. 5. Graphic representation of logging results from the prospecting borehole given in Fig. 4

5. ábra. A 4. ábrán látható szelvényezési eredmények részletes grafikus ábrázolása

Рис. 5. Графическое изображение результатов измерения в разведочной скважине, указанной на Рис. 4.

4. Conclusions

Digitally recorded logs from prospecting boreholes in brown coal basins are evaluated using the system of SG programs for an Eclipse C 300 minicomputer. Such a manner of evaluation has the following advantages:

1. The time consuming process of manual evaluation can be omitted; the results of computer log evaluation are available to the mining enterprise or the geological service of the prospecting organization in a very short time.
2. The subjective human factor and the unreliability of manual calculations are excluded.
3. The possibility is given for thorough statistical analysis of logging and laboratory data to determine the characteristic and limit values of rock parameters and the corresponding interrelations.
4. Calculation of rock parameters VSH, EPOR and of technological coal parameters (AD with an absolute error not exceeding $\pm 5\%$, QD with a relative error not exceeding $\pm 10\%$).
5. Representation of logging results in a form convenient for geologists. (The most desired form is that combining listing and simple graphic presentation (*Fig. 4*) with a depth step of 0.5 m).
6. Preservation of measured and evaluated data in the external memory of a computer for the future assessment of coal reserves in the area under consideration or for any other integrated evaluation of logging data together with the descriptive geological (lithology, intensity of weathering, density of jointing) and laboratory data (bulk density, matrix density, porosity, moisture content, grain-size distribution, mechanical properties) obtained from core samples.

BIBLIOGRAPHY

- BOND L. O., ALGER R. P., SCHMIDT A. W., 1969: Well Log Applications in coal mining and rock mechanics. Soc. Mining Engineers of AIME, 99th Annual AIME Meeting, Washington (Feb. 16–20, 1969), Paper 69-F-13
- CHRISTALLE H., STEINBRECHER D., 1981: Estimation of brown coal quality parameters using well log data. Proceedings of the 26th International Geophysical Symposium, Leipzig, Sept. 22–29
- GRECHUKHIN V. V., 1965: Geophysical methods of investigation coal boreholes (in Russian). Moscow, Nedra
- HAVLENA V., 1964: Geology of coal deposits. Czechoslovak Academy of Sciences, Academia, Prague (in Czech)
- KREŠŤAN J., MAREŠ S., 1977: The System of SG programs for effective well log evaluation. Paper read at the Geophysical Symposium, Sept. 13–16, Prague
- KŘEŠŤAN P., 1978: Digital Recorder DKR-32-MH (in Czech). Natural Gas and Petroleum, XXIII, la. pp. 171–175, Hodonin
- MATOUSEK J. ET AL., 1978: Digital recorder for well logging SG-77 (in Czech). Natural Gas and Petroleum, XXIII, la. pp. 163–169, Hodonin
- MAREŠ S., KŘEŠŤAN J., 1981: Minicomputer processing of log data from Engineering Geological Boreholes. Proceedings of the 26th Geophys. Symp., Sept. 22–25, Leipzig
- SCHLUMBERGER, 1974: Log Interpretation. Vol. II—Applications, New York
- TIXIER M. P., ALGER R. P., 1967: Log evaluation of nonmetallic mineral deposits. Trans. SPWLA Eighth Annual Logging Symposium

SZÁMÍTÓGÉPES SZELVÉNYKIÉRTÉKELÉS HARMADKORI SZÉNMEDENCÉKBEN

S. MAREŠ. J. KŘESTÁN

Az észak-csehországi harmadkori szénmedencékben külszíni fejtéses lignitbányászat jelenleg is folyik. A területen intenzív földtani és fúrásos kutatás folyik, további szilárd fűtőanyag-készletek feltárása céljából. Valamennyi fúrásban széles körű szelvényezést végeznek, többek között meghatározva az ellenállás-, gamma-, sűrűség-, neutron- és lyukátmérő szelvényt. A szelvényezési adatok digitalizálását közvetlenül a terepen végzik, egy Eclipse 300 típusú számítógép segítségével. A számítógépes feldolgozás eredményét az agyag-homokkő fedőközetben térfogati elemzés, a szénrétegben hamutartalom-szelvény formájában adják meg.

МАШИННАЯ ОБРАБОТКА КАРОТАЖА ПРИ РАЗВЕДКЕ БУРОГО УГЛЯ

С. МАРЕШ. Й. КРЖЕСТЯН

В третичных угольных бассейнах северной Чехии бурый уголь добывается в открытых разработках. В новых районах этого бассейна производятся буровые работы для подсчёта запасов твёрдого топлива. Во всех скважинах производится относительно широкий комплекс каротажных методов (измерение сопротивления, ГК, ГГК, ННК, кавернометрия). Каротажные диаграммы регистрируются в цифровой форме прямо на буровой, машинная обработка производится на ЭВМ типа Eclipse С 300 системой программ SG. Результаты машинной обработки представляются в виде кривых отдельных составляющих (глина, песок, пористость) в пустых третичных отложениях и в виде кривой зольности углей в угольных пластах.

STATISTICAL INTERPRETATION TECHNIQUES FOR INCOMPLETE SET OF LOGS IN SAND-SHALE COMPLEX

Bertalan KISS*, László KORMOS*

The increasing demand for data produced by quantitative well logging interpretation, especially in areas where the old and incomplete set of logs cannot be interpreted by traditional methods, has led to the elaboration of a method capable of creating synthetic logs and thus enabling a complete quantitative interpretation procedure. This method produces reliable results for well correlating areas especially in sand-shale complexes.

d: well-logging, computer programs, statistical analysis, sand-shale complexes

1. Introduction

In Hungary in recent years it has been shown that there is an increasing demand for data produced by quantitative well-logging. The applicable interpretation techniques and depending on these, the number, accuracy, and reliability of determinable reservoir-parameters depend on the set of available logs and their quality. For sandstone reservoirs in sand-shale complexes out of the three necessary porosity-indicating logs (neutron logs, density logs and transit time logs) generally only the neutron logs were available until now in Hungary.

In 1982-83 the Oil Exploration Company put into action Dresser Atlas-made well-logging equipment, a home-made acoustic-probe and a 3-parameter, hole-compensated neutron probe. The logs produced by these satisfy the interpretation demands. The neutron-probe is able to measure calibrated limestone-porosity. The reproduction capability of both methods is very good.

In the case of integrated regional interpretation of hydrocarbon reservoirs only in some recently completed wells was available the following complete set of logs

— spontaneous potential	SP,
— gamma-ray	TG,
— neutron-log	NL,
— density-log	DEL,
— acoustic log	ATL,
— laterolog deep	RLLD,
— induction deep	RILD,
— pseudo-laterolog	RPLH,
— laterolog shallow	RLLS,

* Oil Exploration Company, POB 85, Szolnok H-5001, Hungary Paper presented at the 28th International Geophysical Symposium, 28 September—1 October, 1983, Balatonszemes, Hungary

— induction medium	RILM,
— micro-laterolog	RMLL
— laterolog-8	RLL8,
— caliper log	DL

In the other wells the set logs is incomplete, even sometimes logs cannot be used for interpretation because of calibration or other errors. Generally, the following incomplete choice of logs is available:

— spontaneous potential	SP,
— gamma-ray	TG,
— neutron-log	NL,
— optimum laterolog	ROL,
— micro-laterolog	RMLL,
— caliper log	DL

Thus the well known interpretation techniques cannot be used for all wells of a given territory.

Lately, for a more exact interpretation of seismic data there is a demand for acoustic (ATL) and density (DEL) logs in each borehole, and where these parameters are lacking we must try to create them. To solve these problems a new technique was elaborated to determine parameters which cannot be calculated owing to the incomplete set of logs.

2. Elaborating the new technique

Dependig on the origin of the available data (rock physical properties *measured* on core samples, or parameters *computed* from well-logs) two different approaches should be followed.

2.1 Use of laboratory measurements on core samples

Laboratory analysis of core samples generally provides the following data and relationships:

- porosity (FILA);
- absolute permeability (KLAA);
- capillary pressure (PC) versus water saturation (SWLA)— $PC = f(SWLA)$.

Knowing the hydrocarbon—water phase boundary and capillary pressure curves (PC) it is possible to work out the distribution of water saturation and residual water saturation (SWRLA) in all intervals of the reservoir, [TÓTH 1972]. The results of about 1000 core sample analyses have been processed. After averaging these data on “homogeneous intervals” we gained characteristic values for 150 such intervals. (*Fig. 1*) For these we read out the corresponding values from well logs [KISS 1972]. We then studied the connection between

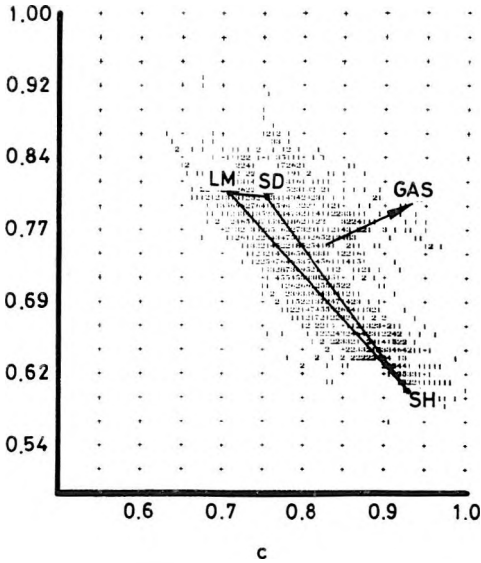
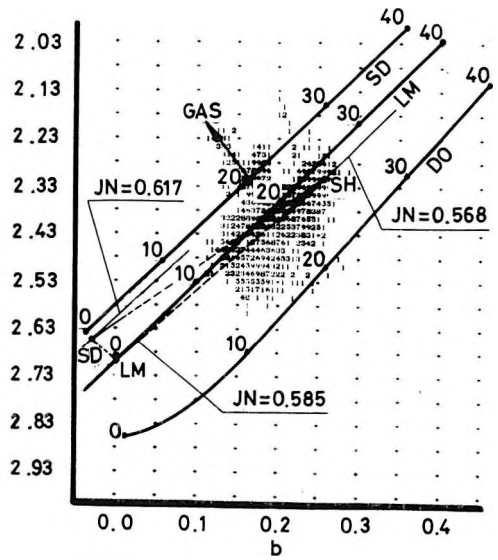
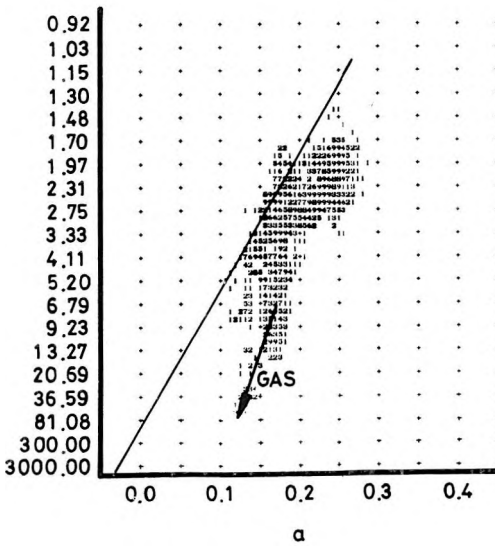


Fig. 1. Results of laboratory core analysis a) Limestone porosity versus resistivity frequency plot b) Limestone porosity versus density frequency plot c) Lithological parameters: JO versus JM frequency plot

1. ábra. Maginták laboratóriumi elemzésének eredményei a) Mészköporozitás — fajlagos elektromos ellenállás gyakorisági eloszlás b) Mészköporozitás — közsűrűség gyakorisági eloszlás c) JO — JM litológiai paraméterek gyakorisági eloszlása

Рис. 1. Результаты измерений в разведочной скважине а) Частотная диаграмма отношения пористости известняка и удельного электрического сопротивления б) Частотная диаграмма отношения пористости известняка и плотности пород в) Частотная диаграмма литологических параметров JO — JM

laboratory and logging data by means of multivariable regression analysis [BÁNLAKE ET AL. 1977].

$$\text{FILA, SWLA, SWRLA, KLAA} = f[(1 - \text{JSP}), \text{JTG}, \text{EXP}(\text{NG}/\text{NGSH}), \text{LN}(\text{RW}/\text{ROL}), \dots] \quad (1)$$

- where
- 1-JSP = shale indicator (see Equ. 2a),
 - JTG = shale indicator (see Equ. 2b),
 - NG = neutron-gamma log,
 - NGSH = neutron-gamma intensity of shale line,
 - RW = resistivity of pore water.

In a given territory the reservoir parameters (FI, SW, SWR, K) were determined by the above relations leading to the following conclusions:

— As most of the cores are taken from more or less clean sandstone, core sampling is not random. The calculated parameters are reliable in such reservoir intervals;

— To extend the applicability of the method contaminated cores should also be included in the investigations.

2.2. Quantitative interpretation in one or a few boreholes

By means of joint interpretation of the logs we obtain continuous information along the borehole. The following reservoir parameters are regularly determined:

- effective porosity (FI);
- shale content (VSH);
- volume of rock matrices (VMA1, VMA2);
- water saturation in the virgin zone (SW);
- water saturation in the flushed zone (SXO);
- residual water saturation (SWR);
- permeability index (K).

Determination of shale content (VSH) takes place on the basis of "shale indicator minima", or by properly chosen shale indicators [POUPON-GAYMARD 1970].

The following shale indicators were used:

$$\text{VSH1} = (1 - \text{JSP}) = \left(1 - \frac{\text{SP}}{\text{SPS}}\right) \quad (2a)$$

$$\text{VSH2} = (1 - \text{JSP})^2 \quad (2b)$$

$$\text{VSH3} = \text{JTG} = \frac{\text{TG} - \text{TGMN}}{\text{TGMX} - \text{TGMN}} \quad (2c)$$

$$\text{VSH4} = 0.33(2^{2\text{JTG}} - 1) \quad (2d)$$

$$\text{VSH5} = (1 - \text{JSP})\text{JTG} \quad (2e)$$

$$\text{VSH6} = \left(\frac{\text{RSH}}{\text{RT}}\right)^{\frac{1}{\text{BRSH}}} \quad (2f)$$

$$\text{VSH7} = \left(\frac{\text{RSH}}{\text{RT}} \cdot \frac{\text{RTMX} - \text{RT}}{\text{RTMX} - \text{RSH}}\right)^{\frac{1}{\text{BRSH}}} \quad (2g)$$

where

SP = logged spontaneous potential,

SPS = static spontaneous potential,

TG = logged gamma-ray value,
 TGMX = maximum value of gamma-ray log (shale-line),
 TGMN = minimum value of gamma-ray log (sand-line),
 RT = resistivity of the virgin zone,
 RSH = resistivity of shale,
 RTMX = maximum value of resistivity of the virgin zone (in pure CH reservoir),

$$\text{BRSH} = \text{exponent } (\sim 1-2), \text{BRSH} \approx \text{BM} \left(1 - \sqrt{\frac{\text{RSH}}{\text{RTMX}}} \right),$$

BM = cementation exponent.

Porosity and matrix volume can be calculated by solving the balance equations of rock components based on three porosity indicator logs [Schlumberger Document 1969]:

$$\text{FINLM} = \text{FI} \cdot \text{FINF} + \text{VMA1} \cdot \text{FINMA1} + \text{VMA2} \cdot \text{FINMA2} + \text{VSH} \cdot \text{FINSH} \quad (3a)$$

$$\text{DE} = \text{FI} \cdot \text{DEF} + \text{VMA1} \cdot \text{DEMA1} + \text{VMA2} \cdot \text{DEMA2} + \text{VSH} \cdot \text{DESH} \quad (3b)$$

$$\text{AT} = \text{FI} \cdot \text{ATF} + \text{VMA1} \cdot \text{ATMA1} + \text{VMA2} \cdot \text{ATMA2} + \text{VSH} \cdot \text{ATSH} \quad (3c)$$

$$1 = \text{FI} + \text{VMA1} + \text{VMA2} + \text{VSH} \quad (3d)$$

Equation 3d is applicable as a means of control, where
 FINLM = apparent limestone porosity calculated from the neutron-log,
 FINMA1, FINMA2 = apparent neutron porosity of rock matrices,
 DEMA1, DEMA2 = density of rock matrices,
 ATMA1, ATMA2 = acoustic transit time in rock matrices,
 FINSH = neutron porosity of shale,
 DESH = density of shale,
 ATSH = acoustic transit time in shale,
 FINF = neutron porosity of pore fluid,
 DEF = density of pore fluid,
 ATF = acoustic transit time in pore fluid.

The equations of rock components (3a-c) contain 4 unknowns therefore shale content will independently be calculated by the earlier described shale indicators.

The matrix values (FINMA1, DEMA1, ATMA1, FINMA2, DEMA2, ATMA2), and the shale characteristics (FINSH, DESH, ATSH, RSH) can be determined on the basis of the resistivity of the virgin zone, porosity-indicators ($1/\sqrt{\text{RT}} - \text{FINLM}$, $1/\text{RT} - \text{AT}$, $1/\sqrt{\text{RT}} - \text{DE}$, $\text{FINLM} - \text{DE}$, $\text{FINLM} - \text{AT}$, $\text{AT} - \text{DE}$), and frequency plots (JN - JM, JO - JM, JO - JN) formulated by lithological parameters as JM, JN, JO (Fig. 1/a, 1/b, 1/c),

where

$$JM = \frac{ATF - AT}{DE - DEF} 0.003,$$

$$JN = \frac{FINF - FINLM}{DE - DEF},$$

$$JO = \frac{FINF - FINLM}{ATF - AT} 330.$$

Plots can be used to check logs and to determine the main rock-components, because the point-set must fall on a predetermined area of the plot-field characterized by the main rock-components, e.g. sandstone (SD), limestone (LM). With the combined use of such plots we can find the faulty or incorrectly calibrated logs.

The following equations are used to calculate water saturation [POUPON ET AL. 1970, WICHTL-DRAXLER 1981]:

$$SW1 = \left[\frac{RT^{-\frac{1}{2}}}{\frac{VSH^{(1-\frac{VSH}{2})}}{\sqrt{RSH}} + \frac{FI^{\frac{BM}{2}}}{\sqrt{BA \cdot RW}}} \right]^{\frac{2}{BN}} \quad (4a)$$

$$SW2 = B + \sqrt{B^2 + \frac{A}{RT}} \quad (4b)$$

where

$$A = \frac{(1 - VSH)BA \cdot RW}{FI^{BM}},$$

and

$$B = -\frac{A}{2} \cdot \frac{VSH}{RSH}$$

$$SW3 = \left[\frac{RW}{RT} \cdot \frac{BA}{FI^{BM}} \right]^{\frac{1}{BN}} \quad (4c)$$

$$SX01 = \left[\frac{RX0^{-\frac{1}{2}}}{\frac{VSH^{(1-\frac{VSH}{2})}}{\sqrt{RSH}} + \frac{FI^{\frac{BM}{2}}}{\sqrt{BA \cdot RMF}}} \right]^{\frac{2}{BN}} \quad (4d)$$

$$SX02 = B + \sqrt{B^2 + \frac{A}{RX0}}$$

where

$$A = \frac{(1 - VSH)BA \cdot RMF}{FI^{BM}} \quad (4e)$$

and

$$B = -\frac{A}{2} \cdot \frac{VSH}{RSH}$$

$$SX03 = \left[\frac{RMF}{RX0} \cdot \frac{BA}{FI^{BM}} \right]^{BN} \quad (4f)$$

where

- BA = tortuosity coefficient,
- BM = cementation exponent,
- BN = saturation exponent,
- RX0 = resistivity of flushed zone,
- RMF = resistivity of mud filtratum.

Two water saturation calculations are used in order to select the more favourable one from the following parameters: SW1, SW2, and SX01, SX02, respectively. The third calculation serves for the control of coefficients, like tortuosity (BA), cementation exponent (BM), and saturation exponent (BN) in pure sands.

After calculating the water saturation we correct the layer contents of the porosity indicator logs when, into equations 3a, 3b, 3c we place respectively

$$FINF^* = FINW \cdot SX0 + (1 - SX0) FINCH \quad (5a)$$

$$DEF^* = DEW \cdot SX0 + (1 - SX0) DECH \quad (5b)$$

$$ATF^* = ATW \cdot SX0 + (1 - SX0) ATCH \quad (5c)$$

where

- FINW = neutron porosity (H-index) of pore water,
- DEW = density of pore water,
- ATW = acoustic transit time in pore water,
- FINCH = neutron porosity (H-index) of hydrocarbon,
- DECH = density of hydrocarbon,
- ATCH = acoustic transit time in hydrocarbon.

Next we perform an iteration procedure on equations (3a), (3b), (3c), (4a), (4b), (4d), (4e), (4f), (5a), (5b) and (5c) to improve the values of FI, VMA1, VMA2, SW and SX0 until

$$FI - FI_{former} \leq 1 - 2\% \text{ and}$$

$$\Delta V \leq 5\% \text{ in average}$$

where

$$\Delta V = 1 - (FI + VMA1 + VMA2 + VSH) \text{ on the basis of Equ. (3d).}$$

Determination of the residual water saturation is carried out from the following relationship:

$$SWR = BSWRC + BSWRM \frac{VSH}{FI} \quad (6)$$

BSWRC and BSWRM can be determined from $\frac{VSH}{FI}$ versus SW cross-plots. The permeability index can be calculated by the following equation:

$$K = 250 \left(\frac{FI^3}{SWR} \right)^2. \quad (7)$$

2.3. Creating of indicators

Besides the knowledge of reservoir-parameters, determined from core analysis or quantitative well log interpretation other indicators derived from logs are also needed which are closely related with the reservoir-parameters. To create these indicators such logs are used which are available in all the boreholes of the area of investigation.

As indicators other values can serve as well, like

$$FI = f \left\{ (1 - VSH), (FINLM - FINSH), \left[\left(\frac{BA \cdot RW}{RT} - VSH \frac{BA \cdot RW}{RSH} \right) (1 - VSH) \right], \dots \right\} \quad (8a)$$

$$VSH = f \left\{ (1 - JSP), JTG, \frac{FINLM}{FINSH}, \left(\frac{RSH}{RT} \frac{RTMX - RT}{RTMX - RSH} \right), \dots \right\} \quad (8b)$$

$$SW, SX0 = f \left\{ \left(\frac{RX0}{RMF} \frac{RW}{RT} \right), \frac{FI}{FIMX}, \left[\frac{RT}{BA \cdot RW} (FINLM - FINSH) \right], (1 - VSH), \dots \right\} \quad (8c)$$

Determination of SWR and K takes place in the same manner as described in Section 2.2.

Next we must find the optimum relationship between reservoir parameters and indicator values to enable us to ensure the determination of reservoir parameters in the other boreholes of the territory.

3. Determination of relationships between reservoir parameters and indicators, computation of reservoir parameters

In order to solve this problem it was necessary to develop a so called statistical indicator system program (SIP) which functions as a subsystem of the well logging interpretation system (KISS).

3.1. Determination of relationships

Main steps:

- calculation of indicator values for the entire investigated interval,
- determination of partial correlation coefficients between reservoir parameters and indicators,
- selection of indicators showing a good correlation with a view to improving the total correlation coefficient,
- determination of relationships between indicators and reservoir parameters on the basis of multivariate linear regression,
- calculation of total correlation coefficient for checking purposes [VINCZE 1975].

When making the primary choice of indicators the value of the partial correlation coefficient is decisive because an indicator with larger partial correlation improves the total correlation. (Among the chosen indicators there is no need for those with weak partial correlation). In spite of their relatively high partial correlation among the chosen indicators those which do not improve the value of the total correlation will also be eliminated.

This method must be used for determining all reservoir parameters. If the relationship is not good enough regarding the total correlation coefficient, it is necessary to find further indicators to improve this relationship.

3.2 Calculation of reservoir parameters

Relationships determining the reservoir parameters and the indicator values form a phase of a computational subsystem of the KISS-system. In the other boreholes of the area of investigation calculation of reservoir parameters are carried out in this phase. Indicator systems and coefficients of different investigation areas form a phase of the above mentioned subsystem. *Table 1* shows the determined parameters and their total correlation coefficient for one of the investigated areas.

Table 1

Reservoir parameter	Abbreviation	Total correlation coefficient
Effective porosity	FI	0.972
Shale content	VSH	0.993
Volume of matrix No 1	VMA1	0.868
Volume of matrix No 2	VMA2	0.759
Water saturation	SW	0.95
Water saturation of flushed zone	SX0	0.913
Residual water saturation	SWR	0.956

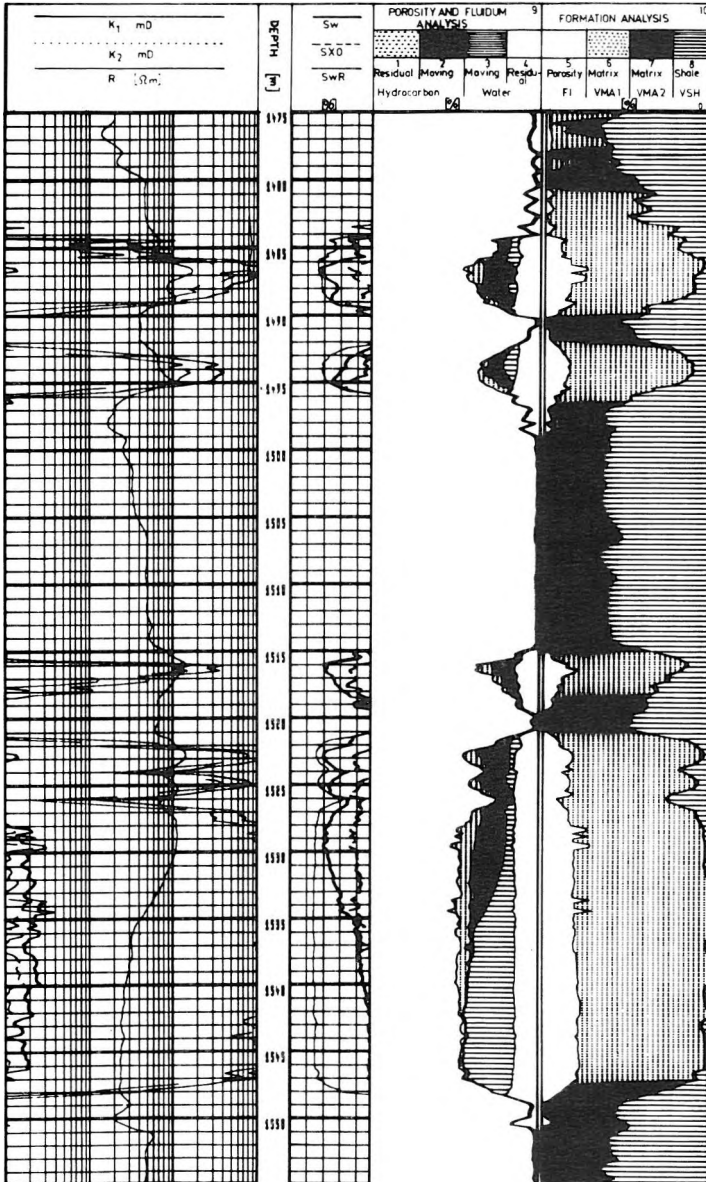


Table I shows that the total correlation coefficient is greater than 0.9, except for the two matrix volumes. Relationships thus seem good enough except for the two used for the volumes. Since these do not really belong to the reservoir parameters we omit their calculation.

Using the relationships for boreholes KIS-3 and KIS-38 of the investigated area, Figs 2 and 3 present the results of the interpretation obtained by the SIP program.

Fig. 2. Results of quantitative well logging interpretation

K_1 , K_2 — permeability indices; R — resistivity log; SW — water saturation in the virgin zone; SX0 — water saturation in the flushed zone; SWR — residual water saturation

2. ábra. A komplex kvantitatív karotázs interpretáció eredménysszelvénye

K_1 , K_2 — permeabilitás indexek; R — ellenállás szelvény; SW — víztelítettség az érintetlen zónában; SX0 — víztelítettség a kisépért zónában, SWR — maradék víztelítettség; 1 — maradék szénhidrogén térfogat; 2 — mozgó szénhidrogén térfogat; 3 — mozgó víz térfogat; 4 — maradék víz térfogat; 5 — effektív porozitás; 6 — 1. mátrixtérfogot (homok); 7 — 2. mátrixtérfogot (mészkö); 8 — agyagtartalom; 9 — porozitás és rétegtartalom elemzés; 10 — formáció elemzés

Рис. 2. Результаты комплексной количественной интерпретации каротажных данных

K_1 , K_2 — индексы проницаемости; R — кривая сопротивления; SW — водонасыщенность в ненарушенной зоне; SX0 — водонасыщенность в промытой зоне; SWR — остаточная водонасыщенность; 1 — остаточный объем углеводородов; 2 — подвижный объем углеводородов; 3 — подвижный объем воды; 4 — остаточный объем воды; 5 — эффективная пористость; 6 — объем вмещающей породы 1 (песок); 7 — объем вмещающей породы 2 (известняк); 8 — содержание глины; 9 — анализ пористости и содержания пласта; 10 — анализ формации

3.3 Generation of synthetic logs

As in the case of the reservoir parameters, synthetic logs can also be created. This method basically corresponds with the described one, but instead of reservoir parameters it needs well calibrated logs of the type to be synthesized measured in some of the boreholes of the study area. As a means of solving seismic interpretation tasks the demand has arisen for acoustic and density logs. The left side of *Fig. 4* shows the calculated and measured density (DE) logs; on the right side is situated the result of statistical quantitative interpretation. (N.B. The logged density curve did not serve as a basic parameter for creating the relationship, but we used it for checking purposes only.) It can be seen that the measured log corresponds well with the synthetic log (deviation 0.05 g/cm^3). Deviation is greater in hydrocarbon bearing intervals, but if we use reservoir parameters to create indicators, the accuracy can be increased by iteration.

4. Conclusions

The method discussed is expected to give reliable results in geologically well correlatable regions, first of all in sandstone formations. One of its advantage, that it can transform the old, incompletely logged well data into a set that is already suitable for a complex, quantitative well-log interpretation. Missing, or poor quality logs can be replaced, at a later date, by synthetic logs computed by the proposed method, and these synthetic logs can be subjected, together with the „real” ones, to a regional processing.

The accuracy of log synthetization can be improved by iteration if reservoir parameters are included into the indicator system.

The method can be used for filtering of measured logs—as verified in the course of log synthetization—i.e. filtering can be used in the first phase of data processing.

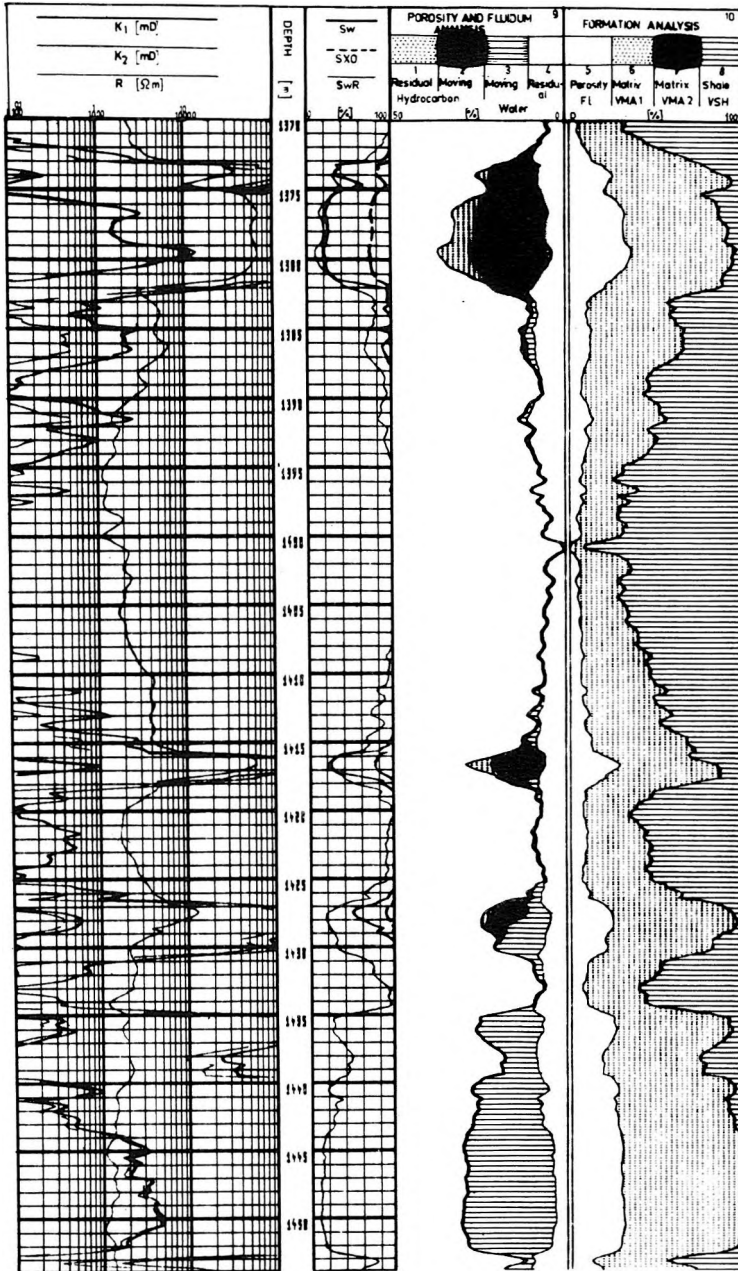


Fig. 3. Results of quantitative interpretation by the statistical program SIP. Legend as in Fig. 2.

3. ábra. Statisztikus módszerrel készült kvantitatív kartertészeti interpretáció (magyarázatok a 2. ábrán)

Рис. 3. Количественная интерпретация данных каротажа по статистическому методу. (Объяснения даны на Рис. 2)

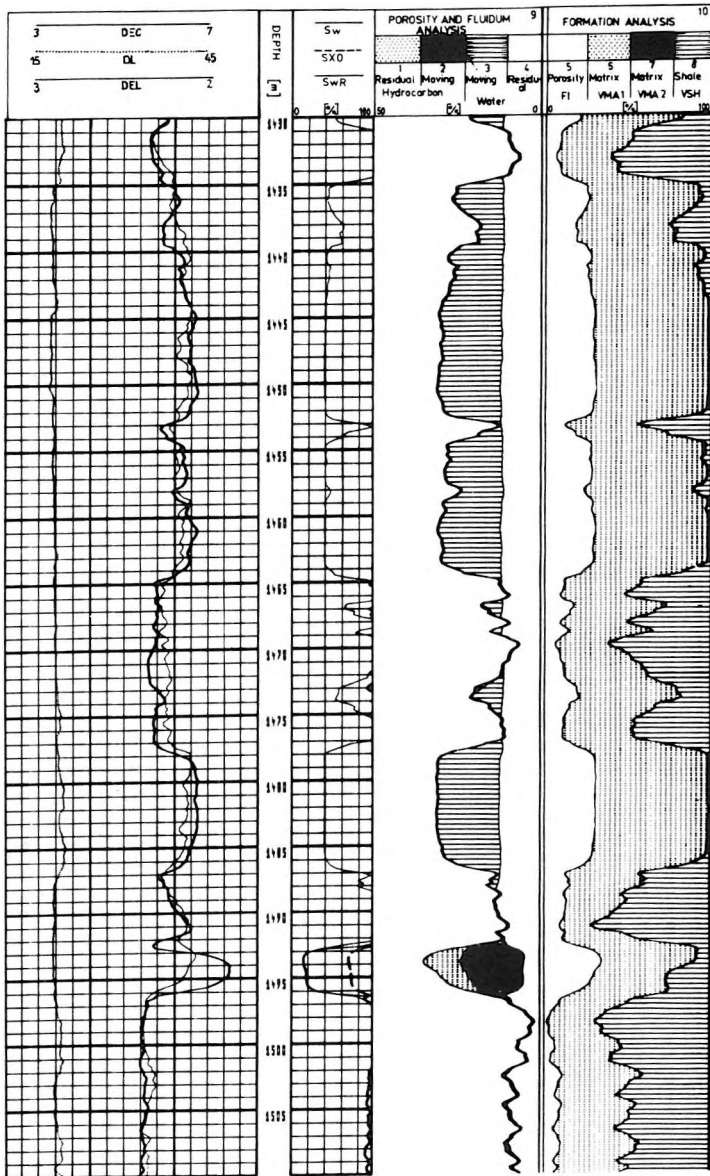


Fig. 4. Comparison of synthetic density log with a measured one
 DEL — measured density log; DEC — synthetic density log; DL — caliper log. Legend as in Fig. 2

4. ábra. Szintetikus sűrűség szelvény összehasonlítása a fúrólukban mért szelvényvel
 DEL — mért sűrűség szelvény; DEC — számított sűrűség szelvény; DL — lyukátmérő szelvény;
 (további magyarázatok a 2. ábrán)

Рис. 4. Сопоставление синтетической диаграммы плотности с измеренной в скважине диаграммой

DEL — измеренная кривая плотности; DEC — расчетная кривая плотности;

BIBLIOGRAPHY

- BÁNLAKI E., KISS B., KORMOS L., PÉKÓ M., 1977: Determination of the reservoir properties of the Szőreg-2 deposit (Algyő) by quantitative well-log interpretation. A statistical method (in Hungarian) Oil Exploration Co. Report
- KISS, B., 1972: Connection between lithological, petrophysical and geophysical properties in the lower Pannonian sandstones of Algyő, Hungary (in Hungarian) Manuscript
- POUPON A., GAYMARD R., 1970: The evaluation of clay content from logs. SPWLA Eleventh Annual Logging Symposium, May, 1970
- POUPON A., CLAVIER C., DUMANOIR J., GAYMARD R., MIRK A., 1970: Log analysis of sand-shale sequences—a systematic approach. Journal of Petroleum Technology, July, 1970
- Schlumberger Log Interpretation Principles. Schlumberger Document, New York, 1969
- TÓTH J. 1972: Surface properties, capillary phenomena in homogenous and heterogenous rocks; humidification conditions (in Hungarian). Publication of Ass. of Hung. Geophys.
- VINCZE I., 1975: Mathematical Statistics with Industrial Applications (in Hungarian) Műszaki Kiadó, Budapest
- WICHTL K., DRAXLER J.K., 1981: Schlumberger CPI Seminar, Budapest

STATISZTIKUS ÉRTELMEZÉSI ELJÁRÁSOK ALKALMAZÁSA AGYAGOS HOMOKKŐ TÁROLÓKBAN, HIÁNYOS SZELVÉNYVÁLASZTÉK ESETÉN

KISS BERTALAN, KORMOS LÁSZLÓ

Az utóbbi években egyre nagyobb igény mutatkozik a kvantitatív karotázs interpretáció által szolgáltatott adatok iránt olyan területeken is, ahol a nagyjából régen készült, hiányos szelvényválaszték — az ismert módszerekkel — ezt nem teszi lehetővé.

Az alábbiakban vázolt eljárással lehetővé válik egy eltérően — hiányosan — szelvényezett kutatási terület hasonló módon és hasonló minőségben történő mélyfúrás geofizikai feldolgozása. Előállíthatók — utólagosan — szintetikus szelvények, melyeknek a fúrólukban történő felvételére már nincs mód.

A módszer geológiaiailag jól korrelálható területeken, elsősorban homokos-agyagos formációkban szolgálat megbízható eredményt.

ПРИМЕНЕНИЕ СТАТУСТИЧЕСКИХ МЕТОДОВ ИНТЕРПРЕТАЦИИ ДЛЯ ПЕСЧАНО-ГЛИНИСТЫХ КОЛЛЕКТОРОВ В СЛУЧАЕ НЕПОЛНОЙ КОМПЛЕКТНОСТИ КАРОТАЖНЫХ КРИВЫХ

Б. КИШ, Л. КОРМОШ

За последнее время увеличивающийся спрос предьявляется к результатам количественной интерпретации каротажных данных, хотя эти требования не всегда могут быть удовлетворены с применением известных методов, в связи с некомплектностью имеющихся каротажных кривых.

В работе предлагается метод, дающий достоверные результаты в геологически хорошо коррелируемых районах, в первую очередь в песчано-глинистых формациях. Вместо отсутствующих видов каротажных кривых, которые уже нельзя получить в скважинах, можно создать расчетные синтетические кривые.

Предлагаемый метод позволяет проводить достоверную обработку каротажных данных в районах, недостаточно изученных промыслово-геофизическими методами.

COMPARISON OF ACCURACY OF CONTROL SYSTEMS FOR VARIOUS FOCUSED-CURRENT LOGGING INSTRUMENTS

István KUBINA*

This paper deals with the errors of the various types of focused-current (laterolog) control systems taking into account all the characteristic features of the control loop, as well as those of the borehole and bearing in mind the influence of the surrounding formations on the accuracy of the various controls.

The relationship is shown between the error of the measured apparent resistivity and the insufficient control, and their links with the main features of the control-loop and the four transfer functions representing the physical properties of the borhole and the surrounding formations.

It is emphasized that the applied theoretical treatment has less rigorous requirements than the real cases, as the ground contact resistance of the current electrodes are taken into account by that of the equipotential surfaces matching at the S_1 and S_2 electrodes. This involves neglecting the effect of the gaps (filled with low resistivity mud) between the current electrodes and the mentioned potential-surfaces. This results in no significant difference if the values of R_0 are high enough while for low values of R_0 it acts as if the output-resistivity of the control-loop in question was increased.

d: focused-current logging, control system, accuracy, I_1 control, I_0 control, I_1/I_0 ratio

1. Introduction

Focused-current (laterolog) well-logging methods have been used universally, in boreholes drilled with conductive mud, since the beginning of the seventies, pushing into background all the classical resistivity measurements. On the one hand this can be attributed to their having the deepest penetration of all logging methods, a good selectivity along the borehole and additionally, they are independent of the disturbances of mud-resistivity, as opposed to the conventional devices; on the other hand, with regard to their features and selectivity, they can better be associated with the other modern logging methods (sonic-, induction-, nuclear-) than the conventional ones. In the near future the focused method can look forward to a further boom as now this is perhaps the only one which offers the possibility of increasing its penetration and sensitivity. It is also likely that this method will play an important role in the planning of enhanced production methods. For these reasons it is necessary to get acquainted with some of the factors influencing its accuracy.

Among the well-known focused current tools (LL3, LL7, LL9 and DLL), those with seven or nine electrodes have so far proved the most useful because there is no flow either of I_0 measuring- or of I_1 focusing currents through the electrodes which give the control-signal and the measured information and this means that they are more accurate than the others. Moreover, one can form the

shape of the I_0 current-beam by means of the I_1 current flowing through the properly located A_1 electrodes, to yield an advantageous measuring characteristic. Therefore this paper deals with the common effects of mud- and rock-resistivities and electrical parameters of the control circuit on the accuracy of control and measurement.

2. Errors of the control and measuring processes

Let us now consider the errors of the control and measuring process caused by these characteristic parameters, as a function of the current ratio $n = I_1/I_0$. We will find that not only the error of n is proportional to this influence, but that of the measured resistivity too.

Our intention is to examine this influence on the wellknown seven-electrode focused sonde (Fig. 1/c) but the same method is also suitable for the nine-electrode sonde as well as for dual types with elongated electrodes.

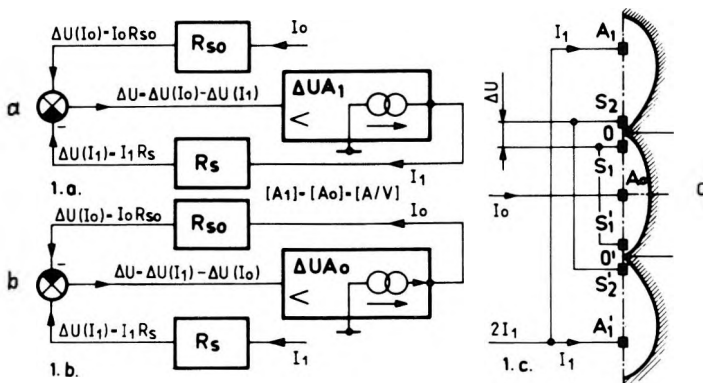


Fig. 1. Schematic diagrams of I_1 and I_0 control circuits (a, b) and an LL7 sonde (c)

1. ábra. Az I_0 és I_1 szabályozó egyszerűsített tömbvázlata és a hét elektrodás szonda

Рис. 1. Упрощенная блок-схема регулирующего устройства I_0 и I_1 и семиэлектродный зонд LL7

One can read in Fig. 1/a, representing the simplified block-scheme of the I_1 control, the expressions

$$\Delta U = \Delta U(I_0) - \Delta U(I_1) = I_0 R_{s0} - I_1 R_s \tag{1}$$

$$I_1 = \Delta U A_1 \tag{2}$$

If $\Delta U = 0$, then (1) gives

$$I_1^*/I_0 = R_{so}/R_s = n_0 \tag{3}$$

where n_0 is the ideal I_1^*/I_0 ratio. The existing current ratio, if $\Delta U \neq 0$, using (1) and (2), is

$$n = I_1/I_0 = A_1 R_{so}/(1 + A_1 R_s) \tag{4}$$

Let us define the error of the control as

$$h_{I_1} = (n - n_0)/n_0 = -1/(1 + A_1 R_s) \approx -1/A_1 R_s \tag{5}$$

this is, in fact, the known expression for automatic control systems.

If the I_0 current is controlled, the expression of the error is

$$h_{I_0} = -1/(1 + A_0 R_{so}) \approx -1/A_0 R_{so} \tag{6}$$

Thus in both cases the errors are functions of the gain of the control circuit as well as of the transfer functions, having values defined by $R_{so} = \Delta(I_0)/I_0$ and $R_s = \Delta(I_1)/I_1$, and they apparently depend on whether we control the I_1 or I_0 . Our aim is to examine the effect on the control of these parameters. The characteristic features of these transfer-functions and those of the n ratio are shown in Fig. 2 for a so called optimum-sonde and two-parameter resistivity-distribution in the direction perpendicular to the borehole axis.

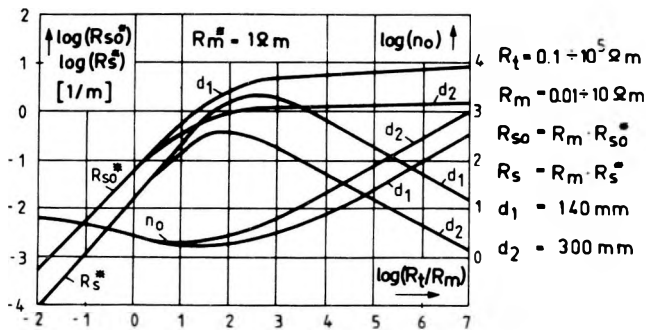


Fig. 2. R_{so} , R_s and n_0 as functions of rock- (R_t), mud-resistivity (R_m), and diameter of borehole (d)

2. ábra. A szabályozás transfer-függvényei és az n_0 áramarány a kőzet- (R_t), az iszap-ellenállás (R_m) és a lyukátmérő (d) függvényében

Рис. 2. Функции передачи регулирования и соотношение токов n_0 в зависимости от сопротивления породы (R_t), раствора (R_m) и диаметра скважины (d)

The characteristic behaviour of R_{s0} and R_s in expressions (5) and (6) fosters the idea that the I_0 control needs far less gain (A_0) than does the control of I_1 (A_1), especially in cases demanding high n ratio. Some experts consider I_0 control to be more beneficial than the other, in particular if they wish to vary, beyond the controlled current, the n ratio too, e.g. so that the more the I_0 is decreased the more the I_1 is increased, or vice versa. One can achieve this process with an additional control circuit driven by the signal produced on R by the controlled current.

Unfortunately, these ideas are rather irrational since they do not take into account either the effects of the output resistances of the generators (R_0, R_1), or the ground contact resistances of the electrodes (R_{f0}, R_{f1}). The control schemes shown in *Figs. 1/a and b* serve for the study of the characteristics of functions R_{s0} and R_s only, they cannot be applied in the actual design of an instrument.

Next we use a general model which is suitable for studying the errors attributed to the inadequate control both of the n ratio and the R_a apparent resistivities. In both cases of the controls the R_0 and R_{f0} are connected series in the I_0 circuit as well as R_1 and R_{f1} in the I_1 circuit, see *Figs. 3 and 4*. The transfer functions make connections between the current flowing through two given points of the rock-space and the voltage caused by this current between another two points of the same space. They are fictitious, thus have no primary effect on the currents. Besides the transfers already defined, the other two are $R_k = U_M(I_1)/I_1$ and $R_{k0} = U_M(I_0)/I_0$.

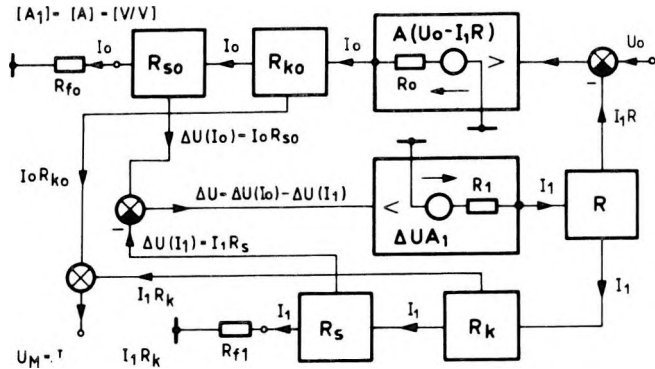


Fig. 3. Schematic diagram of I_1 control using all transfer-functions

3. ábra. Az I_1 szabályozás a mérés transzfer-függvényes tömbvázlata

Рис. 3. Блок-схема регулирования I_1 и измерения с применением всех функций передачи

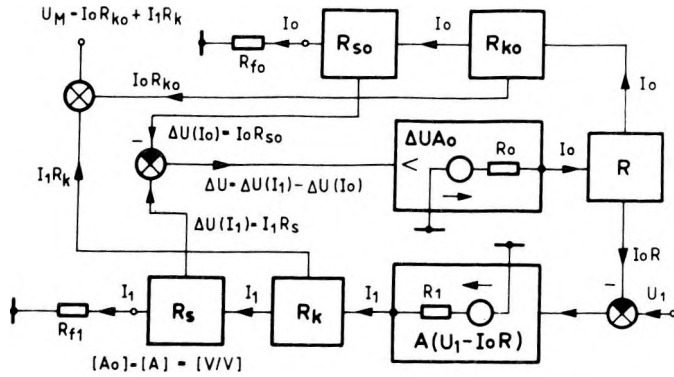


Fig. 4. Schematic diagram of I_0 control using all transfer-functions

4. ábra. Az I_0 szabályozás és a mérés transzfer-függvényes tömbvázlata

Рис. 4. Блок-схема регулирования I_0 у измерения с применением всех функций передачи

$$\Delta U = \Delta U(I_0) - \Delta U(I_1) = I_0 R_{s0} - I_1 R_s \quad (7)$$

$$I_1 = \Delta U A_1 / (R_1 + R_{f1}) \quad (8)$$

Thus one can express the existing I_1 value and the n ratio as

$$I_1 = I_0 A_1 R_{s0} / [(R_1 + R_{f1}) + A_1 R_s] \quad (9)$$

$$n = I_1 / I_0 = A_1 R_{s0} / [(R_1 + R_{f1}) + A_1 R_s] \quad (10)$$

The relative error of I_1 and the gain due to the parameters are given by:

$$h_{I_1} = (n - n_0) / n_0 = -(R_1 + R_{f1}) / [A_1 R_s + (R_1 + R_{f1})] \leq \leq -(R_1 + R_{f1}) / A_1 R_s \quad (11)$$

$$A_1 = [(1 + h_{I_1}) / h_{I_1}] / [(R_1 + R_{f1}) / R_s] \quad (12)$$

Accordingly, (11) and (12) show that the error and the gain are not only functions of R_s or h_{I_1} but also of R_1 and R_{f1} , however they are independent from the R_0 , R_{f0} , R and A values. The error of R_a caused by I_1 is

$$h_{R_1} = (R_a - R_a^*) / R_a^* \quad (13)$$

where R_a^* exists if $\Delta U = 0$, and R_a is measured if $\Delta U \neq 0$

$$R_a^* = k(R_{k0} + n_0 R_k) \quad (14)$$

$$R_a = k(R_{k0} + n R_k) \quad (15)$$

Equations (14) and (15) are merely modified forms of the basic equation of geophysical resistivity measurement:

$$R_a = kU_M / I_0 \quad (16)$$

if we consider the U_M value to be the superposition of the two potentials $I_0 R_{k0}$ and $I_1 R_k$ (fig. 3). From (14) and (15) one can express the error of resistivity:

$$h_{R1} = (n - n_0)R_k / (R_{k0} + n_0 R_k) \quad (17)$$

Now, taking (3) and (10) one can reformulate (17), viz.

$$\begin{aligned} h_{R1} &= -(R_1 + R_{f1}) / [(R_1 + R_{f1} + A_1 R_s)] \cdot [n_0 R_k / (R_{k0} + n_0 R_k)] = \\ &= h_{I1} n_0 R_k / (R_{k0} + n_0 R_k) = h_{I1} e_k \end{aligned} \quad (18)$$

Hence the error h_{R1} is proportional to h_{I1} , moreover

$$e_k = n_0 R_k / (R_{k0} + n_0 R_k) \quad (19)$$

representing the influence of the rock- and mud-resistivities and their distribution always having a value less than unity. On the basis of (18) it can be stated that h_{R1} , the error of the apparent resistivity, is less than the error of I_1 .

Similarly one can determine the characteristics of the I_0 control using Fig. 4.

$$\Delta U = \Delta U(I_1) - \Delta U(I_0) = I_1 R_s - I_0 R_{s0} \quad (20)$$

$$I_0 = \Delta U A_0 / (R_0 + R_{f0}) \quad (21)$$

From these one gets the characteristic formulae

$$I_0 = I_1 A_0 R_s / [R_0 + R_{f0} + A_0 R_{s0}] \quad (22)$$

$$n = I_1 / I_0 = (R_0 + R_{f0} + A_0 R_{s0}) / A_0 R_s \quad (23)$$

$$\begin{aligned} h_{I0} &= (I_0 - I_0^*) / I_0^* = -(R_0 + R_{f0}) / [(R_0 + R_{f0}) + A_0 R_{s0}] \approx \\ &\approx -(R_0 + R_{f0}) / A_0 R_{s0} \end{aligned} \quad (24)$$

$$A_0 = [(1 + h_{I0}) / h_{I0}] \cdot [(R_0 + R_{f0}) / R_{s0}] \quad (25)$$

If we consider (24) and (25) it can be seen that h_{I0} and A_0 depend on the parameters of the I_0 circuit. It soon becomes obvious that this apparent inequality between (11) and (24) covers a strict identity. Now, similarly to (14), the error of R_a is

$$h_{R0} = (R_a - R_d^*)/R_a^* = (n - n_0)R_k/(R_{k0} + n_0R_k) \quad (26)$$

Using (3), (19) and the right side of (26) one can write

$$h_{R0} = [(R_0 + R_{f0})/A_0R_d] [R_k/(R_{k0} + n_0R_k)] \quad (27)$$

If we then multiply (27) by R_{S0}/R_{S0} and take (3), (19) and (24)

$$\begin{aligned} h_{R0} &= [(R_0 + R_{f0})/A_0R_{S0}] [n_0R_k/(R_{k0} + n_0R_k)] = \\ &= [(R_0 + R_{f0})/A_0R_{S0}]e_k \geq h_{i0}e_k \end{aligned} \quad (28)$$

On comparing (24) and (11), the ratio of the errors from the controlled currents—supposing that h_{I0} and h_{I1} are small—is found to be

$$\frac{h_{I0}}{h_{I1}} = \frac{R_0 + R_{f0}}{R_1 + R_{f1}} \cdot \frac{R_1 + R_{f1} + A_1R_s}{R_0 + R_{f0} + A_0R_{S0}} \approx \frac{R_{f0}}{R_{f1}} \cdot \frac{1}{n_0} \quad (29)$$

This last approximation is derived by setting $A_0 = A_1$, $R_0 = R_1 = 0$ and using (3). The approximate values of R_{f0} and R_{f1} are obtained from (16) and Fig. 1/c, viz.

$$R_{f0} = U_M/I_0 = R_a/k \quad (30)$$

$$R_{f1} = U_M/I_1 = U_M/n_0I_0 = R_a/kn_0 \quad (31)$$

Inserting (30) and (31) into (29) we find that the ratio is practically equal to unity, namely it does not depend on R_a . For this reason the accuracy of the current controls demands the same gain regardless as to whether we control I_0 or I_1 . Making use of (18) and (28), the ratio of the measurement errors is

$$h_{R0}/h_{R1} = h_{I0}e_k/h_{I1}e_k = h_{I0}/h_{I1} \approx 1 \quad (32)$$

In Fig. 5, as further evidence, we present, on the basis of (12) and (25), the values of amplification A for both current controls, as a function of R_a , R_m and R_0 or R_1 respectively, using the transfer functions already presented in Fig. 2. The error of the control has a value as high as $h=0.01$, the diameter of the borehole $d=140$ mm, and $R_0=1 \Omega$ or $R_1=0.1 \Omega$

The continuous curves represent the cases of $R_0 = R_1 = 0$ and the dashed ones correspond to the real R_0 or R_1 values found in practice. The effect of the transitional impedances of the current electrodes is included in R_0 and R_1 , respectively.

The figure shows the values of gain A necessary for measurements having an accuracy of $h=0.01$ and the remarkable effect if R_0 or R_1 have values differing from zero.

It can thus be seen that there is no difference in the technical requirements if one controls I_1 or I_0 . Consequently neither of the control ideas has the slightest advantage over the other. The main factor to be taken into consideration is which kind of measuring system gives the best solution for the most severe conditions, and the extremely high R_i and R_m dynamics occurring in oil and gas prospecting.

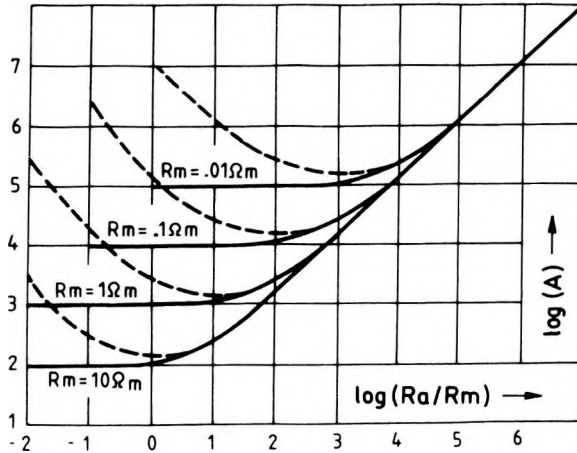


Fig. 5. Values of A versus R_a/R_m and R_0 or R_1 for an LL7 sonde. Continuous lines represent $R_0 = R_1 = 0$

5. ábra. Az A értéke R_a/R_m és R_0 illetve R_1 függvényében egy LL7-szonda esetében. A folytonos vonal az $R_0 = R_1 = 0$ értéknek felel meg

Рис. 5. Значение A в зависимости от R_a/R_m и R_0 или R_1 для зонда LL7. Сплошная линия отвечает значению $R_0 = R_1 = 0$

3. Optimum system for focused-current control and measurement

A simple optimum system is shown in Fig. 6. The value of R_0 is chosen so that it keeps I_0 constant if R_a has low values; if R_a is high, then I_0 is in inverse ratio to R_a , advancing the realization of the n_0 requirement. We produce R_a as a quotient of U_M and I_0 being measured simultaneously while I_1 is controlled. The very advantage of the system is that it covers a high range of R_a resistivities while having possibly the least dynamics in the information channels. The value of U_M and I_0 , that is $U(I_0)$, are shown as a function of R_a in Fig. 6/a.

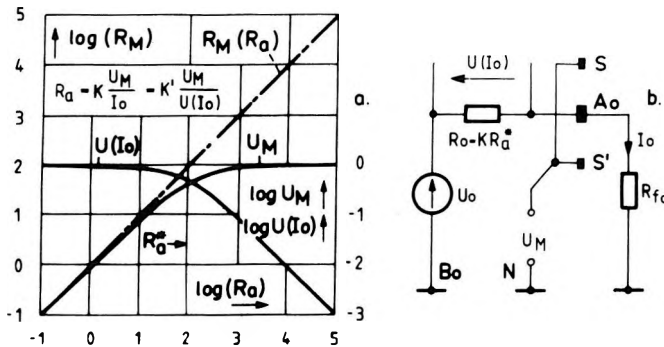


Fig. 6. Characteristics of the sonde measuring the U_M/I_0 ratio and its I_0 circuit

6. ábra. Az U_M/I_0 hányados mérésen alapuló mérőrendszer karakterisztikái és az I_0 áramkör

Рис. 6. Характеристики измерительной установки, основанной на измерении отношения U_M/I_0 и схема I_0

4. Combined controls

Let us consider the possibilities offered by the combined controlling. In the case of I_0 control (cf. Fig. 4) if h_{I_0} (24) is small, supposing $R_0 = R_1 = 0$ and using (22), (23) and (30), one can write

$$I_0 = U_1 k A / (R_a + k A R) \quad (33)$$

$$I_1 = U_1 k A n / (R_a + k A R) \quad (34)$$

hence, I_0 does not depend on n : it is only a function of R_a as well as of constants k , A , and R of the control circuit. If we choose k , A , and R properly, the current will have the same shape as that of the $U(I_0)$ curve shown by Fig. 6/a. The shape of the curve of the measured potentials is similar to that of curve U_M in Fig. 6/a. The position of the crossing point of the U_M and $U(I_0)$ functions depends on the values of R_a and $k A R$ product. Consequently the combined I_0 control, in spite of its having been complicated by using an additional control circuit, realizes only the simple optimum system shown by Fig. 6.

Likewise, we can write for the I_1 control shown in Fig. 3

$$I_0 \approx U_1 k A / (R_a + k A R) \quad (35)$$

$$I_1 \approx U_1 k A n / (R_a + k A R) \quad (36)$$

The currents as function of R_a and n are plotted in Fig. 7. The continuous curves show the I_0 values and the dashed ones those of I_1 . One can see that the values

of I_1 never exceed the maximum of the function $I_0(R_a, n_0)$. Theoretically this control would give the best solution—being both I_0 and I_1 maxima limited—if we did not consider the low values of I_0 i.e. the U_M voltage caused by this current. Whenever R_a is low we can see, bearing in mind expression (16), that U_M can have extremely low values, even lower than the noise level. Moreover the optimum U_M and $U(I_0)$ signal-dynamics is spoiled because the shape and relative values are not optimized as strictly as in the case of the system shown in Fig. 6. Thus, this control requires higher dynamics in each measuring channel than it does in the optimum system. Although the concept seems reasonable it is no more advantageous than the simple system.

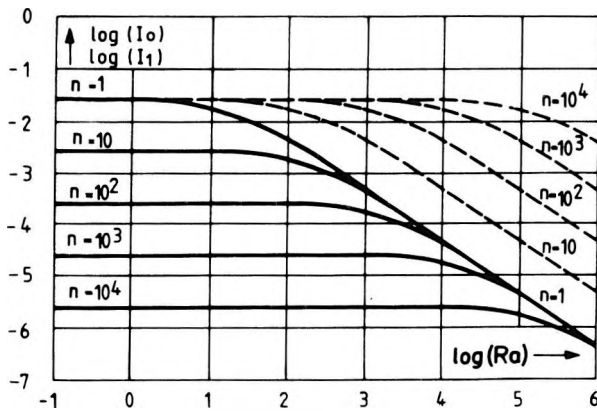


Fig. 7. Typical values of I_1 (dashed line) and I_0 (continuous line) versus R_a and n for I_1 control with additional I_1/I_0 ratio

7. ábra. I_1 (szaggatott vonal) és I_0 (folytonos vonal) jellemző értékei R_a és n függvényében, I_1 és járulékos I_1/I_0 -szabályozás esetében

Рис. 7. Характерные значения I_1 (пунктир) и I_0 (сплошная линия) в зависимости R_a и n при регулировании I_1 и дополнительно I_1/I_0

5. Conclusions

Both cases of I_1 and I_0 controls demand identical control loop gain if the conditions are identical in the borehole. Thus it is not valid that the I_0 control demands less gain than that of the I_1 (see equations (12) and (25)).

Consequently it is important for the highly demanding situation of oil and gas prospecting, especially in hostile environmental boreholes, that such control systems are realized which give adequate gain as well as stable and rapid operation.

The additional I_1/I_0 ratio adjusting cannot make it possible to decrease the gain of the control-loop for I_1 or I_0 control either, since neither gain A nor

coupling-resistance R figuring in the expressions describes the error of the controlled current or that of the apparent resistivity (see equations (11) and (18), or (24) and (28)).

The error of the measured resistivity caused by insufficient control is proportional to the product of the error of current control and the factor depending on the resistivities of the borehole and rock-space and their geometrical distribution. This error is generally less than the error of the current control (see equations (18); (19), or (28)).

A KÜLÖNFÉLE TÍPUSÚ FOKUSZÁLT ÁRAMTERŰ SZELVÉNYEZŐ BERENDEZÉSEKBE HASZNÁLT SZABÁLYOZÓ RENDSZEREK ÖSSZEHASONLÍTÁSA A PONTOSSÁG SZEMPONTJÁBÓL

KUBINA ISTVÁN

A cikk az irányított áramterű (laterolog) szelvényezés különféle változataival foglalkozik, figyelembe véve a szabályozó berendezés, a fúróluk és a kőzetér valamennyi jellemzőjét, amely befolyásolja a szabályozás pontosságát.

Bemutatjuk a mért látszólagos ellenállás hibájának és a szabályozás elégtelenségének összefüggését és azt, hogy ezek milyen kapcsolatban vannak a mérést meghatározó fő műszerjellemzőkkel, valamint a fúrólukat és az azt körülvevő kőzetteret leíró négy átviteli függvénynel.

СОПОСТАВЛЕНИЕ ПО ТОЧНОСТИ РЕГУЛИРУЮЩИХ СИСТЕМ РАЗЛИЧНЫХ ТИПОВ ДЛЯ БОКОВОГО КАРТАЖА

И. КУБИНА

В работе дано сопоставление разных вариантов бокового каротажа с учетом всех характерных черт регулирующего устройства, скважины и вмещающих пород, которые производят влияние на точность регулирования.

Приводятся зависимость погрешности измеренного кажущегося удельного сопротивления от недостаточности регулирования и ее связь с определяющими измерение основными характеристиками аппаратуры, а также с четырьмя функциями передачи, описывающими скважину и окружающее ее пространство горных пород.

